ACCESSIBILITY
OPEN

OsloMet – Oslo Metropolitan University

Department of Civil Engineering & Energy Technology
Section of Civil Engineering

Master Program in Structural Engineering & Building Technology

MASTER THESIS

TITLE OF REPORT	DATE
Development of FEM methodology for analyzing wind-induced loads on transmission lines for sub-arctic terrain and extreme atmospheric conditions	24.05.2022
	PAGES / ATTACHMENTS 125/27
AUTHOR(S) Wojciech Poradowski s349019	SUPERVISOR(S) Prof. Aase Reyes aaser@oslomet.no

IN COLLABORATION WITH	CONTACT PERSON
Høyspent AS, Bogstadveien 27B, 0355 Oslo, org. no.: 911 977 788	Ola Torgrim Eide ola@hoyspent.no

SUMMARY / SYNOPSIS

This thesis presents structural analysis of power lines with the use of the Finite Element Method (FEM). The methodology of analyzing the atmospheric loading on conductors and supporting structures is being developed. The introduction to the problematics of climatic loading that impact transmission lines is proceeded with review of design codes for determination of resulting loads on supports. The final stage is to create parametrized model of suspension structures coupled with conductors in MATLAB and COMSOL Multiphysics software with adequate modelling techniques and boundary conditions. As a result, master thesis contributes to development of structured procedure of overhead transmission lines design in order to facilitate the structural assessment and address the commercial needs.

KEYWORDS
Overhead transmission lines
Wind and ice loads
COMSOL Multiphysics

PREFACE

As the student of *Structural Engineering and Building Technology* master´s degree program at Oslo Metropolitan University, I would like to take advantage of knowledge gained during ongoing studies and contribute to the development of power line design.

Master thesis proposal emerged from ambitions of Høyspent AS with support of Katalyzator AS to supplement the industry with tool for analyzing power lines from the structural integrity point of view and maintaining the power line structures in safe and reliable operation. I would like to thank my supervisor Professor Aase Reyes for imparting the engineering practices and contributing to well organized master-program, as well as Ola Torgrim Eide from Høyspent AS, who supported me with access to COMSOL Multiphysics software and introduced me to exciting branch of industry.

Last but not least, I would like to thank my lovely fiancé Aleksandra that she has always being there for me.

Wojciech Poradowski

Oslo, 25th May 2022

Motivation

Overhead transmission powerlines are often spanned across large distances in order to distribute electrical energy from power plant to several consumption areas. With regards to Nordic sub-arctic terrain, electrical infrastructure crossing diverse landforms is exposed to harsh climatic conditions, such as ice, snow and windstorms, that influence its operation and reliability. Uninterrupted energy supply has a crucial function in the economical dimension and in term of society well-being. As of 2018 [1], electricity accounts for 57,7% of Norway´s energy consumption (see Figure 1), being therefore the dominant energy product in this area with predictions of increase up to 66,8% until 2040 [2]. Norway´s trading capacity contributes to end users in both domestic and international level with over 300 000 km of high voltage grid [3]. The trend of economic growth in Norway and technological advancement will generate increase of energy demand, thereby extension of transmission grid and revitalization of aging infrastructure [4].

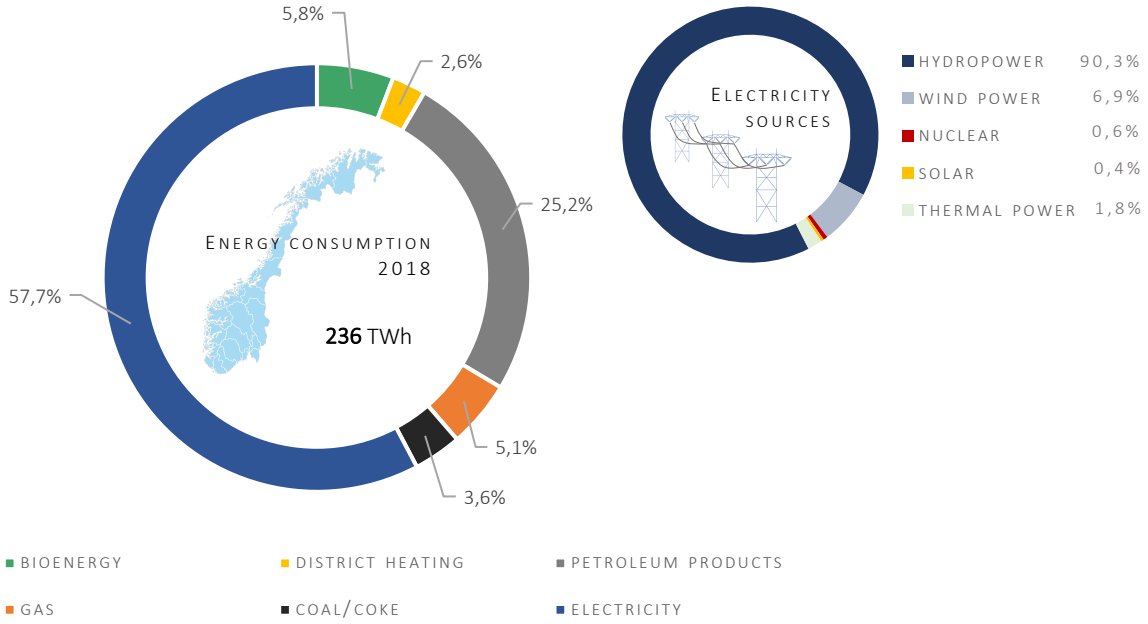

Figure 1. Energy consumption in Norway (2018) with fraction on electricity sources (2020), based on data from [2, 3]

Ice and snow accumulating on transmission network components increase their weight and resulting loading conditions. Combined with wind actions, this may lead to system´s structural imbalance, overloading and collapse. Dynamic loading on conductors, i.e.: aeolian vibrations and galloping, followed by sudden ice shedding, affects the whole structure, leading to lateral forces over system´s design limits [5]. Beyond loss of electrical power supply and high in cost necessity of putting the system into service, power lines surrounding becomes hazardous for human safety.

Atmospheric icing phenomena must hence be taken under consideration while designing overhead powerlines, especially in regions characterized with a high risk of ice and snow accretions. As a part of standardized design

methods, icing phenomena should be considered in the metrological aspect for given region to accurately lay out transmission lines routes, adjust design parameters and analyze the system under various loading conditions. Ice accretion phenomena is although complex and load estimations are challenging, since dependent on many factors, such as temperature, altitude, wind speed, humidity, cloud droplet number concentration, etc. [6]. Loading scenarios varies across Norway and general atmospheric data that is found in standards, with regards to climatic change, might be faulty, leading to hazardous events over structure loading capacity. On account of that, considerable attention is put over collecting the real-time atmospheric data with forecasting models that could complement software for power-line routes design. At the same time, no applications for commercial use with regards to detailed analysis of transmission towers taking advantage of those data were found in Norway.

Objective and Scope

The main objective of this thesis is to obtain in-depth insight into atmospheric loading that acts on power lines and modeling techniques of transmission towers, with regards to those actions. Design codes provides definition of loads on structures; however, it is restricted to general static scenarios. *The finite element method* (FEM) allows engineers to design and analyze constructions with high accuracy but requires structural expertise in order to obtain computational model that reflects physical conditions. If the computational model is built from scratch, application of commercial FEM software would be without any doubts time-consuming regarding modeling routines. Furthermore, the load cases that must be considered for design of power lines might be troublesome for obtaining repeatable convergence of the model.

In order to address the considerations above, the attempt to create user-friendly tool for structural analysis of transmission towers, as a part of the power grid design, was made. The aim of (a) modelling of parametrized multi-spans, (b) tower-conductor interactions, (c) possibilities of including ice-accretions on conductors and (d) dynamic analysis of conductor breakage, were achieved. Moreover, the computational model allows to integrate all the load cases required by design codes[7]. The draft solution is created with computer aided software *COMSOL Multiphysics* and *MATLAB.* It has to be underlined that the thesis represents rather ambitions for such a solution than ready-to-use tool. Creating a software for analyzing power lines that are highly non-linear in its physics, even just from the point of view of the structural design of towers, requires establishing the holistic modeling (see Figure 2), sets of validations with physical references and interdisciplinary cooperation of expertise.

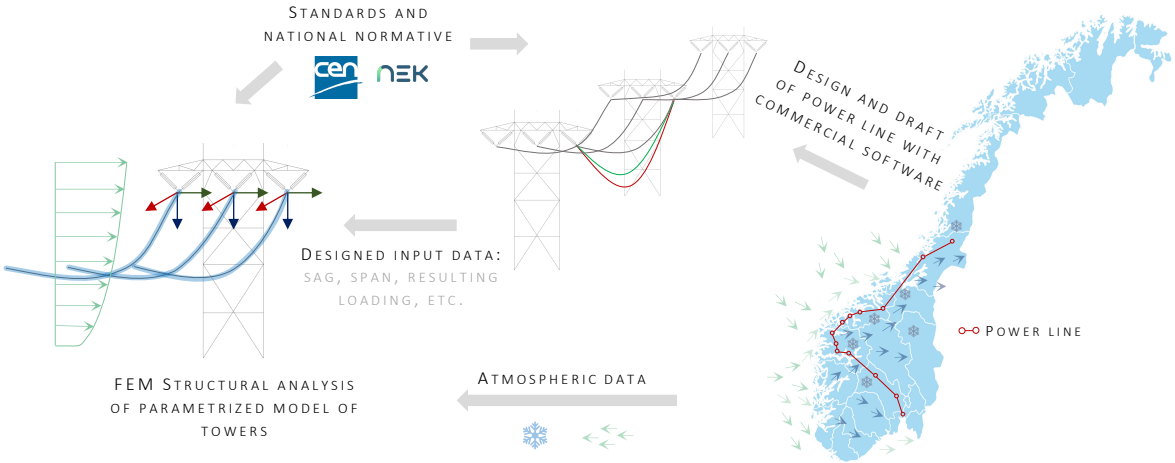

Figure 2. Scheme of interdisciplinary power line design

TABLE OF CONTENTS

1. Atmospheric icing of power lines

1.1. Problem definition

The geographic location of Norway makes the local power lines subjected to atmospheric accretion, i.e.: rime ice, glaze ice, wet snow, dry snow and hoar frost, affecting its durability and increasing risk of disruption in power supply [8]. While dry snow, soft rime and hoar frost may be easily removed from conductors or earth wires, due to low adhesion force, accretion of rime ice, glaze and wet snow might have severe consequences, such as circuit breakage and tower collapse [9]. Furthermore, climate change is going to result in higher climate variability with more extreme atmospheric events, that need to be addressed through design process of power lines and resistance of its components[10]. Several consequences of atmospheric icing are presented in Figures 1.1-1.4. The significance of atmospheric loading on power lines from the mechanical and structural point of view is discussed in the section.

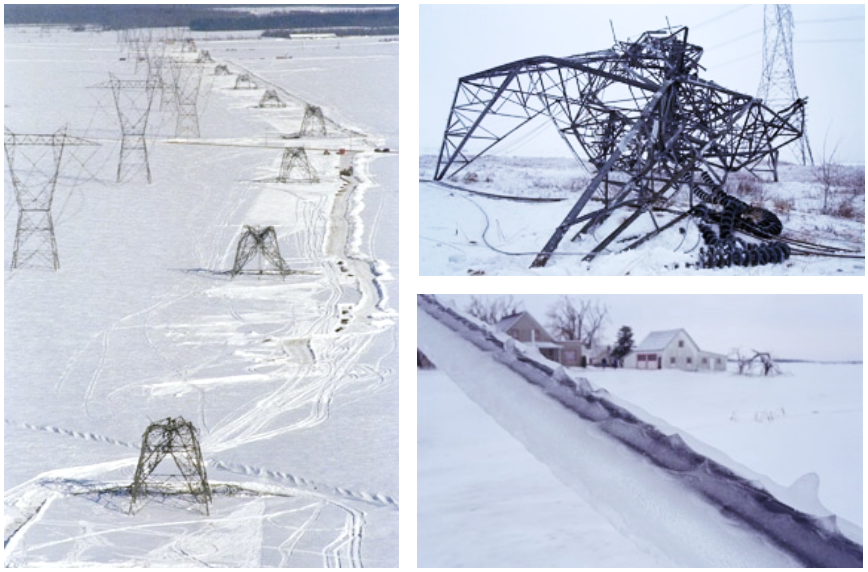

Figure 1.1. Collapse of 1,500 tower power line due to ice storm in Quebec (Canada), 1998 [11]

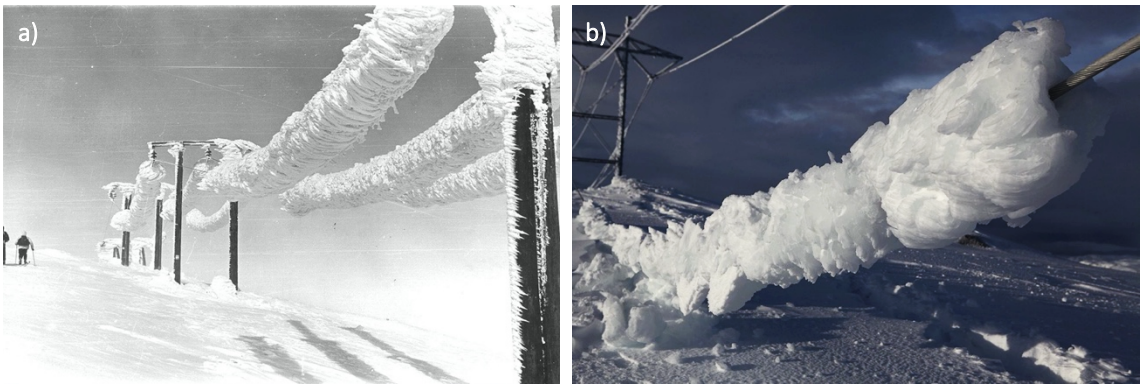

Figure 1.2. Ice and snow accreted on powerlines in (a) Lønahorgi (Norway), 1961 [12] and (b) Ålvik (Norway), 2014 [13]

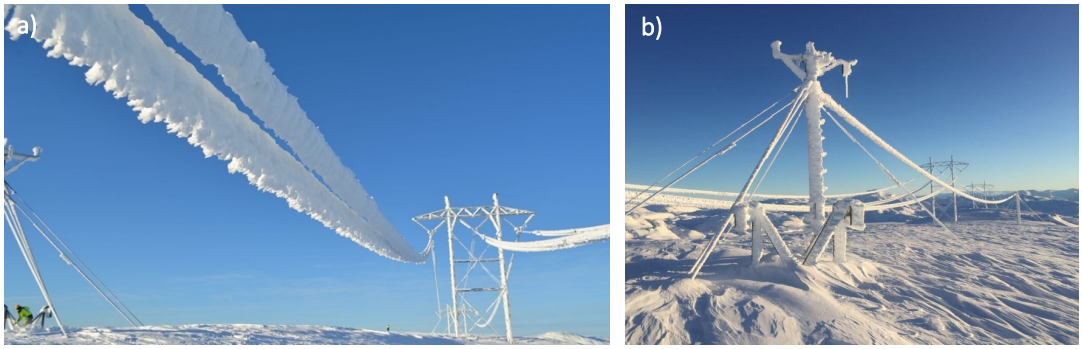

FIGURE 1.3. ICE AND SNOW ON (A) *SIMA-SAMNANGER* POWERLINE WITH WEIGHT UP TO 300 KG/M (NORWAY), 2020 [14] AND (B) ÅLVIKFJELLET WITH ICE ACCRETION 42 KG/M (NORWAY), 2018 [15]

FIGURE 1.4. ICING ON 300KV POWERLINE IN NORWAY [16]

1.2. CLIMATE CHANGE-DRIVEN LOADS ON POWERLINES

According to Norwegian Meteorological Institute report [17] and Norwegian Water Resources and Energy Directorate report [18] with regards to "Climate in Norway" 2100 climate adaptation report [10], wind and atmospheric icing will affect overhead powerlines with loading over its design capacity. Although temperature increase indicates less snow cover across Norway during the year, it will in fact lead to more extreme atmospheric events. More severe icing on powerlines caused by wet snow is certain, leading to load accumulations, especially in Finnmarksvidda plateau and mountain terrain. According to the report, those loads are expected to be reduced across the coastal line. Shorter winter seasons are going to extend conditions favorable for the icing effect and due to temperature increase will be more pronounced in the areas with currently low temperature due to increased specific humidity [19]. In order to get an overview of the significance of climate load change for existing and future power lines, the atmospheric conditions must be assessed with regards to local changes.

1.3. MECHANICAL IMPACTS

With reference to sub-arctic climate, snow and ice accumulating on power lines components increase the system´s static loading. In combination with wind forces the atmospheric impact is amplified. In addition, non-uniform accreted ice, leads to longitudinal unbalanced tension and impact suspension towers with bending and tortional moments. Slender mast structure need to withstand several loading phenomena, characteristic for transmission lines.

1.3.1. AEOLIAN VIBRATIONS OF CONDUCTORS

Cylindrical shape conductor exposed to wind contributes to Karman vortex-shedding pattern formation (see Figure 1.5). Resulting alternating pressure field on the leeward side of conductor creates lift and drag force that trigger vertical motion of the conductor, called aeolian vibrations, [20] leading to fatigue damage [21] (see Figure 1.6). Fluctuating pressure may be present regardless motion of conductor. With regards to Nordic climate, snow cover smooths terrain that works in favor of aeolian vibrations enhancement. Furthermore, ice on conductors reduces its self-damping capability and increased vibration amplitude is observed [22]. This however has been addressed through dampers installed on powerlines that mitigate the effects of severe icing [23]. Frequencies of aeolian vibrations varies between 4 to 120 Hz and usually does not exceed the diameter of conductor [24]. If the conductor oscillates under a certain frequency, it remains *locked* even for wind variations up to $1.3\frac{m}{s}$.

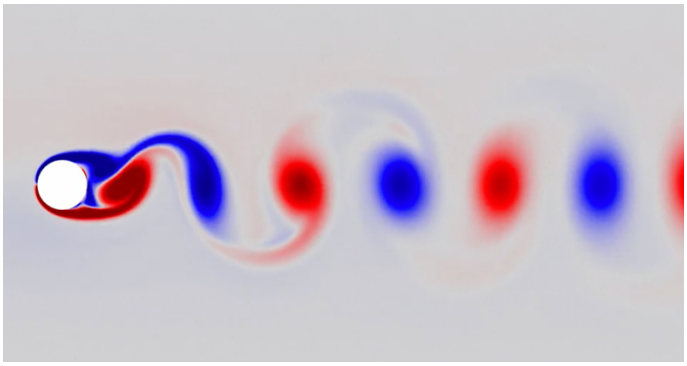

FIGURE 1.5. VORTEX SHEDDING - 2D FLOW AROUND A CIRCULAR BODY FOR RE = 500.0 [25]

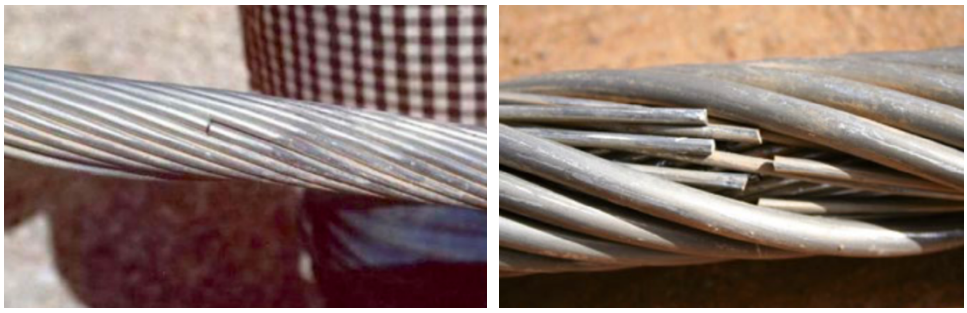

FIGURE 1.6. FAILURE DUE TO AEOLIAN VIBRATION [24]

1.3.2. GALLOPING OF CONDUCTORS AND EARTH WIRES

Ice that accretes on conductors changes its cross-sectional profile to non-symmetrical. Aerodynamically perturbated flow around conductors set the component in lifting drag motion and trigger loading on suspension hardware and transmission towers that may result in mechanical failure, i.e.: tower bracing and legs [26]. Galloping leads to large loading variations with high-amplitude oscillations on both sides of suspension towers, that results with horizontal and vertical bending and torsional loading of suspension towers structure [27]. Galloping mode shapes with the lowest frequency (0.1- 1 Hz) [5, 28] will have the highest amplitude, i.e.: one-loop mode (up and down) for multi span power line, and two-loop modes for anchor

pylon. Farzaneh [23] reports galloping amplitudes up to 15 m in extreme events. Havard [26] points out that galloping for conductors with accreted ice may increase longitudinal loading on towers 2.2 times, whilst vertical loading increases 2.7 times [27]. For overhead powerlines, galloping is thus the most hazardous type of vibrations [21, 23]. Contrary to aeolian vibrations, that results from flow instabilities fluctuating around the conductors, galloping is the result of changing ice coverage's drag, lift coefficient and wind velocity itself. Aerodynamic coefficients vary for different cross-sectional profiles of ice accretions (see Figure 1.7).

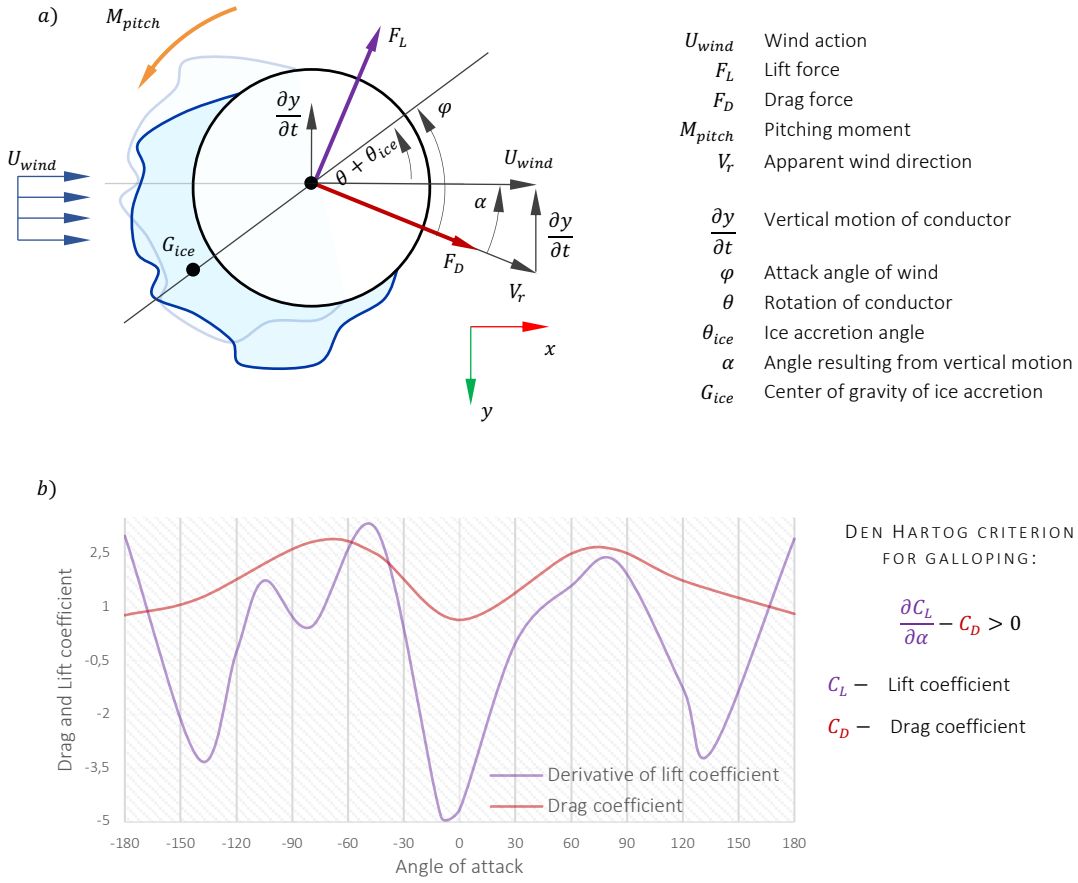

FIGURE 1.7. AERODYNAMIC CHARACTERISTICS OF CONDUCTOR WITH ACCRETED ICE (A) AND DEN HARTOG INSTABILITY CRITERION FOR ICE ECCENTRICITY $\varepsilon = 1.39$ (B). REPRODUCED FROM [23, 27] AS THEORETICAL EXAMPLE

The conductor at time t during upward vertical and tortional motion is subjected to wind U_{wind}, that exerts lift and drag forces (F_L and F_D) and pitching moment M_{pitch} in an aerodynamic center. As this point will not be the same as the center of gravity and is not known a priori [27], moment and forces are assumed to act in the shear center of conductor. Conductor upward motion $\frac{\partial y}{\partial t}$ results in apparent wind direction V_r [29], where φ is the attack angle of wind. The lift, drag and pitching moment coefficient are usually measured for a fixed cylinder in wind tunnels (quasi-static approach) [27]. System instability is defined according to *Den Hartog criterion* [23] (anticlockwise reference for positive angles) as follows:

$$\frac{\partial C_L}{\partial \alpha} - C_D > 0 \tag{1.1}$$

Galloping occurs when the system's net damping (mechanical and aerodynamical), approaches zero. Under these conditions, conductor begins to move with growing amplitude. The severity of the phenomena is then dependent on balance between input energy (aerodynamic action) and energy dissipated during the motion cycle. Most of energy dissipated is due to the drag coefficient, wind and resistance of air over the moving conductor. Mechanical dissipation in horizontal and vertical movements, i.e.: self-damping of the conductors and damping of supporting structure, has little contribution to the energy balance. Self-damping for vertical movements reaches 0.5%, negligible for vertical ones and 2% for torsional movement, with regards to energy balance.

1.3.3. Ice and snow shedding

Ice and snow shedding from conductors exert dynamic response that leads to vibrations of high amplitudes. Such an event impacts towers severely, especially its arms, and may lead to single component failure or cascade collapse. Its consequences are similar to galloping; however, the phenomena exert impulsive load. Due to loss of cohesion in a snow deposit or adhesive load on conductor, under the effect of gravity, wind, solar radiation or temperature of conductors, the surplus weight of accretion suddenly drops that results in horizontal rebound [30].

1.3.4. Rolling of Bundle Conductors

In case of long span powerlines, ice that accumulates on conductors might lead to rolling of bundle conductors (see Figure 1.8), as the effect of torsional instability [31]. This causes conductor damage and exclude powerline from service. The phenomena was addressed by Havard et al. [32] with criterion for critical conditions leading the bundle to roll over. Number of spacers excluding rolling instabilities are chosen based on predefined meteorological conditions that need to be considered individually. Bundle rolling affects especially mountain terrain and powerlines crossing large distances, i.e.: valley and rivers.

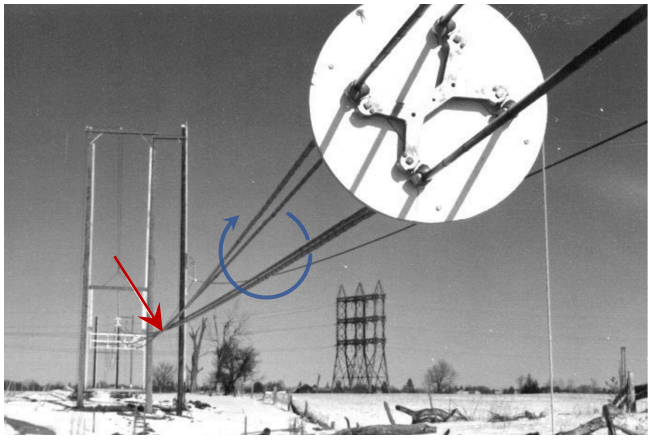

Figure 1.8. Rolling of bundle conductors [5]

1.3.5. Oscillations of sub-conductor

The phenomena affect bundle conductors of transmission lines, that is the result of wake interference between sub-conductors [33, 34]. Based on a simple example of cross-sectional plane of duplex conductor arrangement (two cylinders laying on the same horizontal line presented in the Figure 1.9), due to the air flow, the second cylinder will be affected through unstable zone of alternating pressure field on the leeward side of first conductor. This induces so called wake-induced oscillations of the affected conductor. This might lead to fatigue failure of conductor or its clashing (conductors comes into contact).

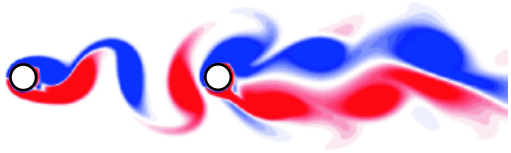

Figure 1.9. Air flow velocity contours around conductors in duplex arrangement [35]

1.3.6. Effect of topography

Although standardized methods for defining wind actions on power lines addresses to topographical features, it does not include certain, critical in terms of loads on structure, terrain characteristic, i.e.: steep hills, valleys, fjords, etc. Highly turbulent flow, such as vortex shedding and aerodynamical rotors on the leeward side of escarpment impacts power lines severely [24]. Design of powerlines with an individual approach is hence crucial.

1.4. Ice accretion protective and preventive techniques – Literature Highlights

In order to prevent power lines´ damage due to excessive ice overloading, the power grid should be either designed to withstand extreme weather events in the structural matter, followed by de-icing methods as the subsequent strategy, or anti-icing design that aims to considerably reduce ice accretion on power line components should be implemented. Several operative and design systems for de- and anti-icing are developed, however as it is a separate field of expertise, it is not being discussed in the thesis. The key-design strategies are found in the recently published "Techniques for Protecting Overhead Lines in Winter Condition" by Farzaneh and Chisholm (2022) [36] that provides a comprehensive review of several measures for improving overhead power lines´ performance under severe ice loading conditions. With regards to the aims of the master thesis, the most relevant design strategies from the literature review are highlighted.

Statnett, the designated transmission system operator in Norway, runs the R&D project "Icebox" that aims to counteract ice loading on the power grid [37]. In addition to development of countermeasures for removing and preventing ice accretion on power lines, the project develops a national icing map (see Figure 1.10) with real-time monitoring systems for creating a probabilistic forecasting system and adequate design values. Both icing phenomena and wind impacts are considered. With regards to master thesis, the up-to-date meteorological data would be crucial for design and optimizing electrical transmission grid.

A forerunner of “ICEBOX”, “FRonTLINES” research project [15], aimed to develop a numerical ice accretion model based on real-time measurements of ice lads at selected locations. Measurements were validated with accurate forecasting of icing event duration and predictions of accretion rates for different conductor diameters.

FIGURE 1.10. STATNETT ICEBOX PROJECT INCORPORATING NATIONAL ICE MAP INTO GIS ELECTRICAL GRID MAP [37]

Damages of overhead power lines in Norway in winter 2013/14 (Hardangerlinjen, Ålvikfjellet) [38], that reached up to five times of the design value [39], and reported climate change-driven extreme snow and icing events [17], prompted the “Wind Ice and Snow Loads Impact on Infrastructure and the Natural Environment“(WISLINE) project from the initiative of Norwegian Meteorological Institute. The main goal is to improve forecasting of atmospheric ice loads that impacts the electrical infrastructure. The project is in an early phase and the accuracy of the analytical model is being developed.

Wolfgang et al. [40] developed ice-prediction and detection model for high voltage overhead lines in “FLEXITRANSTORE” project. The weather-based system predicts ice accretion types with resulting loading. The real-time monitoring supplement the system with data defining conductors sag and tensile strain, so that the danger factor for necessary intervention for powerline is defined.

Havard [41] introduced an analytical approach to predict the motion of galloping conductors, tension in conductors and forces applied to the supporting insulators for single loop mode of galloping for the design parameters as follows: span length, conductor weight, ice weight, initial tension and insulator string length. With reference to the author´s previous model [26] that was limited to inelastic string theory that could not be used to estimate extreme events effects, the updated model includes elastic stretch of conductors.

1.5. NUMERICAL SIMULATION OF TRANSMISSION LINES WITH REGARDS TO ATMOSPHERIC LOADING – LITERATURE REFERENCES

Yongping et al. [42] performed state-of-the-art finite element analysis of the dynamic response of a two-span transmission line system under the effect of wind and ice shedding. Among several aspects, the displacement at the top point of the transmission tower, reaction at supports and maximum stresses on towers were analyzed under varying wind conditions. Both lattice transmission towers and ice on conductors were simulated with BEAM188 element (ANSYS software [43]). The conductor and ground wires were treated as cable elements and modelled with LINK10 element. The birth-death element method simulates ice shedding on conductors.

Zhang et al. [44] analyzed wind-induced vibrations of tower-line system through FEM analysis with focus on coupling effect of multiple tower-line system using ANSYS software [43]. The results indicate prominence of modelling the line system (sequence) for wind speeds above 10.8 m/s, as the single-tower member components were less prone to yield. Dynamic coupling effect can thus not be neglected due to demonstrated self-dependency and amplification of system response. The authors proposed an amplifying coefficient $\delta \geq 1.06$ toaddress the coupling effect for single-tower, quasi-static analysis.

Farshad [45] improved the ice failure model on conductors proposed first by Kalman et al. [46] and later applied ice shedding into a three-dimensional finite element model of multi-span transmission line to investigate cable rupture. Ice deposit on the conductor was modeled with *element death* available in ADINA [47] software, that upon rupture its mass and stiffness contribution is deleted from model.

Fengli et al. [48] established a 3D finite element model of a transmission line with focus on dynamic response due to ice shedding (ANSYS [43]). Under physical design conditions the lattice tower members collapsed, thus authors implemented interphase spacers to reduce system tension imbalance. Ice shedding was simulated with the masses applied uniformly on conductors.

In the successive study, Fengli et al. [49] created a seven-span model of conductors subjected to unbalanced tension due to non-uniformly accreted ice and resulted with its impact on suspension towers. Authors concluded that loading modes of accreted ice (distributed mass on conductors or distributed load on conductors), wind conditions and ice on conductor eccentricity has little effect on the unbalanced tension. The unbalanced tension percentage is thus the function of ice thickness, span length and icing rate.

A numerical method for calculating unbalanced tension for transmission lines under non-uniform accreted ice was proposed by Zhou et al. [50]. The methodology allowed to calculate horizontal tensions and sag with little computational effort. The research provides a guideline for design of head clearance and load on transmission towers.

1.6. Concluding remarks

Reliability of suspension tower design is highly dependent on meteorological data. Modelling of ice accretions on conductors, supporting towers and associated elements, together with wind events, increase the confidence of the construction to withstand meteorological anomalies. Especially for sub-artic climate the contribution of icing effect must be assessed with special consideration. Furthermore, due to climate change the hazardous events on powerlines seems to be apparent and the so-far gathered meteorological data, that can be found in standards, should be updated. The designer should keep in mind that the severity of icing events for the planned and existing power grid is expected to increase. From the very beginning of power line design, the multidisciplinary approach, i.e. holistic model, must be considered. The complexity of structural and atmospheric interactions, with its variability and ice formation physics aspect, requires interdisciplinary expertise.

2. TRANSMISSION GRID

Norwegian electricity network is divided into three levels: the central transmission grid, regional grid, and distribution grid. The central transmission grid carries voltage equal to 300 or 420 kV, although 132 kV lines are installed as well, among others in Balsfjord in Troms. The regional grid is designated for voltages from 33 to 132 kV. The distribution grid supplies with power up to 22kV. Central transmission grid (90%) in Norway is owned by Statnett that holds the role of transmission system operator, whilst regional and distribution grids are operated by approximately 146 different distribution system operators [51].

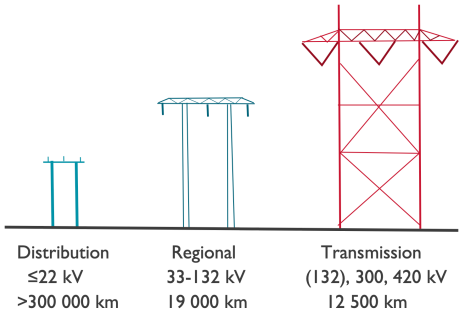

FIGURE 2.1. NORWEGIAN ELECTRICITY GRID [51]

Design of transmission lines gathers expertise across disciplines of civil, structural, mechanical, geological and electrical engineering, natural and geographical science, as well as it includes the regulating and law sector [52]. With regards to key design requirements, this master thesis focuses for the most part on the structural aspect.

2.1. TOWERS AND POLES

The main function of the overhead transmission lines supporting structure is to support conductors with required clearance from ground and other phase conductors. Support design is dependenton both electrical, i.e. transmission voltage and number of circuits, etc., and structural aspect, i.e. loading conditions and sag. This determines the type of supporting structures, either lattice tower or pole. The most common materials used in construction design is steel or other metal alloys, timber, concrete, and composite/fiber reinforced polymers that recently have been gaining attention.

2.1.1. SUPPORT STRUCTURES

Overhead transmission towers are classified in terms of the mechanical support it provides for conductors as follows (see Figure 2.2):

- **Suspension support**
  Carries the conductors along power line network and does not transfer tensile force from conductors. Conductors are attached to tower through suspension insulators.
- **Angle suspension support**
  Provides support for power line that changes direction up to 20°. Suspension insulators are installed under inclined position.

- **Strain and angle-strain support**

  Rigid anchoring of the power line network holding tensile force from conductors from both side of powerline. Designed to prevent from cascade failure. Applied in sequence according to working condition and risk of hazardous events, i.e. angle-strain support on each angle point of power line (up to 90°) and strain support for required distance.

- **Dead-end support/anchor pylon**

  Tensile force from conductors is carried on one side of the construction along power line network. In addition, withstand the loading of conductors that leads to nearby substation portals. Dead end support is being often loaded unevenly that leads to overloading of single members of construction.

- **Termination pylon**

  Type of dead-end support that terminates the power line to connect it to substation equipment of transit to underground cables.

- **Branch pylon**

  Structures designated for supporting and branching off (or starting new) multi circuit powerlines.

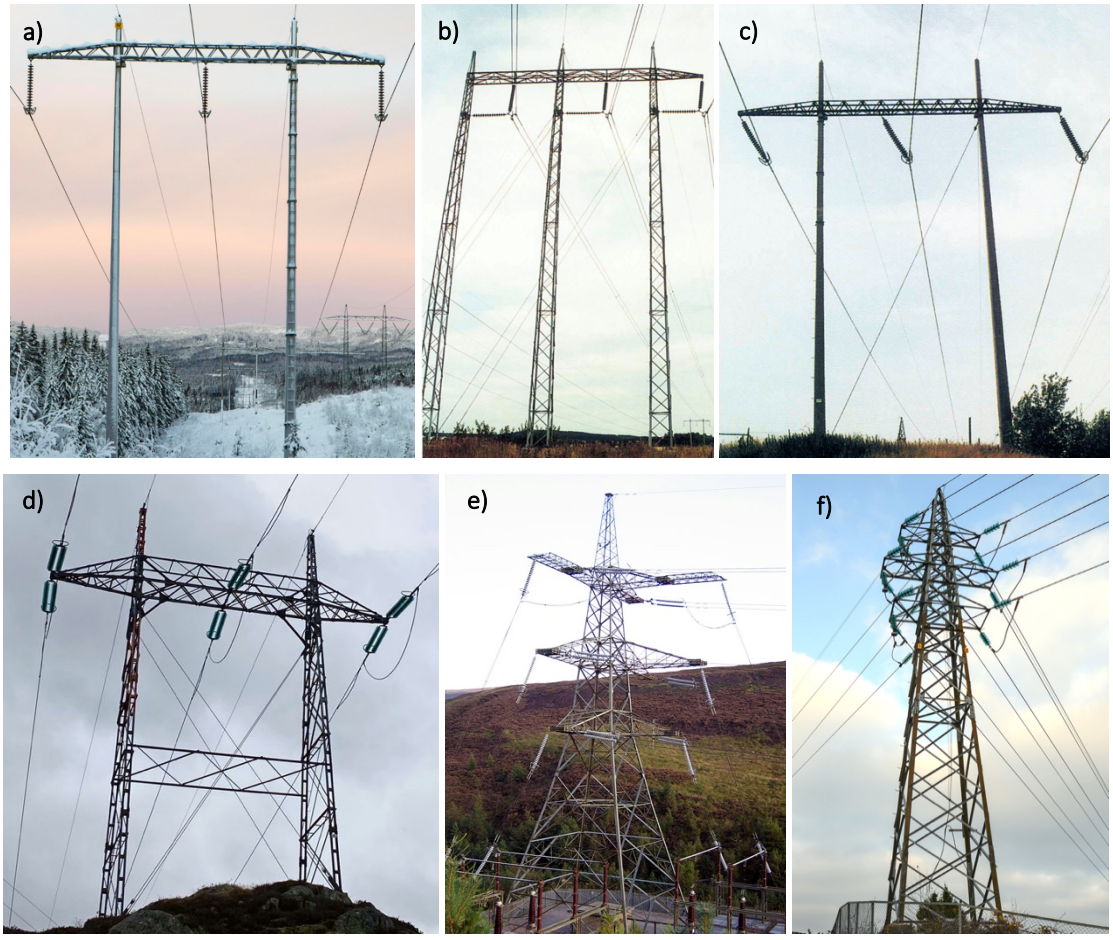

FIGURE 2.2. TRANSMISSION TOWERS EXAMPLES WITH REGARDS TO SUPPORT PROVIDED [53-55]: (A) SUSPENSION SUPPORT, (B, C) ANGLE SUSPENSION SUPPORT , (D) STRAIN SUPPORT, (E) DEAD-END SUPPORT, (F) BRANCH PYLON

2.1.2. Design requirements

The construction must provide reliable support for conductors and withstand ultimate and service loading arrangements, taking into account the safety factors due to design uncertainties. The strength of individual members must be verified to ensure resistance against high deformations, yield stresses and loss of stability. Several load cases must be considered according to EN 50341-1:20212 [7], NEK IEC 60826:2017 [56] and national normative aspects EN 50341-2-16:2016 [57], related to static loads in combination with atmospheric conditions, i.e. wind and ice. The normative requirements are discussed in section 4 of the thesis.

2.1.3. Load on structures

Transmission power line system is highly nonlinear from the structural point of view. It includes behavior of slender towers and conductors spanned across long distances. Conductors exert longitudinal loading on towers due to tensile stress. Wind-induced response of powerlines has a crucial aspect in system efficiency and safety assessment. Ice accretions magnifies the loading effects. Loads on towers are considered in terms of environmental forces, actions from the structure itself, i.e.: dead loads or pre-tensioning of conductors, maintenance loading, as well as discrete events, such as earthquake, landslides and avalanches. Furthermore, change in temperature has a great impact on the conductors' tension due to thermal expansion of the wire.

With regards to normative requirements and engineering practice, wind loads are considered in a steady state condition and must correspond to atmospheric data from power line location. Land features, i.e. mountains, hills, rivers or valleys, contributes to wind condition with a certain extent, accelerating wind dramatically. It is usually considered in horizontal direction, although in mountain terrain it affects the construction in acute angles. Design of wind loads must consider wind directions to power line direction, in order to verify its actual contribution, since wind blowing along the powerline doesn't affect conductors considerably.

Wind loads on lattice towers results in tension and compression forces of the leg members (Figure 2.3). Bracing that is in shear, provides support for legs in compression against buckling. Wind acting on conductors and ground wires results in transverse and longitudinal forces of support structure. According to CIGRE [24] the main cause of support structures collapse is wind loading, followed by a combination of wind and ice load. Mechanical impact of ice loads was discussed in the section 1.2 of the thesis. For powerlines crossing terrain with varying ice loading conditions along the structure, the atmospheric data must be adjusted into several zones to obtain most accurate design adjustment. Ice accreting on power lines structures increase its dead loads that are although not often the reason of structural failure, especially for towers.

When tension in a cable is partially or fully released, i.e. dynamic actions of conductors due to wind, swing of cables or due to conductor breakage, suspension structures experience torsional loading. In addition, unbalanced tension in conductors on both sides of structure, exerts longitudinal load (see Figure 2.3).

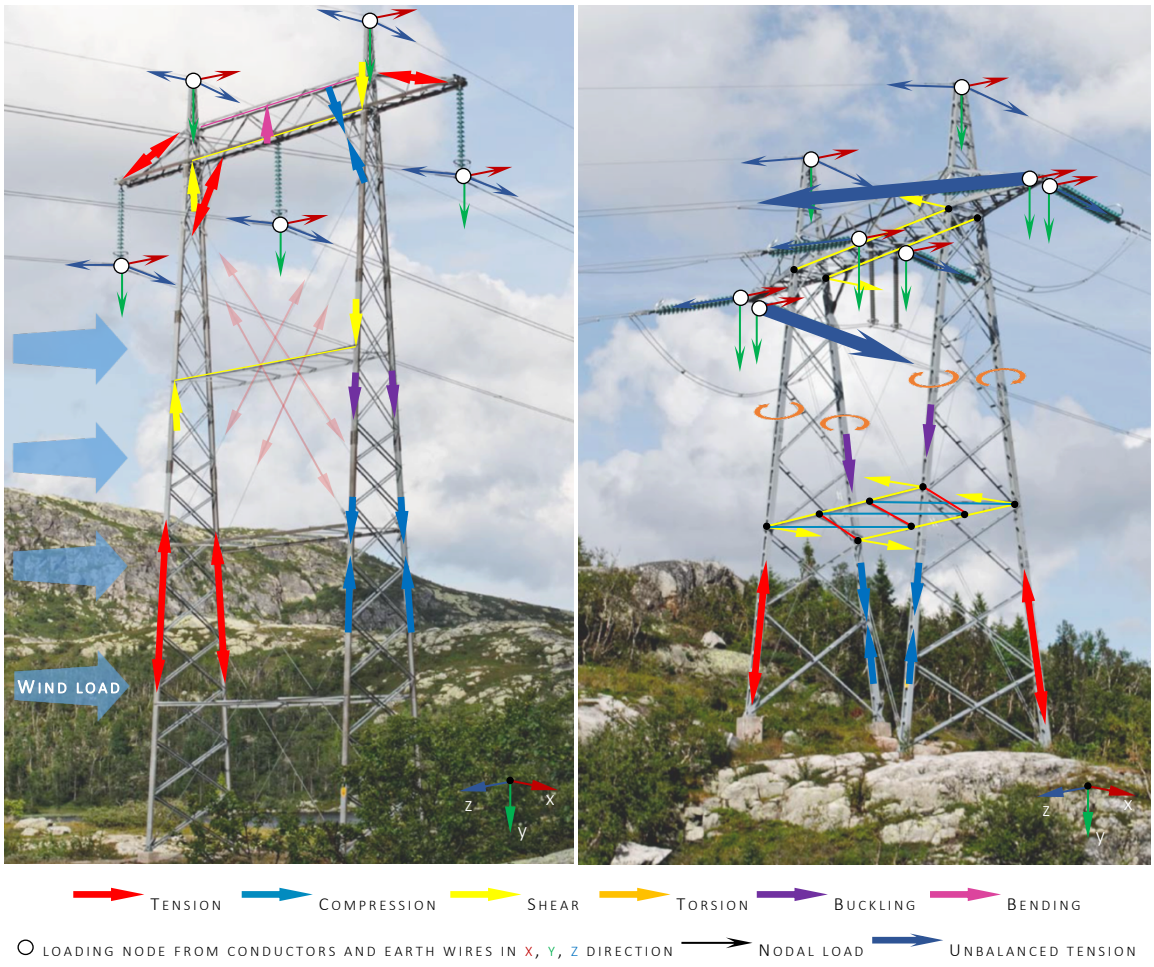

FIGURE 2.3. SIMPLIFIED DISTRIBUTION OF LOADS ON TRANSMISSION TOWERS - VERMORKTOPPEN – FLESAKER 420 KV H-PORTAL PYLONS [58] (A) SUSPENSION TOWER UNDER WIND LOAD PERPENDICULAR TO POWER LINE, AND (B) SUPPORT TOWER UNDER LOAD DUE TO UNBALANCED TENSION OF CONDUCTORS

2.1.4. DESIGN CATEGORIES

There are several design categories of transmission pylons that may serve for different support conditions depending on structural, geographical (location, terrain, etc.) and environmental aspects. Furthermore, number of circuits, required height, lifetime, facility budget and many others would be decisive while choosing the appropriate construction. As a matter of fact, each transmission lines design varies individually. In Norwegian power grid, among others, the following transmission towers designs are highlighted:

- Self-supporting lattice steel towers (different arrangement of crossarms) (Figure 2.4),
- Steel truss H-portal, Tree/steel/composite H-portal and tree/composite H-portal with steel cross beam and bracing (Figure 2.6),
- Guyed steel towers (i.e.: truss H-masts with ropes) (Figure 2.5),
- Self-supporting steel or wooden poles (Figure 2.5).

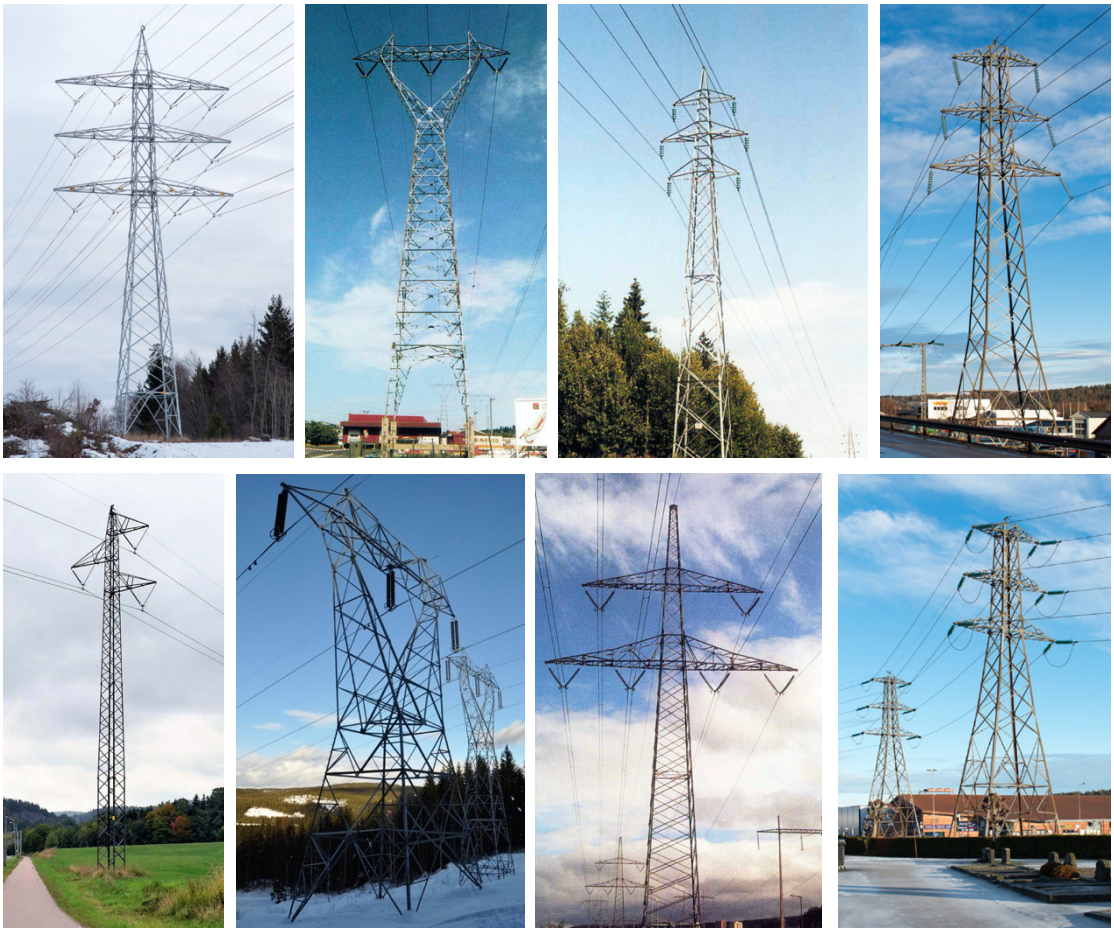

FIGURE 2.4. LATTICE STEEL TOWERS ACROSS NORWAY [59, 60]

FIGURE 2.5. EXAMPLE OF GUYED STEEL TOWERS AND SELF SUPPORTING STEEL POLES [60]

FIGURE 2.6. EXAMPLE OF H-PORTAL PYLONS IN NORWEGIAN POWER GRID [60]

2.2. SUSPENSION AND STRAIN INSULATORS

Insulators provides electrical insulation between the line conductor and the ground, and the support conductors mechanically. Resistance of insulators, both mechanical and electrical, is determined with loading conditions and must be designed with regards to flashovers failure, that is the bypass of the electrical insulation between electrical current in conductors to structure, and short-duration surges due to lightning strikes. Ice and snow accretions on insulators is especially considered in terms of electrical leakage.

Suspension insulator are being installed in tangent or angular form. It is free to swing about its point of support on transmission tower and must thus be designed with safe clearance to other components of power network. The swing is dependent on tension and weight of conductors, temperature from solar radiation, wind conditions, span and line angle. Single or multiple arrangements of insulators, and its orientation varies dependent on designed load, although might be also restricted by contamination conditions that affects its performance. Insulators are being usually installed in vertical, inclined or V-string arrangement.

V-type set of insulators limits the conductor to swing transversally to the conductor direction and reduce construction size [61]. Furthermore, in any load scenario, reduces the overturning moment of transmission

tower [62]. V strings works both in tension and compression (Figure 2.7). The angle of insulators from vertical, weight of conductors and atmospheric loading, i.e.: wind and ice accretions, are the decisive design parameters, whether the insulator working in compression will resist the loading. High angle V string carries large transverse wind loading, but due to clearance to the supporting structure, exert bigger geometries of tower arms. Moreover, its tension capacity diminishes. Mechanical design for both suspension and tension insulators must consider maximum loading scenarios with safety factor set by standards.

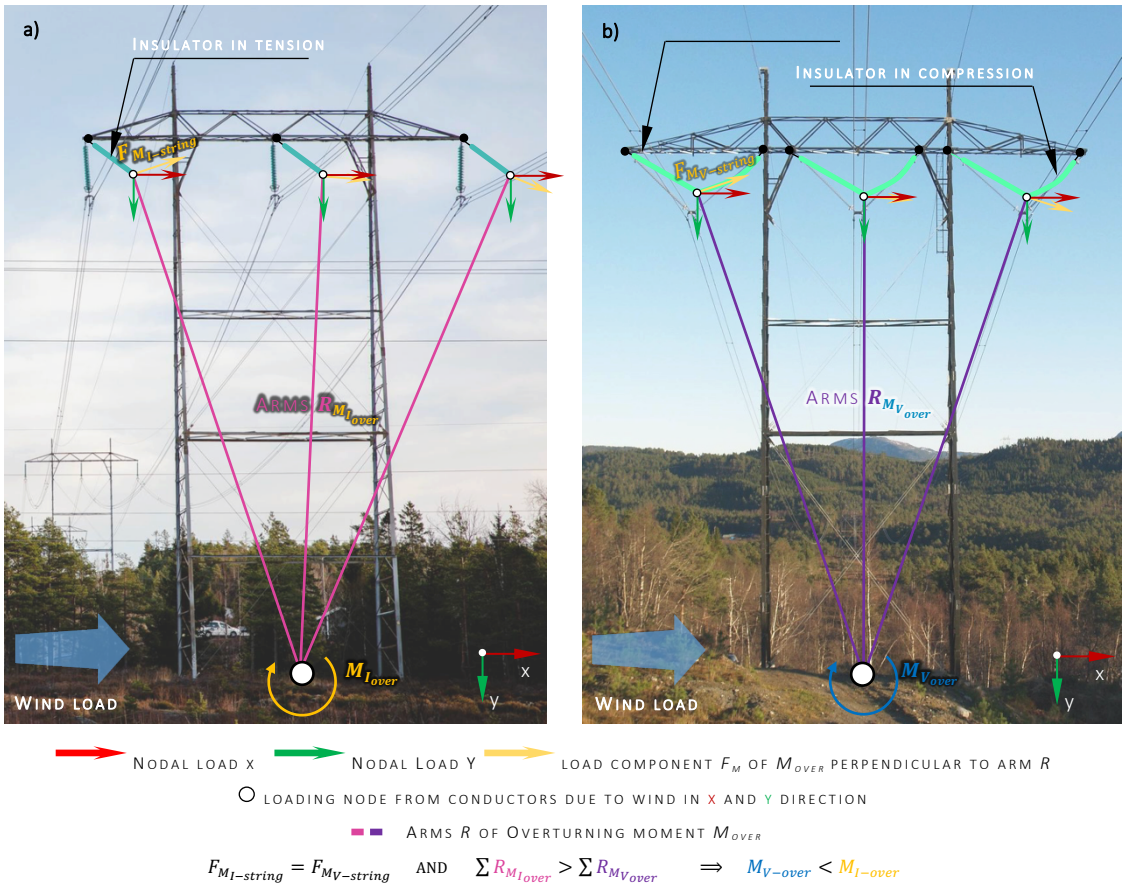

FIGURE 2.7. OVERTURNING MOMENT - LOAD DISTRIBUTION FOR (A) I - STRING INSULATOR AND (B) V -STRING INSULATOR EXAMPLE ON (A) 300 KV HASLE-HALDEN H-PORTAL [63] (B) 420 KV (300 KV BEFORE UPGRADE) ERTSMYRA – TJØRHOM-LYSE POWERLINE H-PORTAL [64],

Requirements and guidelines for insulator design can be found in NEK EN 60383-1 [65] and in the worth mentioning work of Kiessling et al. [66] and Catchpole [62].

2.3. MECHANICAL ASPECT OF CONDUCTORS

Manufacturing specification for conductors is not covered in the thesis. Design and type are primary considered from electrical point of view, such as current rating (that is capability of power transfer); although as a component working under both electrical and mechanical loading, the structural design is crucial.

The conductor, as the major component of power lines, convey electrical current. It is a cable strung on the points of support. Conductors are arranged in single or multiple setups, creating a bundle conductor with equal spacing between each sub-conductor, i.e.: duplex, triplex, etc. Conductors arranged in bundles has a higher efficiency than a single conductor designed for carrying the same current. Conductors should have high tensile strength due to high tensions during operation, good flexibility to avoid vibrational fatigue and low weight. Furthermore, a low coefficient of thermal expansion is desired.

Aluminum-based with central cored steel conductors (ACSR) were the dominant type up to early 90´s, and since then has been successively replaced by *all aluminum alloy conductors* (AAAC) that has greater *strength to weight ratio* due to absence of central reinforcement [52]. For ACSR, aluminum conductors that carry the current are stranded around a central core of galvanized steel providing structural strength. Furthermore, for non-homogenous sections with high differences of linear expansion coefficient, such as Aluminum-Steel with ratio ~2:1, there is a transfer of tension from outer layer to core that increase non-linearity of the component. Other types of conductors are among others *aluminum alloy reinforced* and *steel reinforced aluminum alloy* conductors. Worth mentioning are spiraling elliptical shape, vibration-resistant conductors that reduces or even eliminates Aeolian vibrations and galloping phenomena. Such a conductor can be both AAAC and ACSR type. Different types of conductors' cross sections can be seen in Figure 2.8.

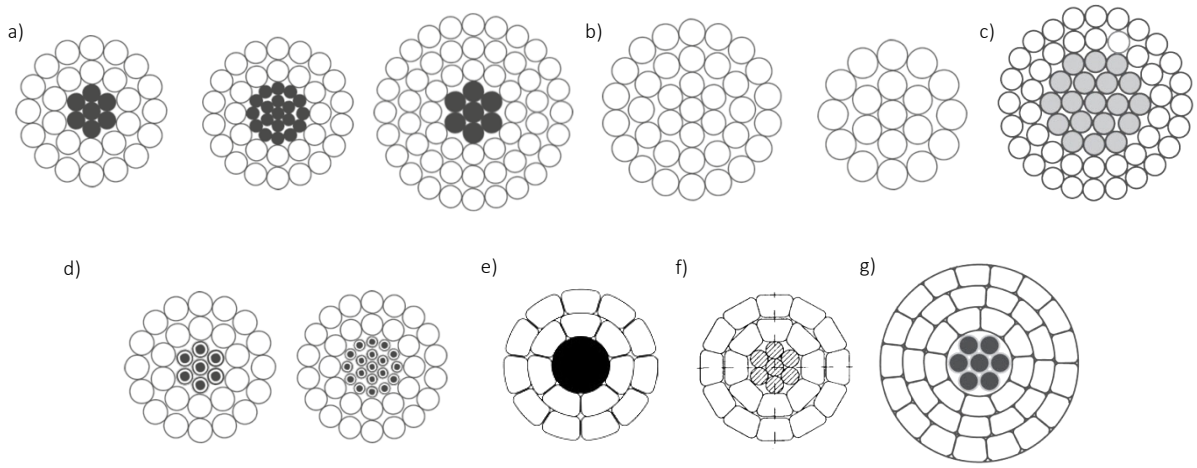

FIGURE 2.8. TYPICAL CROSS-SECTIONS OF CONDUCTOR: (A) ACSR/ACSS ALUMINUM CONDUCTORS STEEL REINFORCED/SUPPORTED, (B) AAC/AAAC ALL-ALUMINUM/ALL ALUMINUM ALLOY, (C) ACAR CONCENTRIC-LAY-STRANDED, (D) ACSR/AW ALUMINUM CONDUCTORS' ALUMINUM CLAD STEEL REINFORCED, (E) ACCC/TW TRAPEZOIDAL ALUMINUM ALLOY CONDUCTOR COMPOSITE CORE (F) ACSR/TW TRAPEZOIDAL ALUMINUM CONDUCTORS STEEL REINFORCED, (G) ACSR/AW/TW TRAPEZOIDAL ALUMINUM CONDUCTORS CLAD STEEL REINFORCED

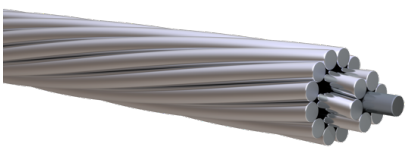

FIGURE 2.9. ACSR CONDUCTOR

Conductors attached to suspension insulators are free to move in longitudinal and perpendicular direction to power line. Unbalanced tension in conductors, i.e. due to uneven distribution of ice loads or due to difference of span lengths, is equalized with free movement of the conductor string end, however, it affects the structural integrity of the supporting structure. For strain support, conductors are terminated on both sides (except dead ends) with insulators that experience full tension of conductors. The geometry of transmission towers depends thus on sag and tension of conductors.

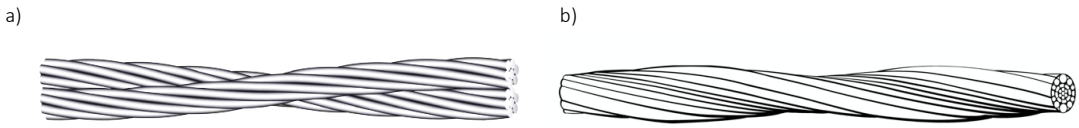

FIGURE 2.10. VIBRATION-RESISTANT CONDUCTORS (A) AAC COMPOSED OF EQUAL CONDUCTORS, AND (B) ACSR COMPOSED OF A COMBINATION OR ROUND AND SHAPED WIRES WITH VARYING DIAMETERS AND CROSS-SECTIONS

2.3.1. SAG

Sag is the vertical distance between line connecting points of attachments of conductors on supports, and conductor. The so-called *sagging curve* or *catenary* is formed due to balance between tension in conductors and its dead load. Engineering practice assumes constant mass of conductor per unit length and constant cross-section of conductor along the span [66]. No bending moment is considered in the point of support; thus, conductors work just under tension. The accepted practice allows substitution of catenary curve with a simpler parabolic equation (0,5% accuracy deviation), as long as the span to sag ratio is higher than 20:1 [66, 67]. The purpose of sag calculation is to provide safe clearance to adjacent infrastructure and sustain power line in a safe operation.

Conductors are being installed up to 35% of its ultimate tensile strength, with regards to NEK IEC 60826:2017 [56]. It elongates due to long-term creep, temperature expansion and plastic deformations while subjected to severe ice and wind actions over its loading capacity. Especially for harsh winter conditions, the sag must provide sufficient self-damping of the conductors to prevent aeolian vibration-driven fatigue. Under specified wind and ice loading, the maximum tensile stress is limited to up to 75% [56]. This is established as a safety limit with regards to extreme loading events.

Development of a numerical tool allows to calculate the sag and tension of power line as a function of temperature and atmospheric load. Nevertheless, the graphical overview with equation derivation is presented to understand the physics of conductors from the structural point of view.

2.3.2. CATENARY CURVE OF CONDUCTOR

Catenary span geometry for different point of support is presented in the Figure 2.11. The shape of catenary is a function of conductor weight per unit length m_c and horizontal component of tension H. The conductor sag f is then a function of those parameters, span a and elevation difference between points of support h.

Force equilibrium yields equal in value horizontal component along conductor:

$$H_A = H_B = H_C = H$$

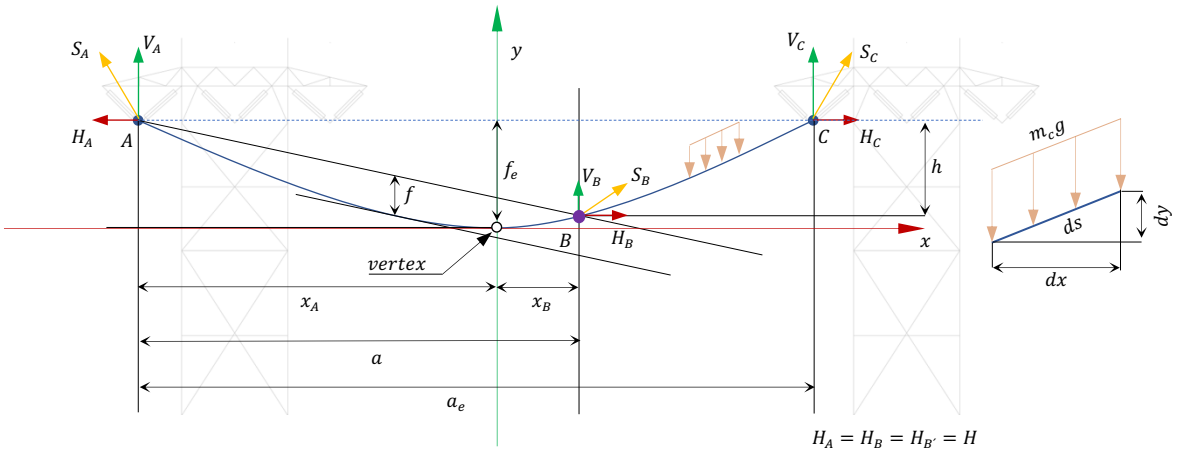

FIGURE 2.11. CATENARY AND SAG OF CONDUCTORS

SUPPORT ON EQUAL HEIGHT

According to CIGRE [67], conductor catenary and its parabolic approximation, with the origin of coordinate system laying in the vertex of curve for x and y coordinates, can be describe with the following hyperbolic cosine function:

$$y(x) = \frac{H}{m_c g}\left[cos\,h\left(\frac{m_c g}{H}x\right) - 1\right] \cong \frac{m_c g}{2H}x^2 \tag{2.1}$$

where:

m_c	mass of conductor per unit length,
g	gravitational acceleration,
H	horizontal component of the conductor tensile force,
$\frac{m_c g}{2H}x^2$	valid for $\frac{(m_c g)^2}{12H^2}x^2 \ll 1$.

With regards to (2.1) conductor sag f_e (max. sag) for points of support at A and C is as follows:

$$y\left(x = \frac{a_e}{2}\right) = f_e = \frac{H}{m_c g}\left[cosh\left(\frac{m_c g a_e}{2H}\right) - 1\right] \cong \frac{m_c g (a_e)^2}{8H} \tag{2.2}$$

$$\frac{m_c g (a_e)^2}{8H} \quad valid\ for \quad \frac{(m_c g)^2 (a_e)^2}{48H^2}x^2 \ll 1$$

The parameter $\frac{m_c g}{H}$ is standardized and defined as catenary parameter or catenary constant with the unit [m]. Catenary constant yields sag to either decrease or increase. The typical values vary between 500 and 2000 m. Sag accuracy between 1% to 2% is acceptable [67]. Conductor length in a function of the x coordinate, measured between points of support A and C is defined as follows:

$$L(x) = \int \sqrt{1 + \left(\frac{d}{dx} y(x)\right)^2}\, dx \tag{2.3}$$

$$L(x) = \frac{H}{m_c g} \sinh\left(\frac{m_c g}{H} x\right) \cong \left(1 + \frac{(m_c g)^2}{6H^2} x^2\right) \cdot x$$

In case of supports remaining on the same level, such as A and C supports (Figure 2.11.), the vertical component of tension is equal to ½ of conductor weight:

$$V_A = V_C = \frac{m_c g L(x=0{,}5a_e)}{2} = \frac{1}{2} H sinh \frac{m_c g a_e}{2H} \tag{2.4}$$

where:

m_c	mass of conductor per unit length,
g	gravitational acceleration,
H	horizontal component of the conductor tensile force,
L	length of conductor.

For those conditions the total tension is:

$$S = \sqrt{H^2 + V^2} \tag{2.5}$$

In the vertex of the catenary, the vertical component is equal to zero, thus tension for this point defines the maximum value of vertical component. The resulting tension from vertical and horizontal component increases while approaching the point of support.

SUPPORT ON DIFFERENT HEIGHTS

The form of catenary equation is not dependent on the difference in point of support elevation. Sag and length of conductor are although in a different form. In order to define sag $f(x)$ of the conductor with point of support at A and B, component x_A and x_B are introduced:

$$f(x) = \frac{h}{a}(x - x_A) + \frac{H}{m_c g}\left[\cosh\left(\frac{m_c g}{H} x_A\right) - \cosh\left(\frac{m_c g}{H} x\right)\right] \tag{2.6}$$

$$x_B - x_A = a \tag{2.7}$$

Powerline design input data usually predefines span length a, points of support elevation difference h and tensile force horizontal component H. Components x_A and x_B must be solved with a set of mathematical transformations (Eq. 2.7 - 2.14). Length of infinitesimal element of conductor (see Figure 2.11) can be defined as follows:

$$ds = \sqrt{dx^2 + dy^2} = dx\sqrt{1 + \frac{dy^2}{dx^2}} \tag{2.8}$$

Conductor length L in a function of x coordinate (Eq. 2.3), measured between points of support A and B:

$$L(x) = \int_{x_A}^{x_B} \sqrt{1 + \left(\frac{d}{dx} y(x)\right)^2}\, dx = \int_{x_A}^{x_B} \sqrt{1 + \sinh^2\left(\frac{m_c g}{H} x\right)} dx = \int_{x_A}^{x_B} \cosh\left(\frac{m_c g}{H} x\right) dx \tag{2.9}$$

$$L(x) = \frac{H}{m_c g}\left[sinh\left(\frac{m_c g}{H}x_B\right) - sinh\left(\frac{m_c g}{H}x_A\right)\right]$$

With respect to identities of hyperbolic function: $sinh\alpha - sinh\beta = 2cosh\frac{\alpha+\beta}{2}sinh\frac{\alpha-\beta}{2}$

$$L = \frac{2H}{m_c g}\cdot cosh\left(\frac{m_c g}{2H}(x_A + x_B)\right)\cdot sinh\left(\frac{m_c g}{2H}(x_B - x_A)\right) \xrightarrow{x_B - x_A = a} L = \frac{2H}{m_c g}\cdot cosh\left(\frac{m_c g}{2H}(x_A + x_B)\right)\cdot sinh\left(\frac{m_c g}{2H}a\right)$$

Based on geometrical assumptions $x_B - x_A = a$. Furthermore, sag f is always equal to zero in points of support A and B, hence:

$$f(x = x_B) \Longrightarrow h = \frac{H}{m_c g}\left[\cosh\left(\frac{m_c g}{H}x_B\right) - \cosh\left(\frac{m_c g}{H}x_A\right)\right] \tag{2.10}$$

With respect to identities of hyperbolic function: $cosh\alpha - cosh\beta = 2sinh\frac{\alpha+\beta}{2}sinh\frac{\alpha-\beta}{2}$

$$h = \frac{2H}{m_c g}\cdot sinh\left(\frac{m_c g}{2H}(x_A + x_B)\right)\cdot sinh\left(\frac{m_c g}{2H}(x_B - x_A)\right) \xrightarrow{x_B - x_A = a} h = \frac{2H}{m_c g}\cdot sinh\left(\frac{m_c g}{2H}(x_A + x_B)\right)\cdot sinh\left(\frac{m_c g}{2H}a\right) \tag{2.11}$$

The length of conductor L in a function of design predefine input data is obtained with following transformation:

$$\begin{cases} cosh^2\alpha - sinh^2\alpha = 1 \\ cosh\left(\frac{m_c g}{2H}a\right) = \frac{1}{sinh\left(\frac{m_c g}{2H}(x_B - x_A)\right)}\cdot\frac{Lm_c g}{2H} \\ sinh\left(\frac{m_c g}{2H}a\right) = \frac{1}{sinh\left(\frac{m_c g}{2H}(x_B - x_A)\right)}\cdot\frac{hm_c g}{2H} \end{cases}$$

$$\frac{1}{sinh^2\left(\frac{m_c g}{2H}(x_B - x_A)\right)}\cdot\left(\frac{Lm_c g}{2H}\right)^2 - \frac{1}{sinh^2\left(\frac{m_c g}{2H}(x_B - x_A)\right)}\cdot\left(\frac{hm_c g}{2H}\right)^2 = 1$$

$$L = \sqrt{\left(\frac{2H}{m_c g}\sinh\left(\frac{m_c g}{2H}(x_B - x_A)\right)\right)^2 + h^2} \xrightarrow{x_B - x_A = a} L = \sqrt{\left(\frac{2H}{m_c g}\sinh\left(\frac{m_c g}{2H}a\right)\right)^2 + h^2} \tag{2.12}$$

The coordinate x_A of conductor with points of support with different elevations is as flows:

$$L - h = \frac{2H}{m_c g}\cdot cosh\left(\frac{m_c g}{2H}(x_A + x_B)\right)\cdot sinh\left(\frac{m_c g}{2H}a\right) - \frac{2H}{m_c g}\cdot sinh\left(\frac{m_c g}{2H}(x_A + x_B)\right)\cdot sinh\left(\frac{m_c g}{2H}a\right) \tag{2.13}$$

$$L - h = \frac{2H}{m_c g}\cdot sinh\left(\frac{m_c g}{2H}a\right)\left[cosh\left(\frac{m_c g}{2H}(x_A + x_B)\right) - sinh\left(\frac{m_c g}{2H}(x_A + x_B)\right)\right]$$

With respect to identities of hyperbolic function: $cosh\alpha - sinh\alpha = e^{-\alpha}$

$$L - h = \frac{2H}{m_c g}\cdot sinh\left(\frac{m_c g}{2H}a\right)\cdot exp\left(-\frac{m_c g}{2H}(x_A + x_B)\right)$$

$$exp\left(-\frac{m_c g}{2H}(x_A + x_B)\right) = \frac{m_c g(L - h)}{2H\cdot sinh\left(\frac{m_c g}{2H}a\right)}$$

$$-\frac{m_c g}{2H}(x_A + x_B) = ln\frac{m_c g(L - h)}{2H\cdot sinh\left(\frac{m_c g}{2H}a\right)}$$

Based on geometrical assumption: $x_A + x_B = a + 2x_A$

$$-\frac{m_c g}{2H}(a + 2x_A) = ln\frac{m_c g(L-h)}{2Hsinh\left(\frac{m_c g}{2H}a\right)}$$

$$x_A = -\frac{a}{2} - \frac{H}{m_c g}\left[ln\frac{m_c g(L-h)}{2Hsinh\left(\frac{m_c g}{2H}a\right)}\right] \tag{2.14}$$

Formula for the vertical component of tension results from balance of moment for infinitesimal element of conductor (Figure):

$$V = \frac{H^2}{m_c g}sinh\left(\frac{m_c g}{H}x\right) \tag{2.15}$$

$$V_A = -H\,sinh\left(\frac{m_c g}{H}x_A\right) \quad and \quad V_B = H\,sinh\left(\frac{m_c g}{H}x_B\right)$$

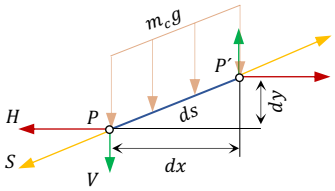

$$\sum M_N(x = dx) = Hdy - Vdx = 0$$

$$V = \frac{Hdy}{dx}$$

FIGURE 2.12. INFINITESIMAL ELEMENT OF CONDUCTOR – MOMENTUM BALANCE

The total tension of the conductor in any point is then:

$$S = \sqrt{H^2 + V^2} \tag{2.16}$$

$$S = \sqrt{H^2 + H^2\,sinh\left(\frac{m_c g}{H}x\right)} = H\sqrt{1 + sinh^2\left(\frac{m_c g}{H}x\right)}$$

With respect to identities of hyperbolic function: $cosh^2\alpha - sinh^2\beta = 1$

$$S = H\,cos\left(\frac{m_c g}{H}x\right) \tag{2.17}$$

Mean value of the conductor tensile force with a span a:

$$S_{mean} = \frac{1}{a}\int_{x_A}^{x_B} S dx = \frac{H}{a}\int_{x_A}^{x_B} H\,cos\left(\frac{m_c g}{H}x\right)dx \overset{Eq.2.9}{\Longrightarrow} \frac{HL}{a} \tag{2.18}$$

COUPLING OF SPANS

The transmission line comprises of strain towers for every n-suspension tower. This divides the power grid into multiple line sections. At suspension, the insulators are free to move both in transverse and longitudinal direction to the power line direction. Free movement of insulators equalize the difference in tension of conductors in adjacent spans L_n, resulting from temperature difference, ice accretion and wind loading. If in considered line section span doesn't change between adjacent towers, the single sag representation can be used ($L_1 = L_2 = L_n, for\ n > 1$). If difference is sag differs considerably, the concept of ruling (equivalent) span L_E can be applied [52, 68]:

$$L_E = \sqrt{\frac{\sum_{i=1}^{n} {L_n}^3}{\sum_{i=1}^{n} L_n}} \tag{2.19}$$

2.3.3. Accuracy factors

Sag formation is non-linear and depends on several factors. With regards to calculation, both analytical and with computer aided tools, the accuracy is always limited [67]. Elongation of conductors depends on tension, temperature and time. For linear model, i.e. linear elastic material model, sag under severe atmospheric loading might be underestimated. Plastic elongation assumes values based on experience and is recommended (although not required) for high accurate estimations of sag under maximum tension loading ang temperature conditions. Under design loading conditions, conductors are assumed to work in elastic limit.

Linear elastic model

Conductors are modelled as linear springs with elastic modulus and thermal elongation coefficient (linear thermal elongation). Elastic elongation (strain) ε of stranded AAC is represented with the following equation [67]:

$$L_{H_c} = L\left(1 + \frac{H_c - H}{EA}\right) \tag{2.20}$$

$$\varepsilon = \frac{L_{H_c} - L}{L} = \frac{\Delta H}{EA} \tag{2.21}$$

where:

L_{H_c}	length of conductor under horizontal tension H_c,
L	reference length of conductor under horizontal tension H,
E	modulus of elasticity,
A	conductor cross-section area.

The equation for linear thermal elongation for AAC:

$$\frac{L_{H_c} - L}{L} = \alpha_{Al} \cdot \Delta T_{con} \tag{2.22}$$

where:

α_{Al}	coefficient of linear expansion for aluminum $\left[23e-06\frac{1}{^\circ C}\right]$,
ΔT_{con}	temperature change of conductor.

The presented linear elastic strain and thermal elongation cannot be directly applied for non-homogenous cross sections, i.e. comprising of different materials. On an example of ACSR, the tension in conductor must be divided into core H_{Steel} and outer layer H_{Al} components. The total tension is hence:

$$H = H_{Steel} + H_{Al} \quad \text{and} \quad \varepsilon = \varepsilon_{Steel} = \varepsilon_{Al} \tag{2.23}$$

The modulus of elasticity for such a composite is derived from equations (2.21) and (2.23):

$$E = E_{Al}\frac{A_{Al}}{A} + E_{Steel}\frac{A_{Steel}}{A} \tag{2.24}$$

The linear thermal coefficient changes accordingly:

$$\alpha = \alpha_{Al}\frac{E_{Al}}{E}\cdot\frac{A_{Al}}{A} + \alpha_{Steel}\frac{E_{Steel}}{E}\cdot\frac{A_{Steel}}{A} \tag{2.25}$$

It is assumed that the equivalent tensile stress in the conductor is equal to horizontal tension divided by cross-sectional area [66, 67]:

$$\sigma = \frac{H}{A} = \sigma_{Al}\frac{A_{Al}}{A} + \sigma_{Steel}\frac{A_{Steel}}{A} \tag{2.26}$$

NON-LINEARITY OF CONDUCTORS

Aluminum strands undergoes plastic deformation under initial pre-tensioning of conductors between point of support. When settled and sagged, the plastic deformation under operational, moderate loading will continue due to time-dependent plastic strain, i.e. creep [69]. Plastic strain of aluminum strands is always greater than steel core plastic strain due to difference in modulus of elasticity ($E_{Aluminum} = 68\,GPa$, $E_{Steel} = 210\,GPa$). The following examples are discussed in order understand nonlinearity of conductors:

a) Plastic strain of aluminum strand is evident based on laboratory testing performed by Aluminum Association [70] on *795 kcmil-26/7 ACSR "Drake"* specimen with UTS 300 MPa (see mFigure 2.13). Even for stress reaching *50%* of UTS, the elongation of conductor is less than 0,1%, although it is considerable for aluminum strands. It can be deducted that tensile stress of aluminum wires decreases in time, whilst increases for steel core. This is advantageous in terms of alternating bending stress (see section 2.3.6.) that may lead to fatigue failure of conductor for mono-metallic conductors.

b) The stress-strain creep curve for *795 kcmil-37 AAC "Arbutus"* conductor in presented in the Figure 2.14 [71]. In the laboratory test, specimen was subjected to tension reaching 125 MPa, that was intended to correspond severe ice and wind event. Conditions yielded plastic deformation below 0,2%. Furthermore, specimen was subjected to moderate constant tension of 30 MPa in order to interpolate the permanent elongation due to creep for period of 6 months, 1 year and 10 years. This resulted, respectively to loading duration, the following strain: 0,11%, 0,12% and 0,15%. Due to creep, the sag after settling the conductor increases and total component of tension decreases. It can be predicted in the design process.

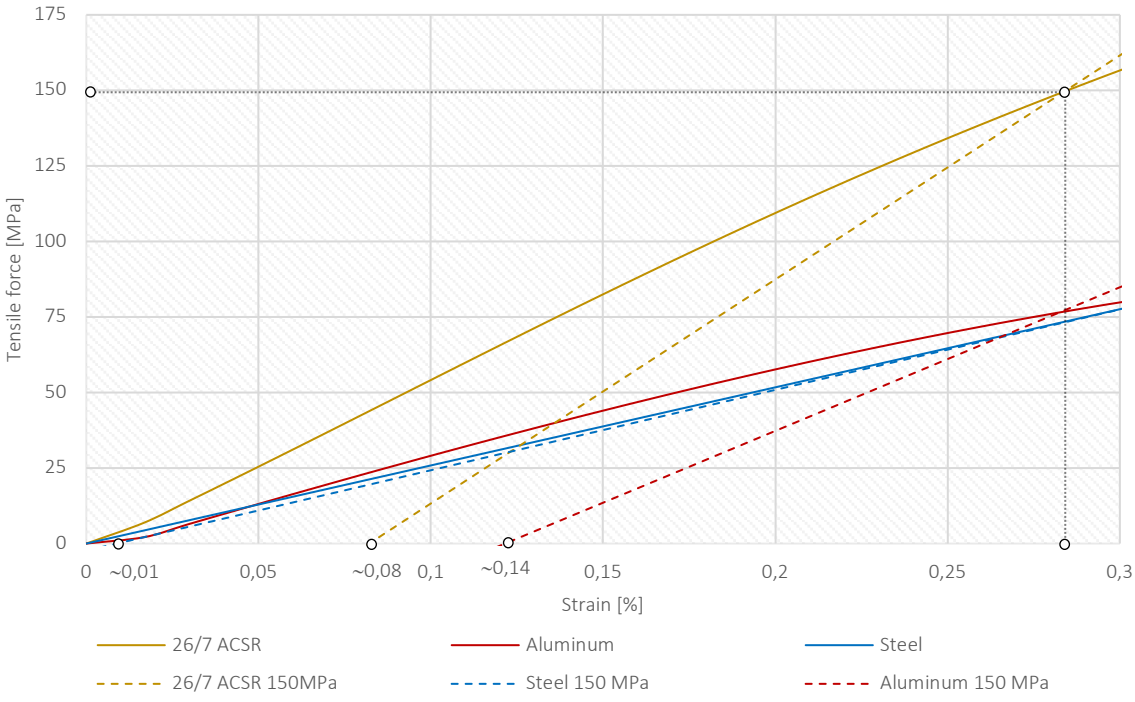

FIGURE 2.13. STRESS – STRAIN CURVE FOR *795 KCMIL-26/7 ACSR "DRAKE"* CONDUCTOR SPECIMEN UNDER TENSION 150MPA

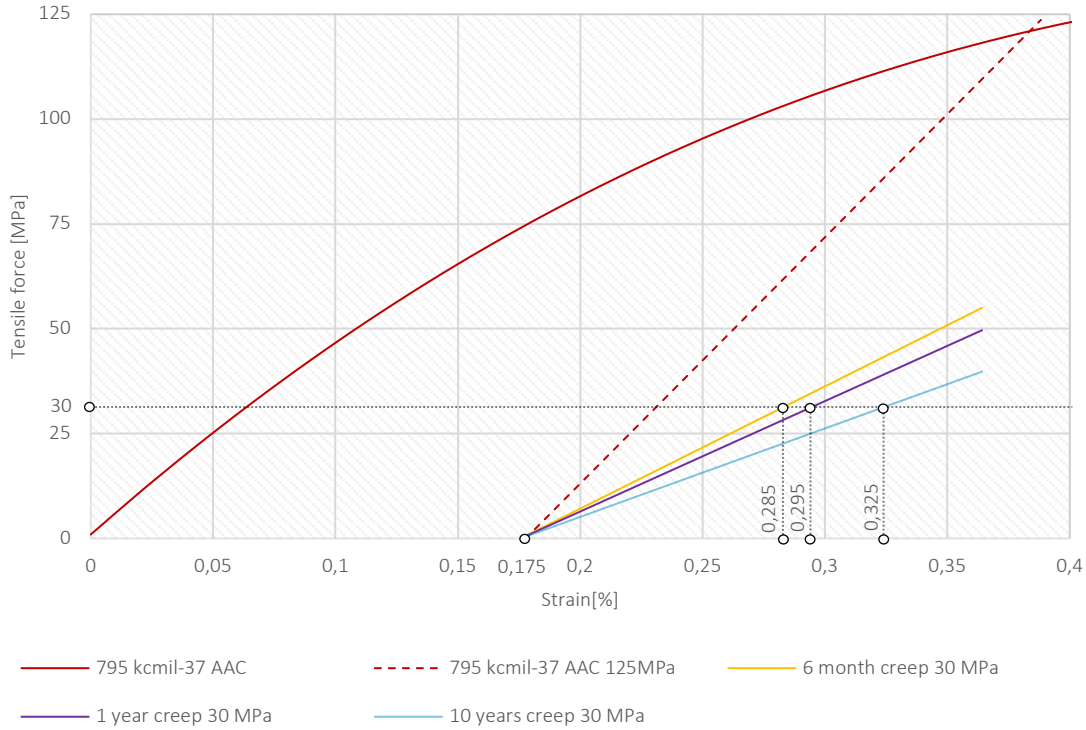

FIGURE 2.14. STRESS – STRAIN CREEP CURVE FOR *795 KCMIL-37 AAC "ARBUTUS"* CONDUCTOR SPECIMEN

BILINEAR ELASTIC-PLASTIC MODEL

Conductors are modelled similarly to discussed liner elastic model. The parameter of plastic elongation is added based on experience and represents combined effects of strand settlement, creep and extreme load

events. For homogenous aluminum conductors, established amount of plastic strain is added to initial length of conductor. For non-homogenous conductors, such as ACSR, the total elongation can be calculated as follows (plastic strain of steel core neglected):

$$\varepsilon_{pl} = \frac{H}{EA} = \frac{H_{Al}}{E_{Al}A_{Al}} + \varepsilon_{pl_{Al}} = \frac{H_{Steel}}{E_{Steel}A_{Steel}} + \overset{0}{\cancel{\varepsilon_{Steel}}} \tag{2.27}$$

where:

H	horizontal component of the conductor tensile force,
ε_{pl}	Longitudinal plastic strain,
E	modulus of elasticity,
A	conductor cross-section area.

Non-linear elastic model

Conductors are modelled as non-linear springs that elongates elastically in a function of tension, plastically as a function of tension and time and thermally as a function of temperature. Plastic elongation due to loading arrangements, as well as creep is based on laboratory testing. Stranding of aluminum wires is taken into consideration while pre-tensioning and settling the wire between point of support. After this point conductor elongates linearly up to point of plastic deformation.

Relatively small changes in length of the conductor leads to substantial changes of sag. Elastic and plastic elongations of conductors spanned across long distances (see Figure 2.15) can not be neglected. During the life cycle of conductor, humidity might increase its weight up to 2.5%. Subjected to environmental conditions, the corrosion occurs, resulting in higher dead load. As mentioned before, conductors are not considered to work in bending in the point of support. If pinned to suspension clamp, the reduction of sag might reach 0.9%.

Figure 2.15. Powerline crossing fjords (a) 3350 m Fjærlandsfjorden powerline [4] and (b) 4570 m Refsdal – Fardal powerline over Sognefjorden [72]

Variation of conductor´s tension due to change of temperature

Conductors expand and contract with changes in temperature. The rate of thermal elongation is dependent on linear coefficient of thermal expansion, temperature change and type of conductor. For conductors

consisting of core and strands with different properties, the thermal elongation will exert additional tensile shift between those sections. As presented in Figure 2.16, change in temperature has non-negligible change in tension of conductors, that must be considered during design of power lines.

For homogenous conductors of length L with predefined coefficient of thermal expansion α_T, the elongation of the conductor ΔL, under change of temperature ΔT can be then defined as follows:

$$\Delta L = \alpha_T L \, \Delta T \tag{2.28}$$

For non-homogenous conductors, that usually is the case, the elastic behavior is more complex. For instance, the linear thermal elongation coefficient of aluminum is twice that of steel. The unification of this aspect describes equation 2.24.

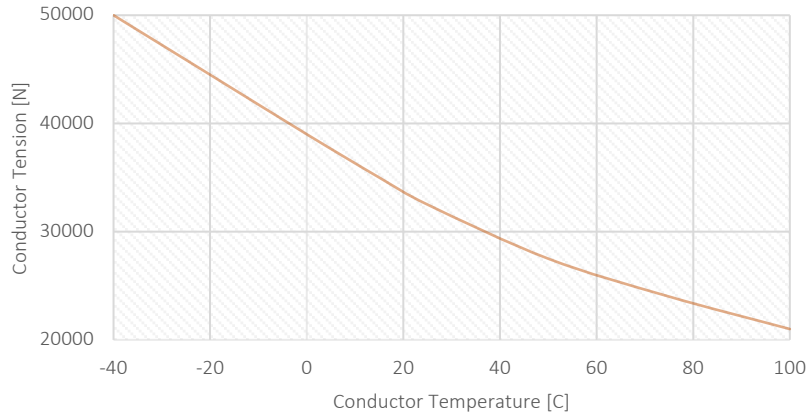

FIGURE 2.16. VARIATION IN TENSION OF CONDUCTOR DUE TO CHANGE OF THE TEMPERATURE. EXAMPLE OF CONDUCTOR DRAKE A1/S1A (ACSR) REPRODUCED FROM [68] FOR SPAN 250 M

2.3.4. SLACK

Slack is a difference of conductor length L and span a. It is usually expressed as a percentage of span length:

$$\left(\frac{L-a}{a} \cdot 100\right)\% \tag{2.29}$$

With an increase of slack, tension decreases.

2.3.5. ATMOSPHERIC LOADS ON CONDUCTOR

The degree of ice and wind loads varies across Norway. Line design must address to the local conditions in order to prevent hazardous events and failures. The design loads of ice and wind load, combined and individually, is discussed in section *4. Law regulations and normative references.* Conductors are designed with regards to long-term stresses, that may reach 75% of rated tensile strength over the period of one year [66]. Furthermore, any extreme peak loading must be addressed through the design.

2.3.6. Conductors fatigue

During vibrations stranded conductors are subjected to alternating stresses resulting from bending at the point of support. This may lead to fatigue damage. Furthermore, bending yields conductors to slip longitudinally to the power line in the supporting clamp that may result in disproportional distribution of tensile loading [73].

The lifetime of aluminum-based conductors subjected to vibrations can be approximated with bending stress σ_b related to number of cycles N_f, proposed by CIGRE [74]. The conservative approach is based on data collected out of fatigue test of conductors on suspension clamp.

$$\sigma_b = \begin{matrix} 450 \cdot {N_f}^{-0.2} & for \quad N_f \leq 1.56e07 \\ 263 \cdot {N_f}^{-0.17} & for \quad N_f > 1.56e07 \end{matrix} \tag{2.29}$$

Fatigue life estimations are usually based on laboratory testing, although Lalonde et al. [75, 76] obtained highly accurate estimations of service life via FEA model of conductors subjected to high and low amplitude deflections adequate to line galloping phenomena. Authors reached similar results to above-mentioned CIGRE approximation.

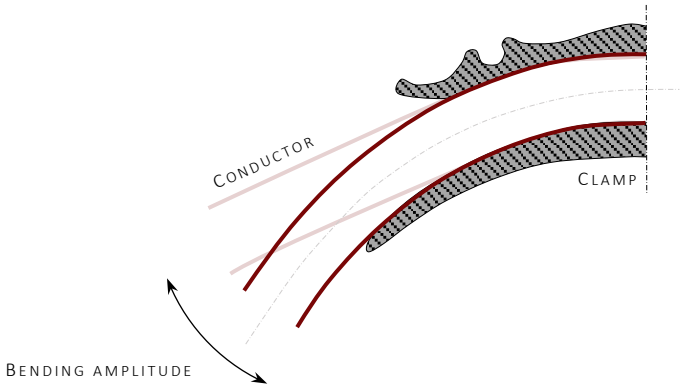

Figure 2.17. Schematic sketch of fatigue bending due to dynamic oscillations of conductor in clamp

Figure 2.18. (a) Aluminum alloy suspension clamp, (b) aluminum alloy clamp with armor rod against bending and (c) aluminum alloy clamp with armor grip against bending (*Preformed Line Products*)

2.3.7. Earth wire

Earth wires (ground wires) improves the lightning performance of power lines. Strength of support structures must consider overhead earth wires that are suspended longitudinally to conductors. According to Farzaneh et al. [23]. Combination of ice and wind loading will have thus the same consequences as for conductors.

FIGURE 2.19. EXAMPLE OF ALUMINUM CLAD STEEL EARTH WIRES CROSS SECTION

Earth wires might also incorporate fiber optic telecommunication circuits (OPGW) as the multi-purpose utilization of powerline (Figure 2.20). Fiber optics are resistant to electromagnetic interference, thus commonly applied.

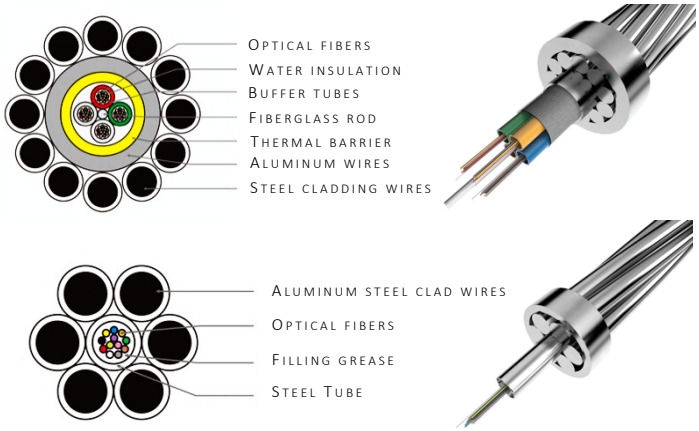

FIGURE 2.20. EXAMPLES OF OPGW EARTH WIRES (*HUNAN GL TECHNOLOGY CO., LTD*)

2.3.8. RECENT CONSTRUCTION DEVELOPMENT

The following design highlights related to development of high voltage infrastructure are worth mentioning:

- Composite poles has little environmental contribution and with regards to timber poles are not subjected to rooting and damage due to woodpeckers [14]. Furthermore, it has high strength-to-weight ratio that facilitates construction operation with reduction of time and cost. This additionally reduces hazardous events while poles are erected by helicopter [77]. It has become more popular in the recent years in Norway to replace wooden and steel poles with composite design. Statnett delivered 130km long 132kV powerline for Skogfoss – Varangerbotn. Construction consists of fiberglass pole and resin material, with steel crossbeams and steel crosses for bracing (Figure 2.3.). Although composite towers have been so far designated for voltages up to 132kV, Statnett developed 420kV CFRP (carbon fiber reinforced polymer) mast (Figure 2.21) [78]. A comprehensive study over design of composite pylons can be found in reference by Jahangiri et al. [79].

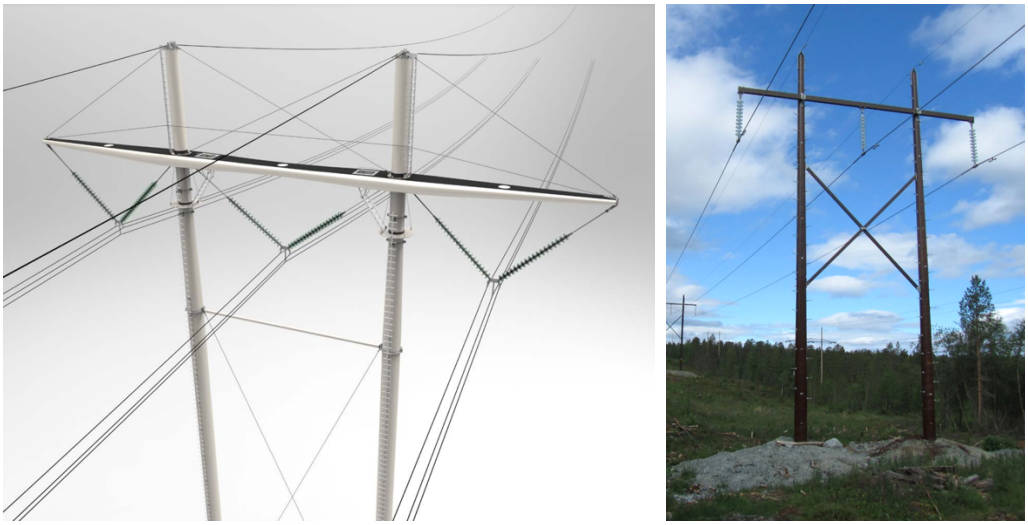

FIGURE 2.21. STATNETTS 420KV POLYMER MAST DESIGN [78] AND 132KV SKOGFOSS – VARANGERBOTN FIBERGLASS POWERLINE [80]

- Statnett and EFLA runs an R&D project on the development of new aluminum tower for 420kV transmission network [80]. Use of aluminum reduces weight of construction, time and cost related to construction site and reduces the carbon footprint with comparison to traditional steel lattice towers. The tower has already been tested and installed on site near Kobbvatnet substation in Nordland for preliminary assessment (Figure 2.22, 2019). The construction has exposed high fatigue failure resistance.

FIGURE 2.22. STATNETT´S AND EFLA´S ALUMINUM TOWER FOR 420KV POWERLINE [80]

- Renewal of 132 kV Løvbergsmoen, Lutufallet and Trysil (eastern Norway) transmission line was executed with application of two pilot aluminum H-portal pylon by Hyndla [81] (Figure 2.23). Company provides solution, production and instillation of light transmission towers for 132 kV regional grid.

FIGURE 2.23. 132 KV ALUMINUM TRANSMISSION TOWER BY HYNDLA [81]. 18M H-PORTAL PYLON FOR RENEWAL OF LØVBERGSMOEN, LUTUFALLET AND TRYSIK TRANSMISSION LINE AND 21 M TOWER TEST PROJECT

- The new type of 420 kV steel mast was designed by Widenoja Design AS in cooperation with EFLA for BBK in Norway (Figure 2.24). The construction was assembled in Mongstad-Kollsness powerline in 2015 as the alternative for visual impact on environment [80].

FIGURE 2.24. DESIGN OF NEW STEEL SUPPORTING STRUCTURE FOR 420 KV POWERLINE [80]

3. REFERENCE LITERATURE

Complexity and severity of atmospheric icing phenomena and wind loads on overhead powerlines, gathers engineers, specialist in a field and power operators to address the design problematics, hazardous events and find new solutions for maintenance and evaluation of power grid reliability. International effort is being put to create efficient countermeasures and supplement the monitoring system with accurate icing on power lines projections and forecast future meteorological trends related to climate change. Among large amount of literature, the following has been found most relevant in terms of master thesis and fundamental reference for research:

- "International Workshop on Atmospheric Icing on Structures" (IWAIS) that aims to bring together research society and industry to exchange knowledge, know-how and technological development in a field of atmospheric icing phenomena on structures, such as electrical transmission and telecommunication network, wind turbines and related. Numerous papers have been gathered since first conference held in 1982 and has been continuously expanded with new knowledge database every 2-3 years, until the latest proceeding in Reykjavik in 2019 [82],
- "Atmospheric Icing of Power Networks" [23, 36] – gathering of most essential research supporting design of power lines with reference to atmospheric icing phenomena. Cooperation of internationally acclaimed expertise under supervision of Professor Masoud Farzaneh, who is the leading expert in a field of power engineering, resulted in detailed compendium with power grid design principles from meteorological point of view, including maintenance and preventive techniques,
- "Techniques for Protecting Overhead Lines in Winter Condition" [36] – review of up-to-date strategies to prevent mechanical and electrical damages of overhead power lines due to ice and snow loading, by field experts Professor Masoud Farzaneh and Dr William A. Chisholm.

Furthermore, comprehensive literature positions, covering the most essential aspect of powerlines design with relevant references as the core of the master thesis, are as follows:

- "Overhead lines (GREEN BOOK series by CIGRE)" [24],
- "Transmission Line Reference Book - Wind Induced Conductor Motion" by Electric Power Research Institute [5],
- "High Voltage Power Network Construction" by Kieth Harker [52],
- "Overhead Power Lines: Planning, Design, Construction" by Friedrich Kiessling et al. [66],
- "Structural Engineering of Transmission Tower" by Peter Catchpole [62].

4. DESIGN CODES

The Norwegian Regulations FEF 2006 [83] established by Norwegian Directorate for Civil Infrastructure (DSB) is the major normative reference applicable in Norway with regards to design, construction, operation and maintenance of electrical supply systems in terms of minimum level of required safety. The authorities state operative regulations, guidance and standards, among which *NEK 445:2016* [84] is declared as the accepted design code for risk assessment and basis for facility construction. The compliance of high voltage installation with abovementioned regulations is required for assurance that no danger to life, health and material values emerge.

Application of the electrotechnical standards at the national level in Norway is administered by *the Norwegian Electrotechnical Committee* (NEK), who is a founding member and national committee of *the European Committee for Electrotechnical Standardization* (CENELEC) and *International Electrotechnical Commission* (IEC). Basis of design of overhead electric lines is found in *EN 50341-1:20212* [7] and in related to Norway´s National Normative Aspects *EN 50341-2-16:2016* [57] . With regards to normative consistency, *NEK 445:2016* is Norwegian translation of those standards. Furthermore, reliability-based design principles for overhead transmission lines are provided by International Electrotechnical Commission (IEC) that corresponds *NEK IEC 60826:2017* [56]. As a supplement to *IEC 60826:2017, NEK IEC 61774:1997*[85] provides information of proper use of climatic database and review icing models for computing ice loads.

With regards to the aims of the present master thesis, law regulated structural requirements and normative design of actions on lines are presented according to IEC and CENELEC standards. *NEK IEC 60826:2017*, has been found the most comprehensive and up-to-date in terms of guidance provided and directly related to local meteorological data that could increase reliability of power lines through individual approach. Hence, the presented basics of design originate foremost from *NEK IEC 60826:2017,* supplemented with National Normative Aspect for Norway *EN 50341-2-16:2016.* Reference values for wind actions are found in National Normative Aspect of *NS-EN 1991-1-4* [86].

4.1. Design value

Each element of powerline is rated according to its characteristic strength X_k, i.e. yield limit, that corresponds to the limit state of the material´s ability to operate under loading. For the powerline there is a high dependency between each component in terms of those limits. For instance, insulators, which failure leads both to electrical and mechanical failure of at least one span and results in excessive loads on the support. Partial factors γ are related to severity of possible consequences, unfavorable deviations of actions, material properties and cover geometric uncertainties. The partial factor method assures that the effect of design actions E_d won´t exceed designed resistance of powerline X_d for ultimate limit states and serviceability limit states. The following condition must be checked for each power line component [56]:

$$Designed\ limit\ load\ E_d < designed\ strength\ X_d$$

$$f\{partial\ load\ factor\ \gamma_F \cdot designed\ load\ F\} < \frac{charasteristic\ value\ of\ material\ property\ X_k}{material\ partial\ factor\ \gamma_M}$$

4.2. Reliability level

Characteristic values of climatic actions and design loads on supports of overhead powerlines are accounted for 50 years [7], that corresponds reliability *level 1*, which defines partial factors for actions.

4.3. Ultimate limit states

Ultimate limit states refer to structural failure due to excessive deformations, loss of stability, buckling, etc. It accounts for both permanent and variable actions. Designed resistance of construction, dependent on material properties with considered uncertainties represented by safety factor γ_M (Table 4.2), must withstand the designed loading conditions and actions on structures magnified with partial factors that represents variability of those actions. Recommended values of partial and combined factors are given in Table 4.1.

Type of action	action	Symbol	Value
Variable actions (Climatic loads)	Extreme wind load	γ_w	1,0
	Nominal wind load	Ψ_w	0,4
	Extreme ice load	γ_I	1,0
	Nominal ice load	Ψ_I	0,35
Permanent actions	Self-weight	γ_G	1,0
Security loads	Torsional loads due to conductor tension	γ_{A1}	1,0
	Longitudinal loads due to conductor tension	γ_{A2}	1,0
Safety loads	Construction and maintenance loads	γ_P	1,5

Table 4.1. Recommended values of partial and combined factors for actions in ultimate limit state [7]

	γ_M
Conductors	1,25
Steel towers	1,10
Line fittings	1,50
Insulators	2,0
Guys	1,5

TABLE 4.2. PARTIAL MATERIAL FACTORS γ_M FOR INDIVIDUAL COMPONENTS [7, 57]

The total design value of the effect of combined actions E_d is as follows:

$$E_d = f\{\sum \gamma_G G_k, \gamma_{Q1} Q_{1K}, \sum_{n>1} \Psi_{Qn} Q_{nK}\} \tag{4.1}$$

where:

G_k	permanent action (self-weight),
$\gamma_{Q1} Q_{1K}$	design value of the dominant variable action Q_{1K}, i.e.: wind or ice load,
$\Psi_{Qn} Q_{nK}$	design value of combination of other variable action Q_{nK}.

4.4. SERVICEABILITY LIMIT STATES

Serviceability limits does not consider partial load factors. Limiting values are acceptable deformations and deflections of structural members [7]. Serviceability limit states accounts for effective use of structure. As primary, the required electrical clearance of conductors to ground, structure and adjacent infrastructure must be met. For steel poles appropriate limiting values of deformations and deflections shall be agreed between client and the designer according to Eurocode 3 [87]. For lattice steel towers deflection are not considered, unless specified in the project specifications.

Serviceability limit states design check are performed with commercial software and are the not case for the thesis. Level of vibrations of conductors should be considered as hazardous for towers.

4.5. ACTION ON LINES

Calculation of all types of atmospheric loads, i.e.: wind, ice and combined wind and ice, on conductors and towers are discussed. The climatic data is available in the National Annexes. Statistical data should be taken from field observations or history data. Peak wind pressure is taken as the reference value for calculating the wind actions that corresponds wind velocity fluctuations due to wind gusts. This is represented with factors G_c and G_t [56].

4.5.1. PERMANENT LOADS

Permanent loads are the self-weight of all powerline components, i.e. structural members of towers, conductors, insulators, earth wires, aircraft warning spheres etc. It is expressed with G_k.

4.5.2. WIND LOADS

The normative approach considered is referred to span length a between 200 m and 800 m [56]. For span lengths outside this range the constant values of coefficients discussed can be safely set, i.e. for span length

greater than 800 m coefficients are the same as for 800 m span; for span length smaller than 200 m coefficients remain the same as for 200 m. Furthermore, support height is less than 60 m. For terrain affected considerably with characteristic features (slopes, scarps, hills, river crossings etc.) the individual consideration should be applied.

WIND LOADS ON ANY OVERHEAD LINE COMPONENT

Wind loads on any overhead line component Q_W due to wind blowing horizontally at the reference height above ground $h = 10\,m$, perpendicular to any line component is given by NEK EN 50341 National Normative [57]:

$$Q_W = 0{,}5 \cdot \rho \cdot \tau \cdot {V_T}^2 C \cdot G_L \quad [Pa] \tag{4.2}$$

where:

ρ air density considered for atmospheric conditions. Conservative value of $\rho = \rho_{ref} = 1{,}292\,\frac{kg}{m^3}$ at temperature of $15℃$ and an atmospheric pressure of $101{,}3\ kPa$ at a sea level in normally assumed [57],

τ air density correction factor correlated with altitude and temperature (Table 4.6),

V_T wind velocity with return period T defined as mean value of the wind during 10 min period at a level of 10 m above ground [56] for terrain category B,

C drag coefficient depending on the shape of considered line component,

G_t combined wind factor considering the influence of the height of the considered element (either insulators or supports) above ground level $z[m]$, terrain category, wind gusts and dynamic response (Table 4.5).

DESIGN OF WIND VELOCITY

Wind velocity V_T is dependent on terrain roughness at the location of the line. With increasing terrain roughness, turbulence increase and wind speed decreases near the ground. Tress and mountain chain might additionally contribute with the shielding effect. According to [56] four categories of terrain is considered:

Terrain category	Roughness characteristics	Factor K_R	Factor α
A	Large stretch of water upwind, flat coastal areas	1,08	0,10 to 0,12
B	Open country with very few obstacles, for example airports or cultivated fields with few trees or buildings	1,00	0,16
C	Terrain with numerous small obstacles of low height (hedges, trees and buildings)	0,85	0,22
D	Suburban areas or terrain with many tall trees	0,67	0,28

TABLE 4.3. CLASSIFICATION OF TERRAIN CATEGORIES WITH REGARDS TO NEK IEC 60826 [56]

According to National Normative Aspect for Norway, for lines direction perpendicular to the main direction of fjord or valley, or if the power line along fjord/valley passes the mouth of a branch fjord/valley (opening toward the sea), the calculated wind V_T should be multiplied by factor 1,2.

Factor K_R adjusts the reference meteorological wind velocity for terrain category B, to category of terrain where power line is considered, as follows:

$$V_T = K_R V_{RB} \qquad [m/s] \tag{4.3}$$

where:

K_R roughness factor (Table 4.3),

V_{RB} reference wind speed from meteorological station that usually is measured in stations typical of terrain type B, 10 m above the ground. If meteorological data is not available, the reference values of wind speed for terrain type B, 10 m above sea level, based on return period of 50 years, for Norway are found in National Normative Aspect of NS EN 1991-1-4 [86] ($V_{b,0}$). The correction of wind speed with regards to high of terrain over sea level is represented with factor c_{alt}:

$$V_{RB} = c_{alt} V_{b,0} \tag{4.3.1}$$

$$c_{alt} = \begin{cases} 1{,}0 & for\ V_{b,0} \geq \dfrac{30m}{s} \\ 1{,}0 + \dfrac{(30 - V_{b,0})(H - H_0)}{V_{b,0}(H_{topp} - H_0)} & for\ V_{b,0} \leq 30\dfrac{m}{s} \end{cases}$$

where:

H altitude of power line location over sea level,

H_0 reference height over which the correction is applied, i.e.: $c_{alt} = 1{,}0$ for $H = H_0$ and $c_{alt} \geq 1{,}0$ for $H \geq H_0$,

H_{topp} the height over sea lever where factor c_{alt} reaches maximum value, i.e.: $c_{alt} V_{b,0} \geq 30\frac{m}{s}$

NOTE!

If reference meteorological wind velocity V_{RB} was measured on different altitude than 10 m above the ground, it must be adjusted to the reference height of 10 m from power law as follows:

$$V_{RB} = \frac{V_{h_m}}{\left(\frac{h_m}{10}\right)^{\alpha}} \tag{4.3.2}$$

where:

V_{h_m} reference measured velocity on height h_m above the ground,

α power law coefficient (Table 4.3).

Region	District	Parameter H_0 [m]	Parameter H_{topp} [m]
1	South Norway, excl. North Trøndelag	900	1500
2	North Trøndelag, Nordland, Troms	700	1300
3	Finnmark, Svalbard	400	1000

TABLE 4.4. ALTITUDES FOR CORRECTION FACTOR c_{alt} APPLICABLE IN NORWAY [57]

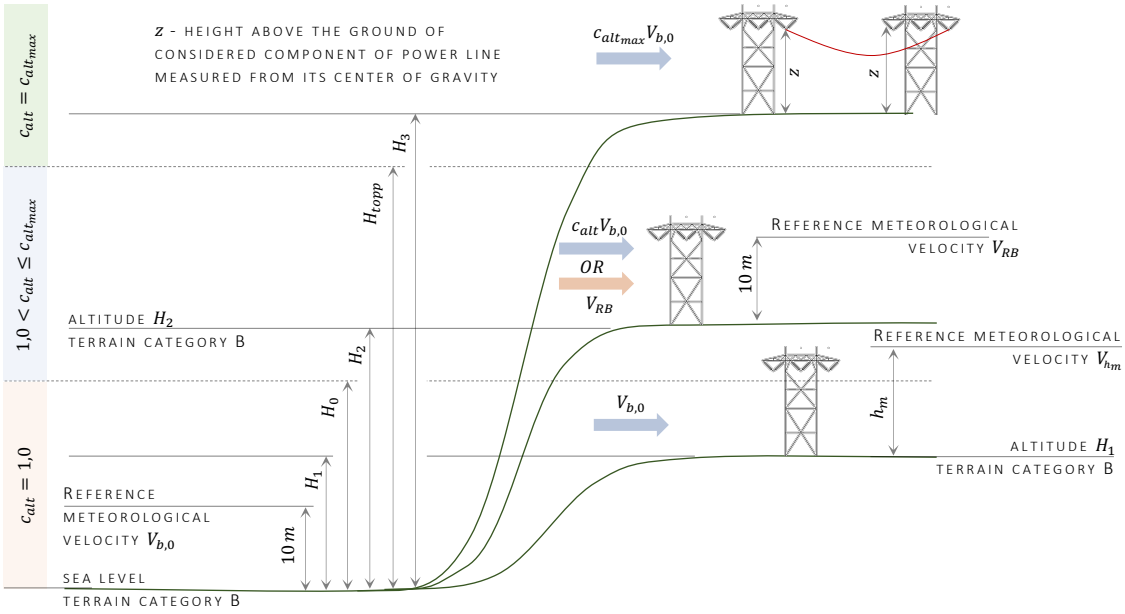

FIGURE 4.1. REPRESENTATION OF APPLICATION OF CORRECTION FACTOR c_{alt} FOR DEFINING WIND SPEED V_{RB}

Terrain category	Combined wind factor G_t
A	$-0{,}0002z^2 + 0{,}0232z + 1{,}4661$
B	$-0{,}0002z^2 + 0{,}0274z + 1{,}6820$
C	$-0{,}0002z^2 + 0{,}0298z + 2{,}2744$
D	$-0{,}0002z^2 + 0{,}0384z + 2{,}9284$

TABLE 4.5. FORMULAS FOR COMBINED WIND FACTOR G_t FOR $z > 10\,m$. FOR $z \leq 10\,m$ VALUE $z = 10\,m$ IS APPLIED [56].

AIR DENSITY IN A FUNCTION OF TEMPERATURE AND ALTITUDE

Air density ρ for atmospheric conditions considered for designed power line should be calibrated to the reference air density $\rho_{ref} = 1{,}292\,\frac{kg}{m^3}$ at temperature of 15℃ and an atmospheric pressure of $101{,}3\,kPa$ at a sea level, as follows:

$$\rho = p_{ref}\frac{288}{T}e^{-1{,}2\cdot 10^{-4}H} = \tau \cdot p_{ref} \tag{4.4}$$

where:

H altitude considered for power line [m],

T temperature for loading conditions [°C].

Temperature T [℃]	Altitude H [m]			
	0	1000	2000	3000
30	0,95	0,84	0,75	0,66
15	1,00	0,89	0,79	0,69
0	1,04	0,94	0,83	0,73
-15	1,12	0,99	0,88	0,77
-30	1,19	1,05	0,93	0,82

TABLE 4.6. CORRECTION FACTOR τ OF AIR DENSITY WITH REFERENCE TEMPERATURE OF 15℃ AND AN ATMOSPHERIC PRESSURE OF $101{,}3\,kPa$ AT A SEA LEVEL [56]

WIND LOADS ON CONDUCTORS AND EARTH WIRES

The wind load on conductors A_c is expressed as follows [56]:

$$A_c = 0{,}5 \cdot \rho \cdot \tau \cdot {V_T}^2 \cdot C_{xc} \cdot G_C \cdot G_L \cdot d \cdot L \cdot sin^2\Omega \quad [\mathrm{N}] \tag{4.5}$$

where:

C_{xc}	drag coefficient of conductor equal to $\mathbf{1{,}00}$ or $\mathbf{1{,}20}$ for conductors with diameter of 15 mm or less and earth wires,
G_c	dependent on height z [m] and terrain category combined wind factor (Table 4.7) taking into account wind gusts and dynamic response. The factor corresponds turbulence intensity factor $I_v(h)$ according to NEK EN 50341-1 [7]. For conductors, height z [m] is taken as distance from ground to point of attachment of conductors at the support,
G_L	span factor $G_L = 4 \cdot 10^{-10} \cdot L^3 - 5 \cdot 10^{-7} \cdot L^2 - 10^{-4} \cdot L + 1{,}0403$,
d	diameter of conductor [m],
L	wind span of the support equal to half the sum of the length of adjacent spans of the support,
Ω	angle between wind direction and conductor (Figure 4.2),
${\rho\tau V_T}^2$	see Eq.4.2.

For bundle conductors the sum of action on each sub-conductor shall be considered. The aerodynamical interaction between sub-conductors is neglected. The height $z[m]$ is assumed as height of point of support on the tower.

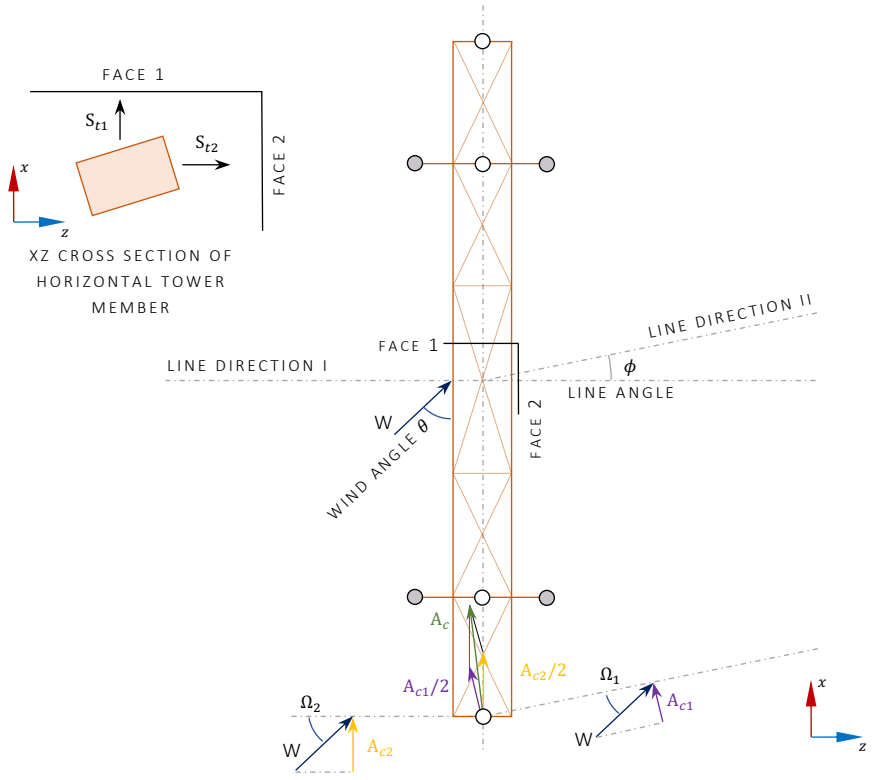

FIGURE 4.2. REFERENCE LATTICE TOWER FOR DEFINING ANGLE Ω AND θ

Terrain category	Combined wind factor G_c
A	$0{,}2914\ln(z) + 1{,}0468$
B	$0{,}3733\ln(z) + 0{,}9762$
C	$0{,}4936\ln(z) + 0{,}9124$
D	$0{,}6153\ln(z) + 0{,}8144$

TABLE 4.7. FORMULAS FOR COMBINED WIND FACTOR G_c FOR $z > 10\,m$. FOR $z \leq 10\,m$ VALUE $z = 10\,m$ IS APPLIED [56].

WIND LOADS ON INSULATOR STRINGS

Wind load acting on insulators is due to discussed loading A_c transferred by conductors, as well as wind acting directly on the insulator strings A_i. Load A_i is applied at the attachment point of insulators to the support in the direction of the wind. According to [56] wind load on insulators has little effect on design of supports.

$$A_i = 0{,}5 \cdot \rho \cdot \tau \cdot {V_T}^2 \cdot C_{xi} \cdot G_t \cdot S_i \quad [\mathrm{N}] \tag{4.6}$$

where:

C_{xi} drag coefficient of insulators equal to $1{,}2$,

G_t dependent on height z [m] and terrain category combined wind factor measured from center of gravity of insulator strings to the ground (Table 4.5). The factor corresponds turbulence intensity factor $I_v(h)$ according to NEK EN 50341-1 [7],

S_i area of insulators string projected horizontally on the vertical plane parallel to the axis of the string,

$\rho\tau{V_T}^2$ see Eq.4.2.

WIND LOADS ON SUPPORTS

NEK IEC 60826 [56] provides a set of formulas for wind loads adjustable to any type of support structures. The reference examples, based on which the adjustment can be issued, are presented.

LATTICE TOWERS -METHOD I

The load $A_{t(l)}$ acting on lattice towers with rectangular cross-section, in the direction of wind, applied at the center of gravity of each member of lattice tower (i.e.: legs and bracing) is defined with the following equation:

$$A_{t(l)} = 0{,}5 \cdot \rho \cdot \tau \cdot {V_T}^2 (1 + 0{,}2sin^2 2\theta)(S_{t1} C_{xt1} cos^2\theta + S_{t2} C_{xt2} sin^2\theta) \cdot G_t \quad [N] \tag{4.7}$$

where:

θ angle of incidence of wind direction (Figure 4.2),

S_{t1} total area of windward surface of tower members, projected on surface perpendicular to power line and ground (FACE 1) (Figure 4.2),

S_{t2} total area of windward surface of tower members, projected on surface parallel to power line and perpendicular to ground (FACE 2) (Figure 4.2),

G_t dependent on height $z[m]$ and terrain category combined wind factor measured from center of gravity of each member of tower to the ground (Table 4.5),

$\rho\tau{V_T}^2$ see Eq.4.2,

$C_{xt1,2}$ drag coefficients of each face of lattice tower members (Figure 4.2),

- for flat-sided members $C_{xt1,2} = 4{,}1727\chi^2 - 6{,}1681\chi + 4{,}0088$ (4.8)
- for round-sided members $C_{xt1,2} = 0{,}2293\chi^3 + 2{,}7091\chi^2 - 3{,}1323\chi + 2{,}2002$ (4.9)

where:

χ solidity ratio related to projected area of members, i.e.:

$$\chi_{1,2} = \frac{S_{t1,2}}{S_{t1} + S_{t2}}$$

LATTICE TOWERS -METHOD II

Wind force on each member is defined based on geometrical relationship between wind velocity vector and axis of the member. Shielding effect is neglected. Force $A_{t(II)}$ is applied in the center of gravity of each member and is perpendicular to the member axis in a horizontal plane XZ plane. Comparing to METHOD I, this is conservative approach and is dedicated for software implementation[56].

$$A_{t(II)} = 0{,}5 \cdot \rho \cdot \tau \cdot {V_T}^2 \cdot G_t \cdot S_t \cdot C_{xt} \cdot sin^2\Omega \qquad [N] \tag{4.10}$$

where:

S_t surface of the flat member exposed to wind $[\ m^2]$,

C_{xt} drag coefficients of each face of lattice tower members. For flat members $C_{xt} = 1{,}6$, round tubes $C_{xt} = 1{,}0$,

G_t dependent on height $z[m]$ and terrain category combined wind factor measured from center of gravity of each member of tower to the ground (Table 4.5),

${\rho\tau V_T}^2$ see Eq.4.2,

Ω angle between wind direction and axis of considered member (Figure 4.1),

SUPPORTS WITH CYLINDRICAL MEMBERS WITH LARGE DIAMETER (d>0,2 m)

The method applies to pole-structures with members with diameter d_{tc} and length l_e. The force A_{tc} is applied in the center of gravity of the component:

$$A_{tc} = 0{,}5 \cdot \rho \cdot \tau \cdot {V_T}^2 \cdot G_t \cdot C_{xtc} \cdot d_{tc} \cdot l_e sin^3\theta' \qquad [N] \tag{4.11}$$

where:

d_{tc} diameter of cylinder $[m]$,

l_e length of the member $[m]$,

G_t dependent on height $z[m]$ and terrain category combined wind factor measured from center of gravity of cylindrical member to the ground (Table 4.5),

θ' angle formed by the direction of the wind and the cylinder axis,

${\rho\tau V_T}^2$ see Eq.4.2,

C_{xtc} drag coefficient of cylindrical cross-section, dependent on Reynolds number Re:

- $C_{xtc} = 1{,}2$ for $Re < 3 \cdot 10^5$,
- $C_{xtc} = 0{,}75$ for $Re > 4{,}5 \cdot 10^5$
- $C_{xtc} = -1{,}1098 lnRe + 15{,}197$ for $3 \cdot 10^5 < Re < 4{,}5 \cdot 10^5$ (4.12)

$$Re = \frac{d_{tc} \cdot V_T}{\nu} \tag{4.13}$$

Where ν is kinematic air viscosity ($\nu = 1{,}45 \cdot 10^{-5} \frac{m^2}{s}$ at 15℃)

For wood poles $C_{xtc} = 1$ due to limited height. For polygonal cross sections the following coefficient might be assumed:

16-side polygonal		0,9
12-side polygonal		1,0
8-side polygonal	C_{xtc}	1,4
8-side polygonal		1,4
Rectangular		2,0

4.5.3. ICE LOAD ON CONDUCTORS AND GROUND WIRES

Atmospheric icing accretion relevant for power line components is considered for precipitation icing and in-cloud icing. The most relevant forms of icing with approximate densities are presented in a Table 4.8 below. According to NS EN 50341 National Annex for Norway [57] *wet snow* and *hard rime* ice are only considered for design.

Icing form			Density kg/m³
Precipitation icing	Freezing rain		800 to 900
	Wet snow[1]		300 to 700
	Dry ice	Soft rime	200 to 600
		Hard rime[1]	700 to 900
In-cloud icing	Glaze		700 to 900
[1]Ice forms to consider according to [57]			

TABLE 4.8. TYPES OF ICE ACCRETING ON COMPONENTS OF POWER LINE [56]

Ice load is defined as a weight per unit length of conductor g (N/m) with a uniform radial thickness t (mm) around conductors and earth wires. Ice accretion is a variable random is shape, size and density. For a purpose of calculation, the ice accreting of power line structures is simplified to the following formula of ice weight per unit length:

$$g = 9{,}82 \cdot 10^{-3} \delta \pi t \left(d + \frac{t}{1000}\right) \quad [N/m] \tag{4.14}$$

where:

δ ice density $\left[\frac{kg}{m^3}\right]$,

t radial ice thickness $[mm]$,

d conductor diameter $[m]$.

Since the ice accretion is strongly influenced with terrain type, the most accurate design of ice load assumes icing data from measuring stations in the area where power line is located. This might not always be available, thus the input for ice accretion often relies on service experience, failure events, statistical ice accretion models involving thermodynamics and fluid mechanics.

The references to recognized icing model are found in NEK IEC 61774 [85].

4.5.4. ICE LOAD ON SUPPORTS

For the support structures of the power line, we distinguish between three major icing condition with regards to ice accreted on conductors:

- uniform ice on conductor leading to weight load on supports,
- non-uniform ice formation on conductors leading to longitudinal and transverse bending conditions on support (unbalanced load),
- non-uniform ice formation on conductors leading to torsional loading on supports (unbalanced load).

Figure 4.3 presents examples of loading arrangements due to unbalanced loading on support structures from the conductors. It is recommended by IEC 60826:2017 [56] to consider unbalanced loading with factors 0,7 and 0,4, so that unbalanced tension results from loading on conductors equal to $g_1 = 0{,}7 \cdot g$ and $g_2 = 0{,}4 \cdot 0{,}7 \cdot g$. With regards to National Normative Aspect for Norway, factors 0,7 and 0,4 are set. For powerlines, where adjacent spans are exposed to considerably different atmospheric loading arrangement due to altitude difference or obstacles, it is applicable to consider maximum loading on one side of support and bare conductors on the other side. On the Figure 4.4 loading arrangement set by NS EN 50431 National Normative Aspect for Norway are presented.

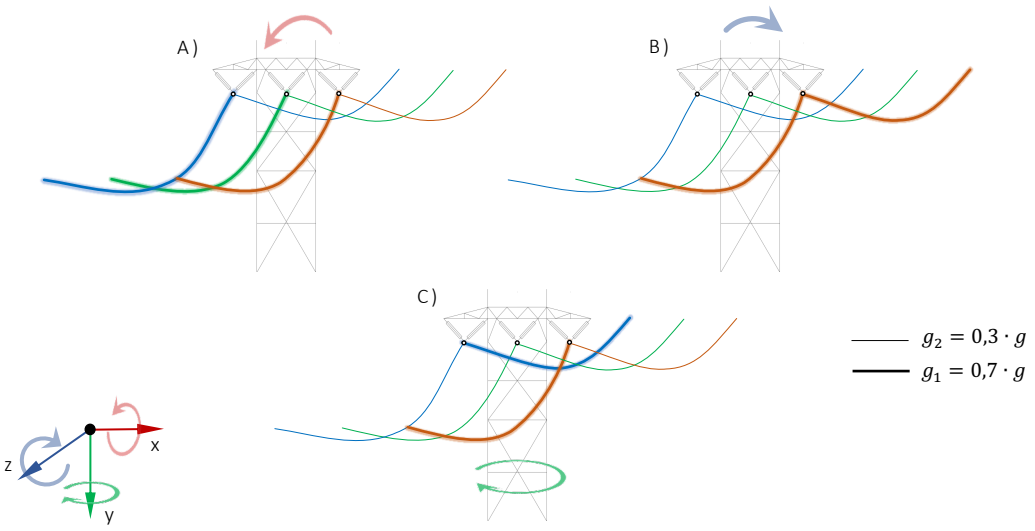

FIGURE 4.3. NON-UNIFORM ICE LOADING CONDITIONS ON SUPPORTS DUE TO ICE ACCRETION ON CONDUCTORS: (A) LONGITUDINAL BENDING, (B) TRANSVERSE BENDING, (C) TORSIONAL CONDITION. THICKNESS OF CONDUCTORS REPRESENTS THE DISPROPORTION IN ICE WEIGHT ON CONDUCTORS.

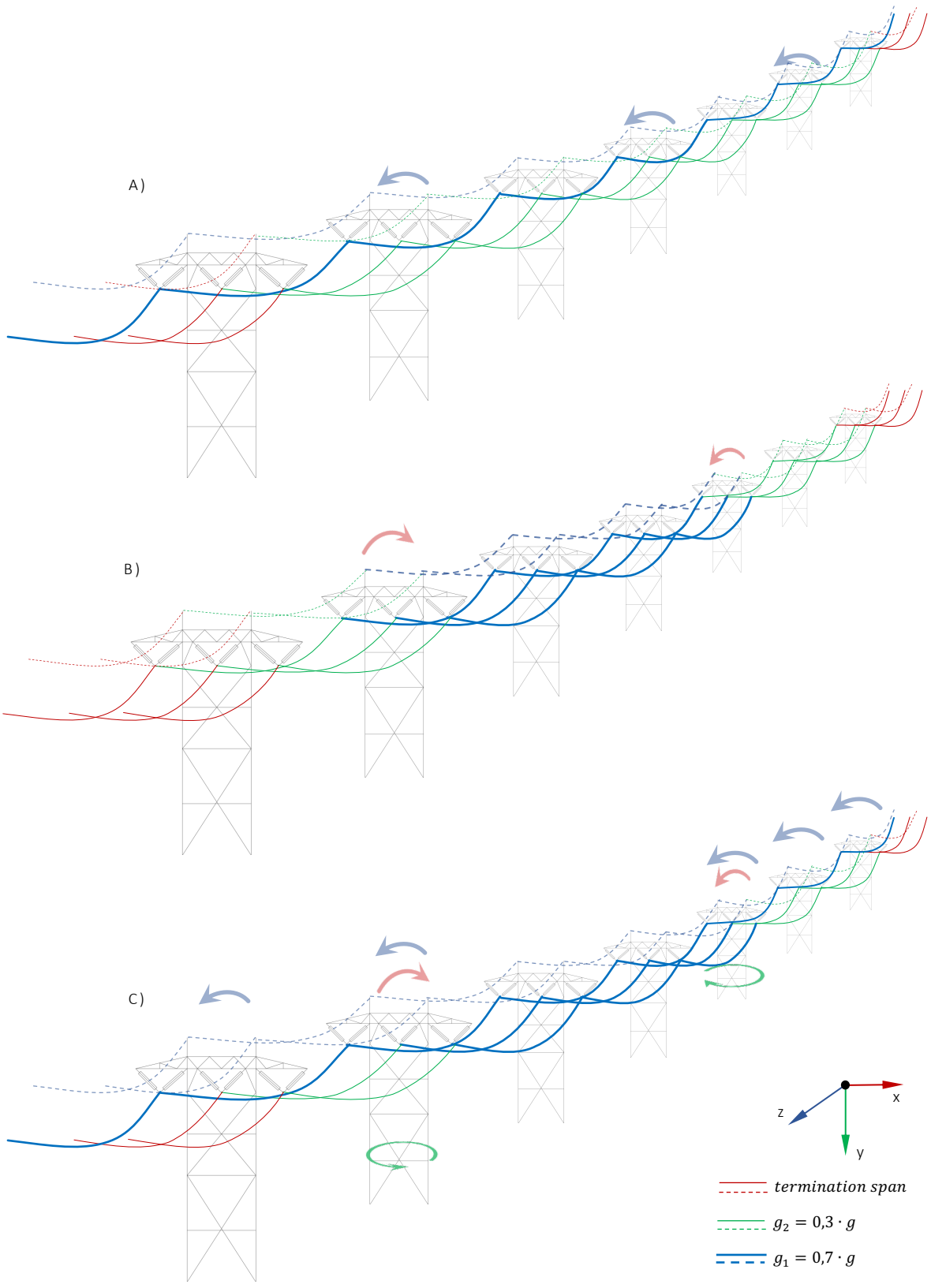

FIGURE 4.4. LOAD CASES 2-4 WITH REFERENCE TO NS EN 50341 NATIONAL NORMATIVE ASPECT FOR NORWAY: (A) **LC 2** TRANSVERSE BENDING, (B) **LC 3** LONGITUDINAL BENDING, (B) **LC 4** TORSIONAL BENDING

4.5.5. ICING ON SUPPORTS AND OTHER COMPONENTS

Ice accreting on structures increases their dead load and should be considered for powerlines where considerable icing has been observed. The weight of ice on individual members of towers can be calculated as additional, geometrical cover with specified thickness and density. Design of loads on supports and other components should be specified in project requirements. According to Eurocode 3 [87] it is valid to assume unform thickness of ice on all structural members of tower.

4.5.6. COMBINED WIND AND ICE LOADINGS

Ice accreting on overhead power lines amplifies discussed wind actions. The magnitude of those actions is dependent on *wind speed*, *ice weight* and effect of *drag coefficient* due to accretion shape (those are called *variables*) With regards to combined actions on structures, wind loads on support for ice accreted conductors are only discussed, as required by NS EN 50341 National Annex [57]. If required by the project specifications, ice on the supports and insulators may be included. For combination of wind and ice, the temperature is set to 0 °C.

In order to obtain combined loading scenarios, the wind data associated with measurements of ice on conductors, should be accessed; although seldom available. Designed loads [56, 57] assumes a combination of maximum loads for *low probability-high value* (L) of one variable, with *high probability-low value* (H) for two other variables. Those combinations would usually not create the critical cases for combination of ice and wind actions. Although not required [56, 57], the critical cases might be included according to project specifications and service experience [56]. *High probability* is the average of extreme yearly values, whilst *low probability* corresponds to return period T (50 years). Combined wind and ice loading cases with reference to NEK IEC 60826 and NS EN 50341 National Normative Aspect for Norway [56, 57] are presented in the Table 4.9. With regards to NS EN 50341 National Normative Aspect for Norway, loading cases LC 6.3.1 and LC 6.3.2 are not required.

Loading Case[3]	Ice weight on conductors [N/m]		Wind speed[2]		Effective drag coefficient				Density [kg/m³]	
					Wet Snow		Hard rime			
LC 6.1.1	g_L	Reference design ice load g^1 or Value from Table 4.10	V_{iH}	$B_{iH} \cdot V_T$	C_{iH}	1,0	-		δ_{11}	700
LC 6.1.2					-		C_{iH}	1,1	δ_{12}	900
LC 6.2.1	g_H	0,4 · Value from Table 4.10	V_{iL}	$B_{iL} \cdot V_T$	C_{iH}	1,0	-		δ_{21}	700
LC 6.2.2					-		C_{iH}	1,1	δ_{22}	900
LC 6.3.1	g_H	0,4 · Value from Table 4.10	V_{iH}	$B_{iH} \cdot V_T$	C_{iL}	1,4	-		δ_{31}	300
LC 6.3.2					-		C_{iL}	1,5	δ_{32}	700

TABLE 4.9.1. COMBINED WIND AND ICE LOADING ON SUPPORTS DUE TO ICE ON CONDUCTORS (APPLICABLE FOR NORWAY) [56, 57]

Loading Case[4]	Ice weight on conductors for return period T = 3 years [N/m]		Wind speed[2]		Effective drag coefficient				Density [kg/m³]	
					Wet Snow		Hard rime			
LC 6.4.1	g_{H3}	Value from Table 4.10	V_{iL3}	$0{,}7 \cdot V_T$	C_{iH3}	1,0	-		δ_{51}	600
LC 6.4.2				$0{,}85 \cdot V_T$	-		C_{iH3}	1,1	δ_{52}	700

[1] Based on statistical data or derived from Eq. 4.12 for known ice thickness,

[2]Wind velocities associated with icing episodes from available meteorological data. If not available, the formulas below are applicable,

[3]Not required by NS EN 50341 National Normative Aspect for Norway [57], originates from NEK IEC 60826,

[4]Required by NS EN 50341 National Normative Aspect for Norway,

B_{iL} reduction factor equal to $0{,}6$ for T = 50 years,

B_{iH} reduction factor equal to $0{,}4\ to\ 0{,}5$ for T = 50 years,

V_T calculated according to Eq. 4.3.

TABLE 4.9.2. COMBINED WIND AND ICE LOADING ON SUPPORTS DUE TO ICE ON CONDUCTORS

(APPLICABLE FOR NORWAY) [56, 57]

No.	Region	Height above sea level	Design ice load (N/m) for return period T = 50 years
1	Main areas of the South East region[1]	0-200	30
2	Main areas of the South East region[1]	200-400	40
3	Main areas of the South East region	400-600	50
4	Østfold and Vestfold	0-200	20
5	Telemark and Agder	0-200	35
6	Telemark and Agder	200-400	50
7	The coast Rogaland - Stad	0-200	35
8	The fjords Rogaland - Stad	200-400	40
9	The coast Stad - Namdalen	0-200	40
10	The fjords Stad - Namdalen	0-400	40
11	The coast Namdalen - Lofoten	0-200	40
12	The inland of Nordland	0-200	30
13	The coast Vesterå len - Nordkapp	0-100	35
14	The inland Troms - Vest-Finnmark	0-200	30
15	The coast of Aust-Finnmark	0-100	30
16	The inland of Aust-Finnmark	0-200	20

[1]Except areas mentioned in no. 3 and 4

TABLE 4.10. DESIGN ICE LOADS FOR RETURN PERIOD T (50 YEARS) FOR NORWAY [57]

4.5.7. LOAD ON SUPPORT DUE TO COMBINED WIND AND ICE LOADING ON CONDUCTORS

UNIT ACTION OF THE WIND ON THE ICE-COVERED CONDUCTOR

Wind loads on ice-covered conductors due to wind blowing horizontally and perpendicular to conductor, corresponding to high and low possibilities of occurrence are given by:

$$A_{c6.1} = 0{,}5 \cdot \rho \cdot \tau \cdot {V_{iH}}^2 C_{iH} \cdot G_C \cdot G_L \quad [Pa] \qquad \text{for LC 6.1} \tag{4.15}$$

$$A_{c6.2} = 0{,}5 \cdot \rho \cdot \tau \cdot {V_{iL}}^2 C_{iH} \cdot G_c \cdot G_L \quad [Pa] \qquad \text{for LC 6.2} \tag{4.16}$$

$$A_{c6.3} = 0{,}5 \cdot \rho \cdot \tau \cdot {V_{iH}}^2 C_{iL} \cdot G_C \cdot G_L \quad [Pa] \qquad \text{for LC 6.3} \tag{4.17}$$

$$A_{c6.4} = 0{,}5 \cdot \rho \cdot \tau \cdot {V_{iL3}}^2 C_{iH3} \cdot G_C \cdot G_L \quad [Pa] \qquad \text{for LC 6.4} \tag{4.18}$$

where:

LC 6.1-4 see Table 4.9.1,

ρ air density $= 1{,}292 \frac{kg}{m^3}$ at temperature of $15℃$ and atmospheric pressure of $101{,}3\ kPa$ at a sea level,

τ air density correction factor correlated with altitude and temperature (Table 4.6),

$V_{iH,iL,iL3}$ wind velocity with regards to loading cases in Table 4.9. The contribution of roughness factor K_R must be included if velocities are taken directly from data associated to ice events,

$C_{iH,iL,iH3}$ drag coefficient with regards to loading cases in Table 4.9,

$G_{L,C}$ combined wind and span factors (see Eq. 4.4).

LOADS ON SUPPORT

Wind load A_t on a considered span L, applied at the support and blowing at an angle Ω to the conductors is considered for loading condition LC 6.1-6.3:

$$A_{t6.1} = A_{c6.1} \cdot D_L \cdot L \cdot sin^2\Omega \quad [\mathrm{N}] \qquad \text{for LC 6.1} \tag{4.19}$$

$$A_{t6.2} = A_{c6.2} \cdot D_H \cdot L \cdot sin^2\Omega \quad [\mathrm{N}] \qquad \text{for LC 6.2} \tag{4.20}$$

$$A_{t6.3} = A_{c6.3} \cdot D_H \cdot L \cdot sin^2\Omega \quad [\mathrm{N}] \qquad \text{for LC 6.3} \tag{4.21}$$

$$A_{t6.4} = A_{c6.5} \cdot D_{H3} \cdot L \cdot sin^2\Omega \quad [\mathrm{N}] \qquad \text{for LC 6.4} \tag{4.22}$$

where:

L wind span of the support equal to half the sum of the length of adjacent spans of the support,

Ω angle between wind direction and conductor (Figure 4.2),

$D_{L,H,H3}$ cylindrical ice accretion around conductors:

$$D_{L,H,H3} = \left(d^2 + \frac{4 \cdot g_{L,H,H3}}{9{,}82\pi\delta}\right)^{0{,}5} \tag{4.23}$$

where:

δ ice density $\left[\frac{kg}{m^3}\right]$ (Table 4.9),

d conductor diameter $[m]$,

$g_{L,H,H3}$ ice loads corresponding to low and high probabilities of occurrence (Table 4.9).

4.5.8. SAFETY LOADS

Loads resulting from temporary guying, lifting arrangements, tower erection, stringing, sagging, general working procedures and maintenance might yield unbalanced and considerable loads on structures. Furthermore, loads related to the weight of linesmen must be included, i.e.: for all structural members, which can be climbed and are inclined with an angle less than 30° to the horizontal, a characteristic load of $1{,}5\ kN$ acting vertically in the center of the member shall be assumed without any other load.

Safety loads design is carried out during the design process of the power line and is not discussed in the thesis, hence not included in any calculations. The design check for safety loads should be performed individually with regards to the installation process and should consider possible unbalanced loading and hazardous events, especially for considerable contribution of atmospheric loading during installation.

4.6. LOAD CASES TO BE INCLUDED – NATIONAL NORMATIVE ASPECT

In order to assure the reliability of overhead power line, the load cases presented in Table 4.11 shall be considered for the structure with regards to National Normative Aspect for Norway NS EN 50341-2-16:2016 [57]. The requirements set might be sufficient to assure safety of the construction, although due to discussed in the thesis atmospheric variabilities and uncertainties, the Normative Aspect was extended with design criteria set by *NEK IEC 60826:2017*.

4.7. ADDITIONAL SECURITY MEASURES

NEK IEC 60826:217 recommends increasing the security for power line when applicable as follows (these are not safety factors):

- Increase the security loads by a factor of $1.5 \div 1.8$ that increases the reliability of structure due to conductor breakage,
- For lines subjected to severe icing conditions the anti-cascading support should be placed in intervals, usually, every tenth support. Those supports shall be designed for all broken conductors (on the one span of support) with limit ice loads during limit wind load event.

Load Case	Load type		Design value of the effect of combined actions $E_{g_{LC}}$	Description	Valid for tower types	Reference section
LC1	Climatic loads	Uniform ice load on conductors	$f\{\gamma_G G_k, \gamma_I g\}$	Ice load g applied on all conductors and ground wires on all spans in the section. Reference temperature is set to 0°C	All towers	4.6.3
LC2		Transverse bending due to ice accreted on conductors	$f\{\gamma_G G_k, \gamma_I g\}$	Loads $0.7g$ and $0.3g$ are applied – Figure 4.3	All towers	4.6.4
LC 3		Unbalanced ice loads – longitudinal bending	$f\{\gamma_G G_k, \gamma_{A2} g\}$		Suspension towers and angle suspension towers	
LC 4		Unbalanced ice loads – torsional bending	$f\{\gamma_G G_k, \gamma_{A1} g\}$			
LC5		Wind loads	$f\{\gamma_G G_k, \gamma_w A_c, \gamma_w A_i, \gamma_w A_t\}$	The wind loads are applied on all conductors and ground wires as well as insulators and supports. Reference temperature is set to 0°C	All towers	4.6.2
LC6		Combined wind and ice loads	$f\{\gamma_G G_k, \gamma_w A_{c6.4}, \Psi_w A_{t6.4}, \gamma_w A_i, \gamma_w A_t\}$	Wind load is applied on ice covered conductors + wind load is applied on insulators and towers. Reference temperature is set to 0°C	All towers	4.6.6
LC7		Load at the minimum temperature	$f\{\gamma_G G_k\}$	The support shall resist the increased conductor tension at the minimum temperature set to -20°C	Angle suspension towers, tension towers, angle tension towers, dead end tower and angle dead end towers	2.3.3.5
LC8	Safety Loads	Construction and maintenance loads	$f\left\{\gamma_G G_k, \sum_{n>1} \gamma_{Pn} P_n\right\}$	Construction must resist 1,45 times designed construction loads P_n	All towers	4.5.8
LC9	Security Loads	Conductor breakage	$f\{\gamma_G G_k\}$	Selection of conductor based on individual assessment resulting in most unfavorable conditions. Reference temperature is set to 0°C	Suspension towers and angle suspension towers	-
LC10		Conductor breakage with full ice load	$f\{\gamma_G G_k, \gamma_{A1} g\}$	Ice load g uniformly distributed on all conductors. Selection on conductor similarly to LC9. Reference temperature is set to 0°C	Tension towers and angle tension towers	-
LC11		One-sided tension with full ice load	$f\{\gamma_G G_k, \gamma_{A2} g\}$	Similar to LC2, load g is applied instead. Reference temperature is set to 0°C	Dead end tower and angle dead end towers	-

TABLE 4.11. LOAD CASES TO BE CONSIDERED ACCORDING TO NS EN 50341-2-16:201 [57]

4.8. Summary of design codes

The reference set of standards provide in detail, iterative guidelines to assure safety and reliability of power lines in terms of structural integrity of supports. The complex calculations of design checks in presented designed codes are nowadays performed most often with software dedicated for power line design, such as PLS-CADD [88]. The three-dimensional engineering model allows for design of the power line routes on exact terrain reference. This helps to keep geometrical compliance with codes, when it comes to clearances, spans, sag calculations and resulting tensions on conductors for ambient conditions. Furthermore, the combination of wind, ice and temperature results in loading vectors on supports and serviceability limit states are verified. The design of unbalanced tension is included. The extension of the software provides structural verification of supporting towers as well, with individual approach to selected spans. This is so far the most comprehensive, reliable, and accessible solution for power line design.

However, the standards do not provide the solution for every case scenario that may occur, thus in many cases the engineering practice should assess the applicability of normative guideline and consider the extension of loading cases with individual adjustment. This can not be done without understanding, primarily, the conditions under which the power line operates, and secondarily, algorithms for which computational software perform analysis. Considering the high variability of terrain, wind and icing events in sub-arctic climate, the powerline will probably be exposed to ultimate limit states that must be verified individually. National Normative Aspect of NS EN 50341-2-16:2016 [57] does not consider ice on supports and insulator for combination of wind velocities and ice loads (4.6.5 in NS EN 50341-2-16:2016). Moreover, extreme ice loads in combination with high probability wind velocities are not required (4.6.6.1 in NS EN 50341-2-16:2016). Power lines crossing mountains, valleys, fjords, and rivers must furthermore be verified individually with on-site data. For instance, loads of wind gusts associated with sloped terrain and acting on power lines located on hills. The discussed design codes do not provide guidance for load cases that consider ice shedding and galloping, which affect the supports dynamically.

5. Prerequisites for Computational Modeling

The computational capabilities of the software *COMSOL Multiphysics* [89] for design of atmospheric actions on the supporting structures of power lines are investigated. Due to the complexity of the power line design process and the variety of data that needs to be considered, several simplifications and predefined solutions are applied in the master thesis. The scope of master thesis is hence not to create software ready to be introduced for commercial use, however, it is aimed to evaluate the computational capabilities of the software for further development.

The following prerequisites are set for computational model:

- The most part of transmission towers in Norway (420 kV) are steel H-portal lattice structures (see Figure 5.2) with arrangement of three duplex parallel conductors. With regards to analysis, Statnett´s H-portal steel lattice structures, with V-string insulators for supporting structures and three parallel simplex conductor arrangement are assumed, as shown in Figure 5.1. Dimensions of both suspension and strain towers are fully parametrized and can easily be adjusted.

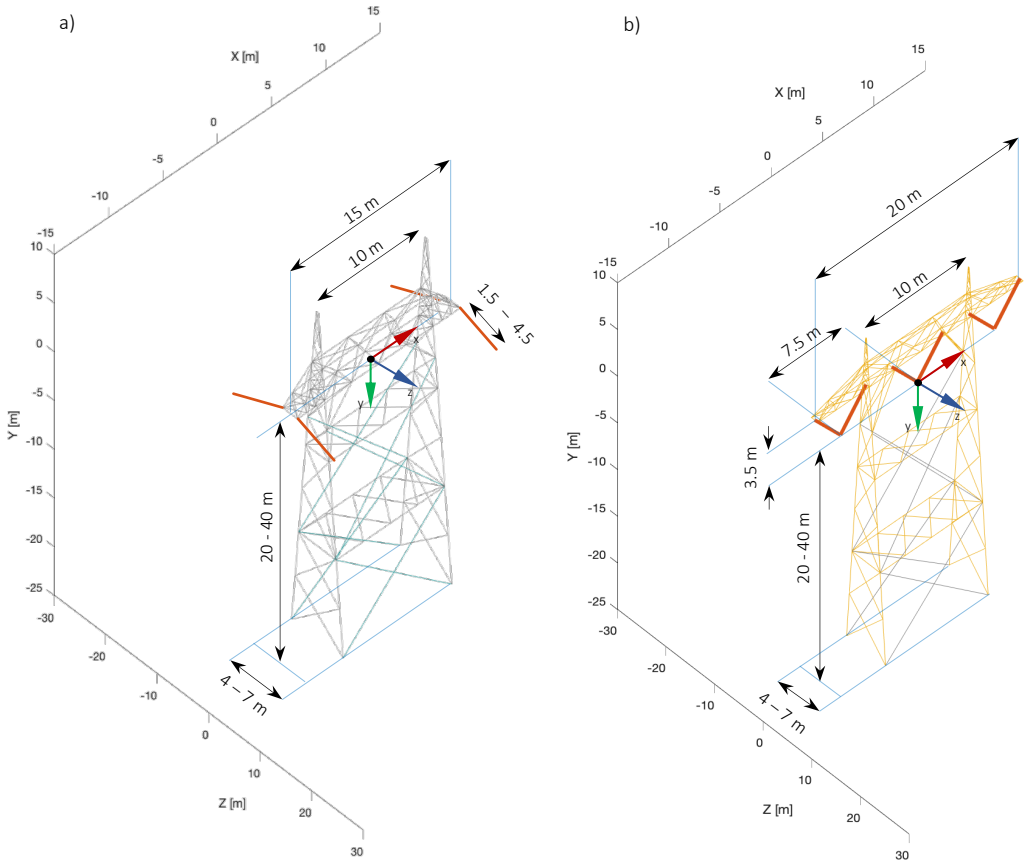

Figure 5.1. Inspired by Statnett´s H-portal geometry considered for structural analysis (a) Strain pylon and (b) supporting tower (MATLAB plot)

- Multi-span powerline, consisting of user-defined n suspension towers (S) supported on both ends with anchoring pylons (A) (Figure 5.3). Anchoring pylons have conductors attached on both sides, that simulates the continuous power line setup.
- Each span has adjustable length a between $100\ m$ and $800\ m$.
- Elevation of each tower can be modified within range $0\ m$ to $50\ m$ above reference level.
- The power line is modelled along the same direction and the orientation of each supporting structure in coordinate system is the same.
- The initial tension of conductors is fixed for the sake of simplifications. The desired solution would include a material database with adjustable tensions with reference to rated tensile strength of the conductor. This is not covered in the scope of master thesis.
- Line of ground is drawn as straight line between each tower, i.e.: no curvatures, except those set by elevation difference is included.
- The initial tension of conductors is adjusted automatically when the conductor collides with the ground,
- Catenary curve (Eq. 2.1) is applied to define geometry of conductors.
- Initial tension of conductors is modified automatically (reduced) for low *span – elevation* ratio, i.e. when the conductor between towers has short sag and catenary approaches straight line (see Figure 6.3).

FIGURE 5.2. STATNETT'S H-PORTAL EXAMPLE [90] – 420KV SUSPENSION TOWER OF *ØRSKOG - SOGNDAL* POWER LINE. PRESENCE OF LINEMEN INDICATES THE SCALE OF CONSTRUCTION

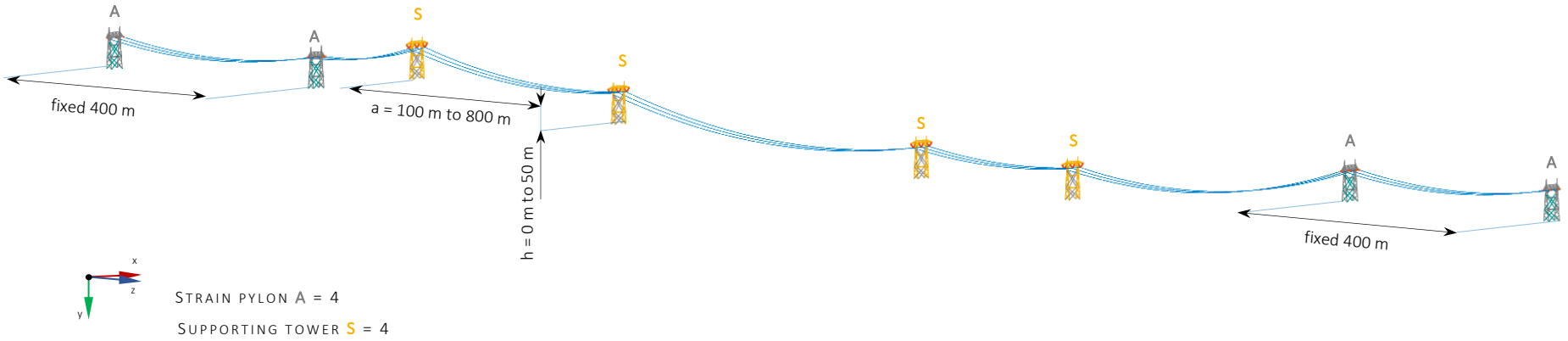

FIGURE 5.3. EXAMPLE POWER LINE SECTION FOR 4 SUPPORTING TOWERS (MATLAB PLOT)

6. COMPUTATIONAL MODELING

Powerlines comprise of several span sections and in a physical scenario each has its own sag and tension conditions varying as a function of elevation of supporting points, ice on conductor distribution, temperature, and wind load. The coupling mechanism of multiple sags requires application of numerical analysis. This is done with commercial software COMSOL Multiphysics. Based on user-defined basic parameters, the power line is modeled with MATLAB interface developed for the purpose of the master thesis. The geometry of the obtained power line is exported into COMSOL Multiphysics where the strength assessment of each tower is performed.

6.1. REFERENCE TOWER MODEL

Both supporting and strain towers are modeled as steel S355, pin joined (EN 50431-1) beam structure. The towers' geometries were designed for the purpose of the master thesis as an example for the individual study. Structural members work under axial loading, i.e. tensile and compressive, as well as shear, bending and torsion. Primarily, linear buckling study is performed to determine the critical load leading to progressive collapse of towers.

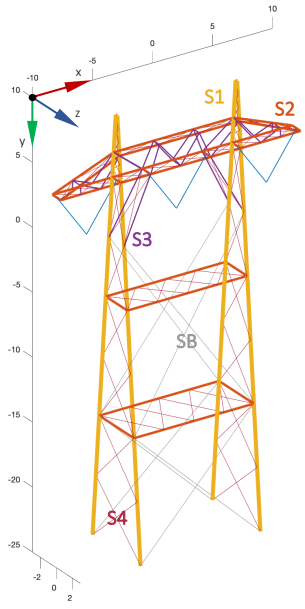

Element	Section	Dimensions [mm]
S1, A1	Rectangular	225x 225 x 15
S2, A2	L-shape	160x 160 x 12
S3, A3		120 x 120 x 10
S4, A4		90 x 90 x 8
SB, AB	Circular bracing	∅15

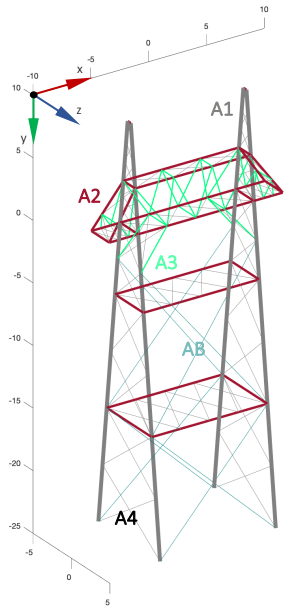

FIGURE 6.1. CROSS SECTIONS OF TRUSS STRUCTURAL MEMBERS (MATLAB PLOT)

The material properties of steel are presented in Table 6.1. A linear stress-strain curve is assumed. Rectangular and L-shaped cross sections are assigned for the individual members (see Figure 6.1. and 6.2). Bracing contributes to the stability of the structure through increasing its stiffness. It counteracts buckling and torsion loads acting on the towers' structural members. Cable bracings are modelled as S355 pretensioned cable element (5% f_y) (truss interface). COMSOL does not support definition of angle cross-sections, thus it must be done by user. Basic section properties for analysis input are presented in Table 6.2

S355[1]	Symbol	Value	Unit
Young´s modulus	E	210	GPa
Poisson ratio	υ	0.3	-
Density	ρ	7 850	kg/m^3
Yield Strength	f_y	355	MPa (N/mm^2)
Post yielding tangent Modulus[2]	E_p	4 120	MPa

[1] Data taken from Eurokode 3 [91]

[2] Example data from analysis of lattice tower [44]

TABELL 6.1. MATERIA DATA OF LATTICE TOWERS´STRUCTURAL MEMBERS

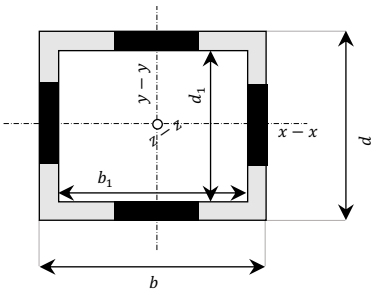

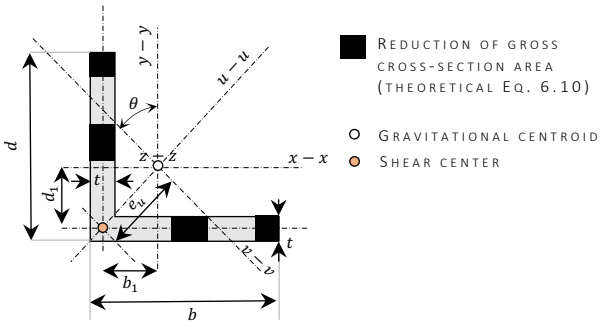

MOMENTS OF INERTIA

$$I_{xx} = \frac{bd^3}{12} - \frac{b_1 {d_1}^3}{12}$$

$$I_{yy} = \frac{db^3}{12} - \frac{d_1 {b_1}^3}{12}$$

$$I_{zz} = I_{xx} + I_{yy}$$

RADIUS OF GYRATION

$$i_{xx} = \sqrt{\frac{bd^3 - b_1 {d_1}^3}{12A}}$$

$$i_{yy} = \sqrt{\frac{db^3 - d_1 {b_1}^3}{12A}}$$

$$i_{zz} = \sqrt{{i_{xx}}^2 + {i_{yy}}^2}$$

MOMENTS OF INERTIA

$$I_{xx} = t^3\left(\frac{b}{12} - \frac{t}{12}\right) + \frac{d^3 t}{12} + t{d_1}^2(b-t) + dt\left(d_1 - \frac{d}{2} + \frac{t}{2}\right)^2$$

$$I_{yy} = \frac{dt^3}{12} + \frac{t(b-t)^3}{12} + t(b-t)\left(\frac{b}{2} - b_1\right)^2 + dt{b_1}^2$$

$$I_{zz} = I_{xx} + I_{yy}$$

$$I_{xy} = b_1 dt\left(d_1 - \frac{d}{2} + \frac{t}{2}\right) - d_1 t(b-t)\left(\frac{b}{2} - b_1\right)$$

$$I_{vv} = \frac{I_{xx} + I_{yy}}{2} - \frac{I_{xx} - I_{yy}}{2} cos2\theta + I_{xy} sin2\theta$$

$$I_{uu} = \frac{I_{xx} + I_{yy}}{2} + \frac{I_{xx} - I_{yy}}{2} cos2\theta - I_{xy} sin2\theta$$

$$d_1 = \frac{d^2 - td}{2(b+d-t)}$$

$$b_1 = \frac{b^2 - tb}{2(b+d-t)}$$

$$e_u = \frac{b_1}{cos\theta}$$

RADIUS OF GYRATION

$$i_{xx} = \sqrt{\frac{I_{xx}}{A}} \qquad i_{vv} = \sqrt{\frac{I_{vv}}{A}} \qquad i_{yy} = \sqrt{\frac{I_{yy}}{A}}$$

CROSS-SECTION AREA

$$A = t(d + b - t)$$

FIGURE 6.2. GEOMETRICAL PROPERTIES FOR *HOLLOW RECTANGULAR*- AND *L*-CROSS SECTIONS OF LATTICE TOWER STRUCTURAL MEMBERS. REFERENCE VALUES FOR DIFFERENT ANGLES CAN BE FOUND IN NS-EN 10056-1:2017 [92]. EQUATIONS WERE DERIVED BY-HAND AND VALIDATED WITH COMMERCIAL SOFTWARE *SKYCIV SECTION BUILDER*

Parameter	Symbol	Angle dimensions [mm] 160 x 160 x 12	120 x 120 x 10	90 x 90 x 8	Unit
Cross-section area	A	36.96E-04	23.00E-04	13.76E-04	m^2
Moment of Inertia about local x axis	I_{xx}	09.17E-06	03.18E-06	01.07E-06	m^4
Moment of inertia about local y axis	I_{yy}	09.17E-06	03.18E-06	01.07E-06	m^4
Distance to shear center in x direction	b_1	38.44E-03	28.70E-03	21.45E-03	m
Distance to shear center in y direction	d_1	38.44E-03	28.70E -03	21.45E-03	m
Torsional constant[1]	J	01.77E-07	0.76E-07	0.29E-07	m^4
Torsional section modulus[2]	w_t	7.61e-04	3.54e-04	1.58e-04	m^3

[1] For angles (L-shapes (Figure 6.10)) [93] $J = \frac{t^3}{3}\left[\left(d - \frac{t}{2}\right) + \left(b - \frac{t}{2}\right)\right]$ [2] $w_t = \frac{I_{pol}}{b_1}$

TABELL 6.2. BASIC INPUT SECTION PROPERTIES FOR COMSOL BEAM MODEL OF ANGLES

6.2. CONDUCTOR MODEL

Conductors in FEM analysis are usually treated as cable structures that support large deflection effects, elasticity, plasticity, and creep. The element works in tension. Under compression the stiffness approaches zero that reflects the relaxation of cable ($E \cdot [1 - 0.99 \cdot if\ in\ compression(truss.en < 0)(true = 1, false = 0)]$). Ground wires are hinged with transmission towers and conductors are hinged with transmission towers through hinged insulator. Bending stiffness near clamps of conductors is neglected. Conductors used in analysis are *Bear ACSR* [94], which characteristic is presented in Table 6.3. The mass of conductor per unit length and its cross-section does not change within span or due to temperature

Parameter	Symbol	Value	Unit
Young´s modulus[1]	E	123.4	GPa
Poisson ratio	υ	0.3	-
Density[2]	ρ	2 811.9	kg/m^3
Diameter[4]	d_{ACSR}	23.5	mm
Mass per unit length[4]	m_c	1.219	kg m
Total cross-section Area	A	433.75	mm^2
Aluminum corss-section[4]	A_{Al}	264.4	mm^2
Rated tensile strength[4]	f_e	116.1	kN
Linear expansion coefficient[3]	α	18.3	-

[1] $E_{Al} = 68\ GPa$, $E_{St} = 210\ GPa$

[2] with regards to reference mass per unit length m_c

[3] $\alpha_{Al} = 23.0$, $\alpha_{St} = 11.0$.

[4] *Bear ACSR* [94]

TABLE 6.3. MATERIAL DATA OF CONDUCTORS

Although not without importance, ground wires are not included in the performed analysis. The modelling principle would be identical to the one applied on conductors. At this stage of research and development of FEA techniques of power lines this might be omitted. The contribution of ground wires on supporting structures for any real-case analysis can not be neglected though.

6.3. Insulators Model

Insulators were modelled as composite beams (FRP Rod) with diameter ∅ 40 mm. The material parameters that were applied [61] are shown in Table 6.4.

Parameter	Symbol	Value	Unit
Young´s modulus (longitudinal)[1]	E_L	44	GPa
Poisson ratio (longitudinal)[1]	v_L	0.5	-
Density[2]	ρ	2 150	kg/m^3
Diameter	d_{ins}	40.0	mm

[1][95]

[2]*Artisan industry trading (Nantong) CO.,LTD* Material data sheet

Table 6.4. Material data of insulators

6.4. Model of power line section

The power line section is modelled with MATLAB interface, that aims to use the solution for practical application. The geometries of conductors and sags are obtained for user-defined input data, i.e.: number of suspension towers, corresponding span lengths and height of point of support for conductor over reference level 0. The horizontal component of initial tension in each span is predefined and fixed to $30{,}338\ kN$ at $16\ ℃$ (reference value from CIGRE [94] for *Bear ACSR* conductor working in heavy ice and wind loading). The numerical algorithm that calculates geometrical parameters of the power line with graphical representation, is developed. The scheme of iterative procedure is as follows:

a. The input data number n_t of suspension towers, span lengths a_e and elevation h of each tower over reference level 0 in the xy coordinate system are defined by user. Furthermore, the initial horizontal component of tension H and mass of conductors per meter $m_c g$ are prerequisites. The catenary y_{AB} is sought (see Figure 6.3). Catenary $y_{AA'}$ is stringed between points A and A' that has the same elevation, where point A' has the same x - coordinate as B. Catenary $y_{AA'}$ in xy coordinate system with origin in vertex of the catenary is defined with the following function:

$$y_{AA'}(x) = \frac{H}{m_c g}\left[cos\ h\left(\frac{m_c g}{H}x\right) - 1\right] \tag{6.1}$$

b. Catenaries $y_{AA'}(x)$, $y(x)$ and $y_{AB}(x)$ are described with the same formula, although are shifted relatively to each other. In order to find the shape of catenary $y_{AB}(x)$ defined between point of support A and B, the numerical procedure solved with MATLAB is introduced:

c. Line AB between points of support of desired catenary $y_{AB}(x)$ is defined with following linear function in xy coordinate:

$$y_{triangle}(x) = \frac{y_B - y_A}{x_B - x_A}x + y_A + \frac{x_A(y_A - y_B)}{x_B - x_A} \tag{6.2}$$

The curve has length L_{AB}:

$$L_{AB}(x) = \int_A^B \sqrt{1 + \left(\frac{d}{dx}y_{triangle}(x)\right)^2}\, dx \tag{6.3}$$

d. Since $y_{AB}(x)$ and $y(x)$ are the same functions, the triangle $AA'B$ must be shifted along vectors $\vec{p}$ and $\vec{s}$ into catenary $y(x)$ in a way that it defines the coordinates A_s and B_s. This is done with iterative procedure solved in MATLAB (see Appendix 1). Triangle $AA'B$ is shifted along catenary $y(x)$ with point A attached with fixed distance Δx, until point B belongs to catenary $y(x)$.

e. Catenary $y(x)$ between points A_s and B_s defines sought catenary for height difference el_{diff}.

f. The developed solution ensures the geometrical compliance of catenaries in case of geometrical singularities, i.e.: wide spans and high in value difference in elevations between towers, where catenary approaches linear curve. This is resolved through tension adjustment. As a result, the solution works for any span and difference of elevation between points of support. Furthermore, the tension is modified automatically if conductor collides with the ground.

g. Catenary for each span is consecutively calculated in xy coordinate system and shifted subsequently afterwards to create single section of power line.

h. For modelling purpose, the power line has two anchoring pylons on each end. First it is designed as a part of considered section, and second as imitation of continuous powerline.

i. Strain insulators are adjusted to the geometry of catenaries with user-defined length.

The example results for the developed iterative solution (Appendix 1) are presented in Figure 6.4. The MATLAB code results in xyz coordinates of each element to be considered with FEA in COMSOL, i.e.: conductors, towers, and insulators.

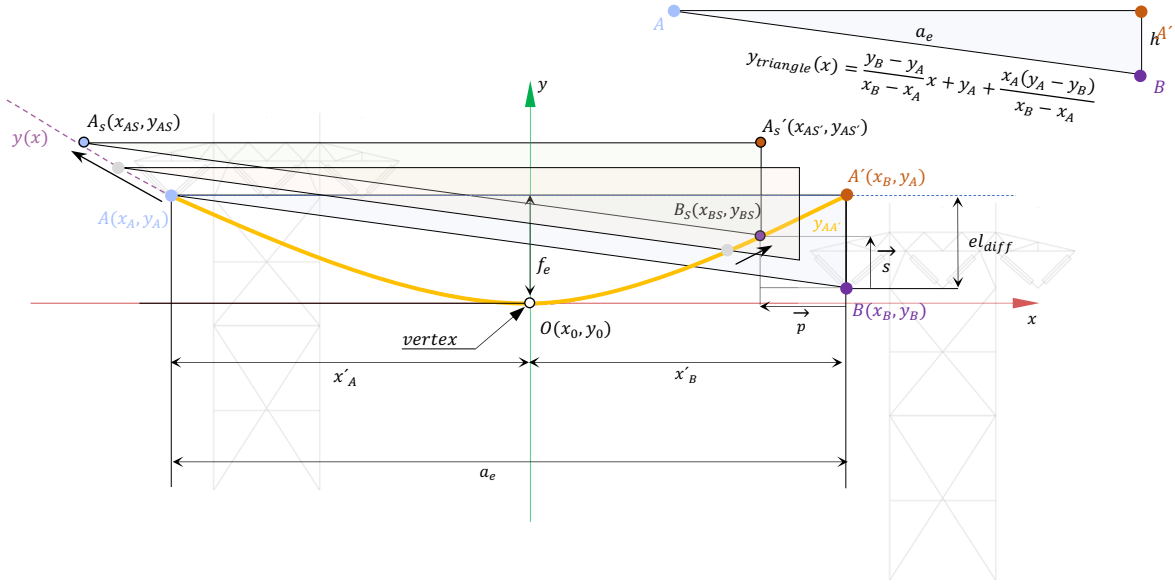

FIGURE 6.3.1. SCHEME OF NUMERICAL ADJUSTMENT OF CATENARY TO SUPPORTING POINTS

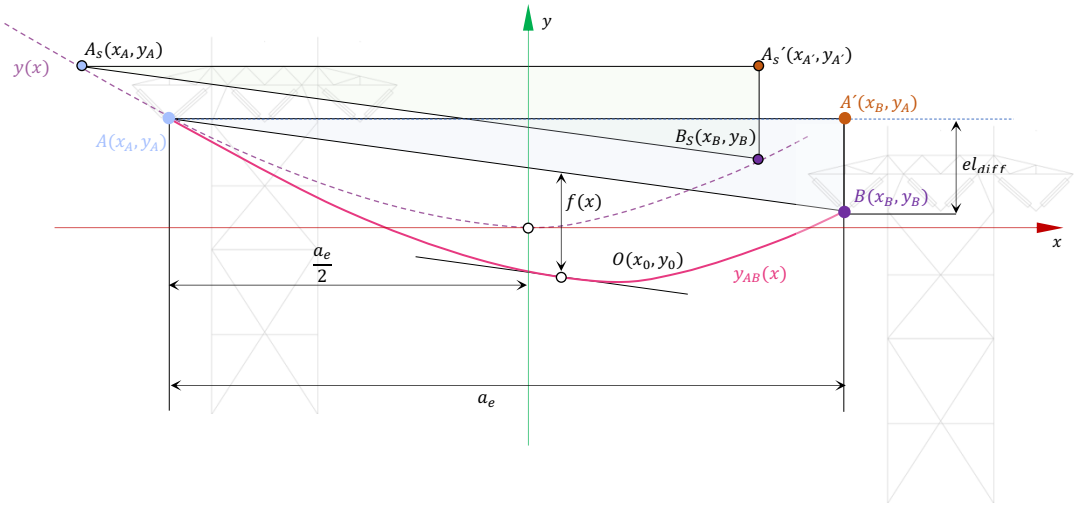

FIGURE 6.3.2. SCHEME OF NUMERICAL ADJUSTMENT OF CATENARY TO SUPPORTING POINTS

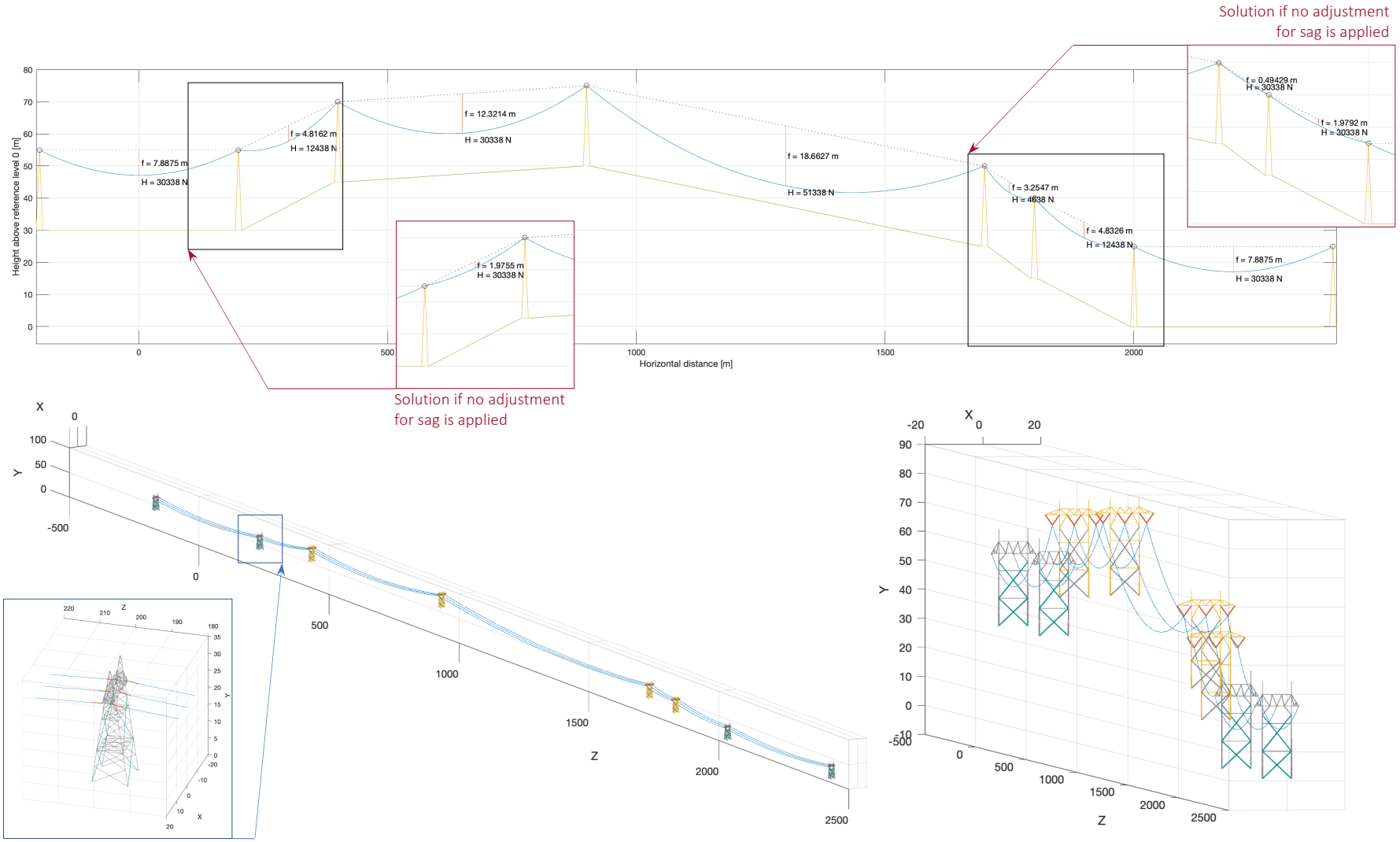

FIGURE 6.4. GRAPHICAL REPRESENTATION OF MATLAB SOLUTION FOR POWER LINE DESIGN EXAMPLE

6.5. Linear buckling analysis of tower members according to design codes

Buckling is considered as a failure mode for the structural members of towers. Towers usually collapse due to instabilities of structural members rather than its plastic failure. The second mentioned is the result of weak fasteners or welding subjected to shear and tension that is not covered in master thesis. The example collapses of towers shown in Figure 6.5 indicates that leg members are most prone to buckling failure under extreme loading conditions. Considering ice and wind actions, buckling may be the dominant failure mode for supporting structures of power lines. This is however not required by National Normative Aspect of EN 50341 for Norway [57]. EN 50341-1 [7] recommends finite element methods for analyzing the second order phenomena (large displacement).

Figure 6.5. Collapse of suspension towers due to buckling – (a) Power line between Kobbelv and Ofoten, due to avalanche on adjacent towers, 17th May 2010 [96] (b) tower collapse due to wind in Suldal municipality in Rogaland, 15th December 2012 [97]

The theoretical *Euler Buckling Formula* predicts the elastic critical load under which the component is expected to buckle (flexural buckling), as shown in Figure 6.6.

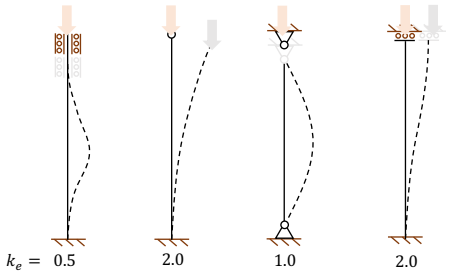

$$N_{Ecr} = \frac{\pi^2 EI}{L_e^2} \quad [\mathrm{N}] \tag{6.4}$$

where:

E	Elasticity modulus of material $[Pa]$,
I	Area moment of inertia of structural member $[m^2]$. If $I_{xx} \neq I_{yy}$, the weaker axis must be considered,
L_e	Effective length of structural member $[m]$.

Figure 6.6. Effective slenderness factor k_e

DNV´s technical standard [98] specifies the effective length with factor k_e, dependent on buckle shape of member ($k_e = 0{,}5 \div 2.0$) as follows:

$$L_e = L \cdot k_e$$

The critical elastic stress σ_{cr} for structural member with cross section A results from equation 6.1. as follows:

$$\sigma_{Ecr} = \frac{\pi^2 EI}{AL_e^{\,2}} \tag{6.5}$$

The formula with introduced radius of gyration $\boldsymbol{i}$ yields the effective slenderness ratio $\boldsymbol{L_e/r}$:

$$\sigma_{Ecr} = \frac{\pi^2 E}{(L_e/i)^2}, \quad \textbf{where radius of gyration } i = \sqrt{\frac{I}{A}} \tag{6.6}$$

$$(L_e/i) \quad - \quad \textbf{slenderness ratio } \lambda$$

The critical stress for which linear buckling is expected can be drawn in *stress-slenderness ratio* curve:

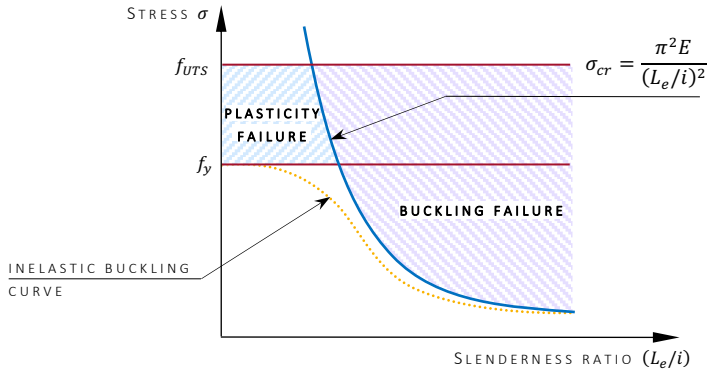

FIGURE 6.7. CRITICAL BUCKLING STRESS IN A FUNCTION OF SLENDERNESS RATIO FOR *EULER´S THEORETICAL APPROACH*

The curve is an idealized example that does not take into consideration material imperfections, eccentricity of load and non-linearities that may occur, i.e. large deformations. The limitation of theoretical critical load design has its solution in Eurocode 3 [99] that introduces the imperfection factor $\boldsymbol{\alpha}$ to draw the abovementioned buckling curves closer to the physical solution. The normative procedure is explained for structural angles (L-shape) of lattice tower under flexural, torsional, torsional-flexural buckling and lateral torsional buckling.

6.5.1. FLEXURAL BENDING

With regards to National Normative Eurocode 3 sets the following requirement for structural members under compression:

$$\frac{N_{Ed}}{N_{b,Rd}} \leq \mathbf{1,0} \tag{6.7}$$

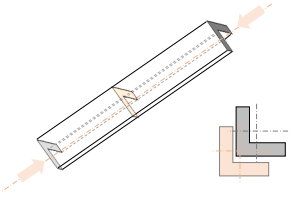

where:

N_{Ed} Design value of compression force for ULS $[N]$,

$N_{b,Rd}$ Design buckling resistance of the structural member $[N]$,

FIGURE 6.8. FLEXURAL BUCKLING OF STRUCTURAL ANGLE

All cross-section areas of structural members of lattice towers are classified as class 3 or 4 according to EN 50341 (Normative Annex J) [7]. The supporting structure is intended to work in elastic limit up to yielding point, however buckling might be present before that point, hence, for class 4:

$$N_{b,Rd} = \frac{\chi A_{eff} f_y}{\gamma_{M1}} \tag{6.8}$$

where:

χ	Reduction factor for relevant buckling mode,
A_{eff}	Effective are of cross section when subjected to compression,
f_y	Yielding strength $[MPa]$,
γ_{M1}	Resistance of members to buckling equal to $1{,}1$ (EN 50341-2-16 [57]).

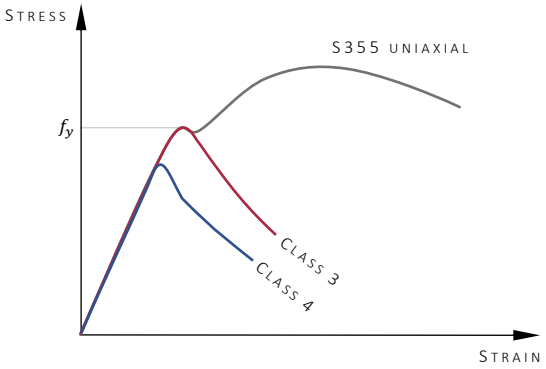

FIGURE 6.9. CLASSIFICATION OF STRUCTURAL CROSS-SECTIONS ACCORDING TO EUROCODE 3 FOR STEEL S355

For axial compression reduction factor $\boldsymbol{\chi}$ is defined as follows:

$$\boldsymbol{\chi = \frac{1}{\phi + \sqrt{\phi^2 - \bar{\lambda}_{eff}{}^2}}} \quad \boldsymbol{for} \quad \boldsymbol{\bar{\lambda} > 0.2} \tag{6.9}$$

$$\boldsymbol{\chi = 1} \quad \boldsymbol{for} \quad \boldsymbol{\bar{\lambda} \leq 0.2}$$

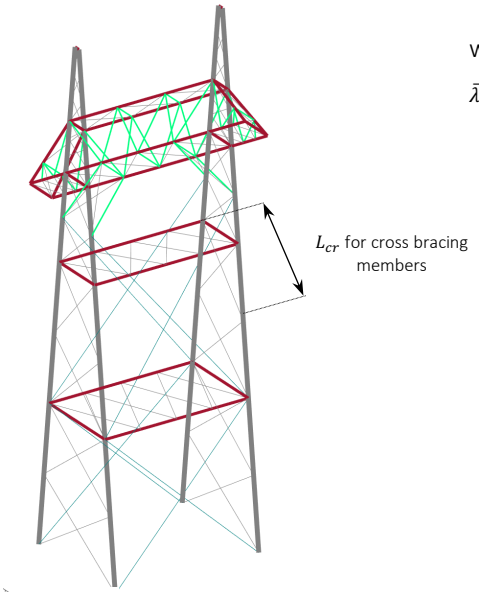

FIGURE 6.10. LENGTH OF EXAMPLE STRUCTURAL MEMBER

where:

$\bar{\lambda}_{eff}$ effective non-dimensional slenderness. For leg member of lattice tower $\bar{\lambda}_{eff} = k\bar{\lambda}$ (EN 50341-1 [7]). Slenderness for flexural buckling $\bar{\lambda}$:

$$\bar{\lambda} = \frac{\lambda}{\lambda_1}\sqrt{\frac{A_{eff}}{A}} = \frac{L_{cr}}{i}\frac{\sqrt{\frac{A_{eff}}{A}}}{\lambda_1} \tag{6.10}$$

where:

i	radius of gyration about the weaker axis for considered cross section (Annex H of EN 1993-3-1 [87]),
k	effective slenderness factor (Annex G of EN 1993-3-1 [87]) dependent on bracing-leg connection. For bolted connection most often $k = 0{,}7 + \frac{0{,}35}{\bar{\lambda}_v}$
L_{cr}	Buckling length. Foremost $L_{cr} = L\ [m]$,
λ_1	slenderness characteristic value

$$\lambda_1 = \pi\sqrt{\frac{E}{f_y}} \tag{6.11}$$

λ	slenderness

$\boldsymbol{\phi}$ characteristic value of reduction factor $\boldsymbol{\chi}$:

$$\boldsymbol{\phi = 0{,}5 \cdot \left[1 + \alpha(\bar{\lambda} - 0{,}2) + \bar{\lambda}^2\right]} \tag{6.12}$$

$\boldsymbol{\alpha}$ Imperfection factor. For S355 *L-section* $\boldsymbol{\alpha_b = 0{,}34}$, for hollow section $\boldsymbol{\alpha_a = 0{,}21}$ (hot finished steel as general case in Norway [57]).

For cross-sections of class 4 it is assumed that the particular portion of the area under compression has no resistance against instabilities. Simply theoretically, it is the area near free edges of cross section, and its central pieces (Figure 6.9). Effective area A_{eff} of gross cross-section A for class 4 (EN 1993-1-1 [91]) is calculated based on effective widths of the compression elements ρ that can be found in EN 50341-1 [7] for hot rolled cross-sections as follows:

$$\begin{cases} \rho = 1 & \bar{\lambda}_p \leq 0.748 \\ \rho = \frac{\bar{\lambda}_p - 0{,}188}{\bar{\lambda}_p^{\,2}} & \bar{\lambda}_p > 0.748 \end{cases} \quad for \tag{6.13}$$

$$\bar{\lambda}_{p(d)} = \frac{(d-2t)}{18{,}62t\sqrt{\frac{235\cdot 10^6}{f_y}}} \qquad or \qquad \bar{\lambda}_{p(b)} = \frac{(b-2t)}{18{,}62t\sqrt{\frac{235\cdot 10^6}{f_y}}}$$

$$A_{eff} = \rho A \tag{6.14}$$

When calculating the effective-cross section, the geometrical details, such as holes for bolts must be considered. The designed critical flexural buckling stress $\boldsymbol{\sigma_{cr}}$ is then:

$$\frac{N_{b,Rd}}{A_{eff}} = \frac{\chi f_y}{\gamma_{M1}} \quad \Rightarrow \quad \sigma_{cr_{flexular}} = \frac{\chi f_y}{\gamma_{M1}} \tag{6.15}$$

6.5.2. Flexural and torsional-flexural buckling

Although EN 1993-1-1 [91] indicates that the structural members with open cross-sections should be considered for both *torsional elastic* and *torsional-flexural* buckling, it does not provide straightforward solution. EN 5034-1-1 [7] states that effective cross section coefficient $\boldsymbol{\rho}$ covers abovementioned buckling modes, however just for legs with L-cross sections where $\boldsymbol{b = d}$ (Figure 6.10). It does not apply to other cross sections. The formula for both *torsional elastic* and *torsional-flexural buckling* is found in EN 1993-1-3 [100], however it applies just to cold-formed members that are symmetrical, i.e. I-beam sections. Finally, for *torsional elastic* and *torsional-flexural elastic* modes of buckling, critical stresses (consecutive $\boldsymbol{\sigma_{ET}}$ and $\boldsymbol{\sigma_{ETF}}$) were found in DNV´s technical standard *DNVGL-CG-0128* [98] as follows:

$$\sigma_{ET(torsional)} = \frac{GI_{sv}}{I_{pol}} + \frac{\pi^2 E c_{wrap}}{I_{pol}(k_e L)^2} \tag{6.16}$$

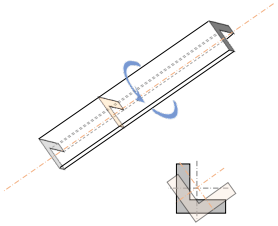

Figure 6.11. Flexural buckling mode

where:

I_{sv} St. Venant´s moment of inertia

For angles (L-shapes (Figure 6.10)) [101]

$$I_{sv} = \frac{[d+b-2t]t^3}{3+0{,}237(t)^4} \tag{6.17}$$

I_{pol} Polar moment of inertia about shear center (Figure 6.2):

$$I_{pol} = I_{zz} + A\left[{b_1}^2 + {d_1}^2\right] \tag{6.18}$$

c_{wrap} Wrapping constant:

For angles(L-shapes (Figure 6.10)) [93]

$$c_{wrap} = \frac{t^3}{36}\left[\left(d-\frac{t}{2}\right)^3 + \left(b-\frac{t}{2}\right)^3\right] \tag{6.19}$$

k effective factor (Eq. 6.1)

G Shear modulus

$$G = \frac{E}{2(1+\upsilon)} \tag{6.20}$$

$$\boldsymbol{\sigma_{ETS(torsional-flexular)}} = \frac{\mathbf{1}}{\mathbf{2\xi}} + \left[\boldsymbol{\sigma_{Ecr}} + \boldsymbol{\sigma_{ET}} - \sqrt{(\boldsymbol{\sigma_{Ecr}} + \boldsymbol{\sigma_{ET}})^2 - \mathbf{4\xi\sigma_{Ecr}\sigma_{ET}}}\right] \tag{6.21}$$

where: $\xi = 1 - \frac{A[{b_1}^2 + {d_1}^2]}{I_{pol}}$

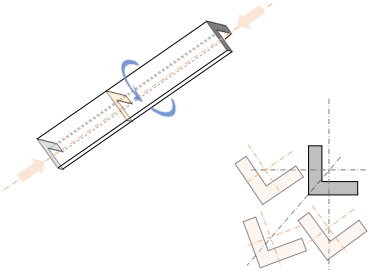

FIGURE 6.12. FLEXURAL -TORSIONAL BUCKLING MODE

With regards to inelastic buckling, the critical *torsional* and *torsional-flexural* buckling stresses are as follows:

$$\boldsymbol{\sigma_{cr}} = \left[\frac{\mathbf{1+\alpha(\lambda_{eff}-\lambda_0)+{\lambda_{eff}}^2-\sqrt{\left(1+\alpha(\lambda_{eff}-\lambda_0)+{\lambda_{eff}}^2\right)^2-4{\lambda_{eff}}^2}}}{\mathbf{2{\lambda_{eff}}^2}}\right] \cdot \boldsymbol{f_y} \tag{6.22}$$

where:

λ_0 coefficient for L-shape $\lambda_0 = 0{,}2$,

α coefficient for L-shape $\alpha = 0{,}5$,

λ_{eff} reduced slenderness

$$\lambda_{eff} = \sqrt{\frac{f_y}{\sigma_{ET(torsional)}}} \quad or \quad \lambda_{eff} = \sqrt{\frac{f_y}{\sigma_{ET(torsional-flexular)}}} \tag{6.23}$$

Alternatively, critical *torsional* and *torsional-flexural* buckling stresses can be obtained through substitution of $\bar{\lambda}_{eff}$ with λ_{eff} in equation 6.9.

Bending curves (Figure 6.13) for example structural members, drawn with reference to Eurocode 3, indicates importance of verification of buckling modes for design of power line towers. Members with high slenderness must thus be verified with second-order analysis to ensure safety of the structure under extreme loading conditions. Design of torsional-flexural buckling according to Eurocode 3 and DNV standards results with comparable bending curves, however both are highly dependent on effective slenderness factor k. This must be chosen with special caution.

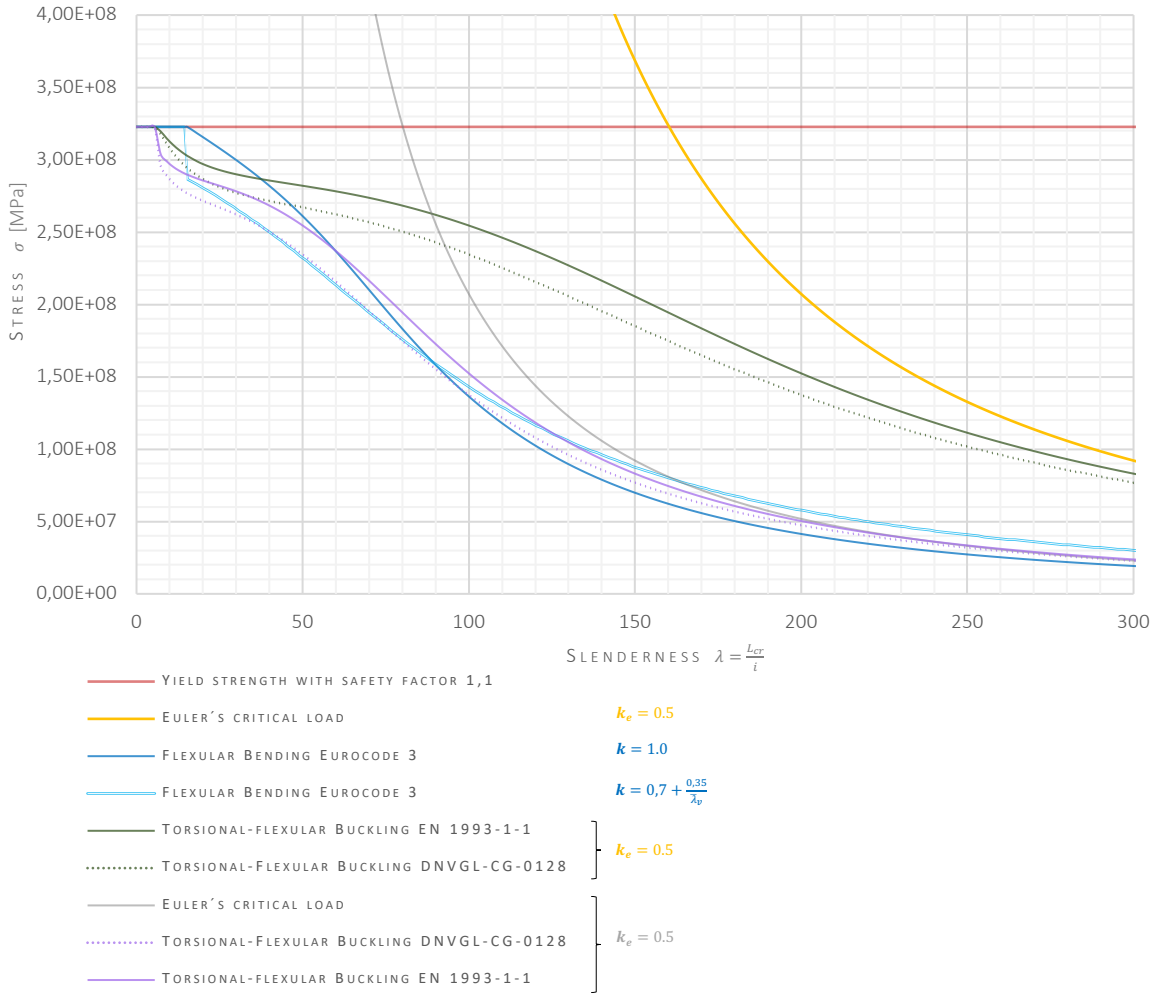

FIGURE 6.13. BUCKLING CURVES FOR EXAMPLE S355 STRUCTURAL BRACING ANGLE 90 X 90 X 8 MM

6.5.3. BUCKLING RESISTANCE OF MEMBERS IN BENDING – LATERAL TORSIONAL BUCKLING

According to EN 1993-1-1, square hollow sections are not prone to lateral torsional buckling. Furthermore, with regards to EN 50341-1, bending moment caused by normal eccentricities in the diagonals of the leg members are negligible. For continuous members, lateral torsional bending may be generally neglected. Nevertheless, in case of susceptibility of cross section to lateral torsional buckling, the following conduction must be met:

$$\frac{M_{Ed}}{M_{b,Rd}} \leq 1{,}0 \tag{6.24}$$

where:

M_{Ed} Design value of moment for ULS $[N]$,

$M_{b,Rd}$ Design buckling resistance moment of the structural member,

$$M_{b,Rd} = \frac{\chi_{LT} W_{eff,min} f_y}{\gamma_{M1}} \tag{6.25}$$

where:

$W_{eff,min}$ effective section modulus for the weaker axis:

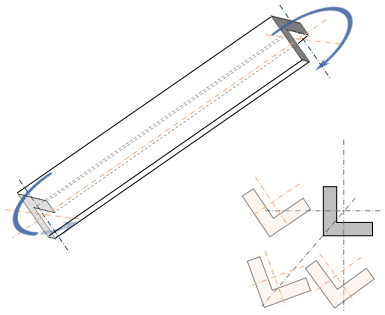

FIGURE 6.14. LATERAL TORSIONAL BUCKLING MODE

$$W_{eff,min} = \frac{I_{xx}}{d_1} \quad or \quad \frac{I_{yy}}{b_1} \tag{6.26}$$

χ_{LT} reduction factor for lateral-torsional buckling,

$$\chi_{LT} = \frac{1}{\phi_{LT} + \sqrt{\phi_{LT}^2 - \beta\bar{\lambda}_{LT}^2}} \tag{6.27}$$

$\boldsymbol{\phi}$ characteristic value of reduction factor $\boldsymbol{\chi_{LT}}$:

$$\boldsymbol{\phi_{LT} = 0,5 \cdot \left[1 + \alpha_{LT}(\bar{\lambda}_{LT} - \bar{\lambda}_{LT,0}) + \beta\bar{\lambda}_{LT}^2\right]} \tag{6.28}$$

where:

$\bar{\lambda}_{LT,0}$ coefficient $0,4$ according to National Annex of EN1993-1-1 for Norway,

β coefficient $0,7$ according to National Annex of EN1993-1-1 for Norway,

α_{LT} imperfection factor 0,76 for torsional buckling curve.

6.6. MATLAB – COMSOL MODEL SETUP

MATLAB and COMSOL Multiphysics can be connected through the scripting environment LiveLink™ for Matlab provided by COMSOL. Through the *Java* syntax it is possible to define the model as well as perform all the pre- and postprocessing from MATLAB´s command line. This however requires additional credentials that were not available during establishing the model for the master thesis. The workaround for exporting the model from MATLAB to COMSOL was issued by defining the model with *mphtxt* file extension. It is automatically generated through the developed MATLAB code (see APPENDIX 1).

6.7. COMSOL MODEL PRE-PROCESSING

The MATLAB geometry output files were uploaded to COMSOL Multiphysics (see Figure 6.15). Model pre-processing was executed by-hand with software interface. For the purpose of automatization of the model definition, it should be further done in MATLAB as well.

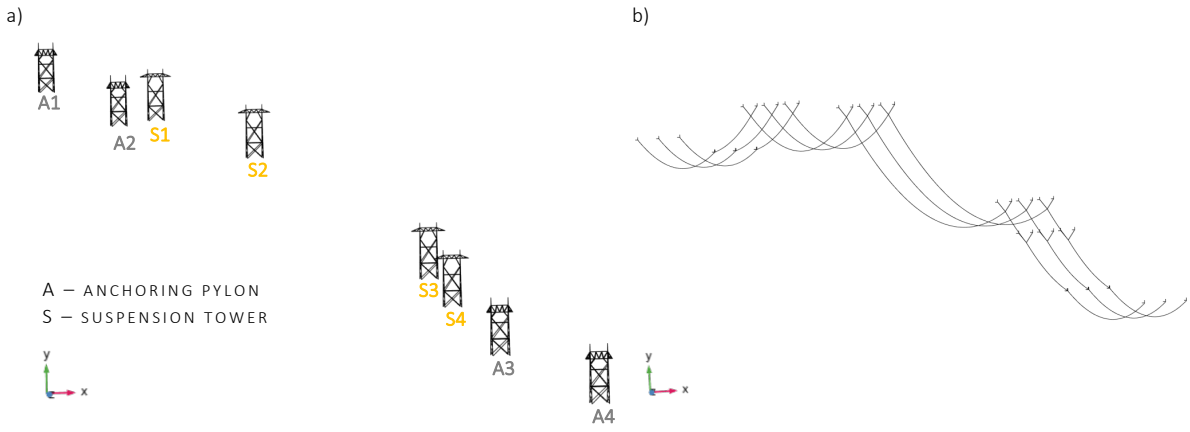

FIGURE 6.15. COMSOL INPUT GEOMETRY OF (A) TOWERS AND (B) CONDUCTORS

6.7.1. Model coupling

Geometrical nonlinearities of sagging phenomena exert different setup of solver for conductors and for towers. Deviations in geometry of towers components (excluding buckling) are slight thus non-linear phenomena may be neglected and geometric linearity is introduced. That means that during analysis equations of equilibrium are formulated for undeformed state of geometry. If components of tower would be defined with geometrical nonlinearity, the solution time of even simple dead-load case would exceed reasonable time limits. Model was thus divided into two geometries - conductors and towers, coupled with set of force and displacement dependencies. Reaction forces in points of supports of conductors determines the initial values for tower analysis with following operator syntax:

C.GC1(withsol('sol', C.CP(C.conductor geometry tag.Nxl)))

where:

C	tag of conductors *component,*
GC1	*Nonlocal coupling* (general extrusion) tag for conductor geometry,
CP	Nonlocal coupling (Integration) tag for coupling node,
sol	solution of analysis of conductor,
withsol	operator,
Nxl	local axial force tag,

Furthermore, displacements of points of support on towers are sent back to conductor model in order to keep geometrical consistency while displaying the results as follows:

T.GC2(withsol('sol', T.CP(displacement field component))

where:

T	tag of tower *component*,
GC2	*Nonlocal coupling* (general extrusion) tag for conductor geometry,

6.7.2. Boundary conditions

Nodes that connect insulators with towers were selected as coupling between interactions of conductors and towers. Because truss elements support only axial forces, workaround of probing of reactions was issued through truss elements modelled in *x, y* and *z* directions for each coupling point (see Figure 6.16).

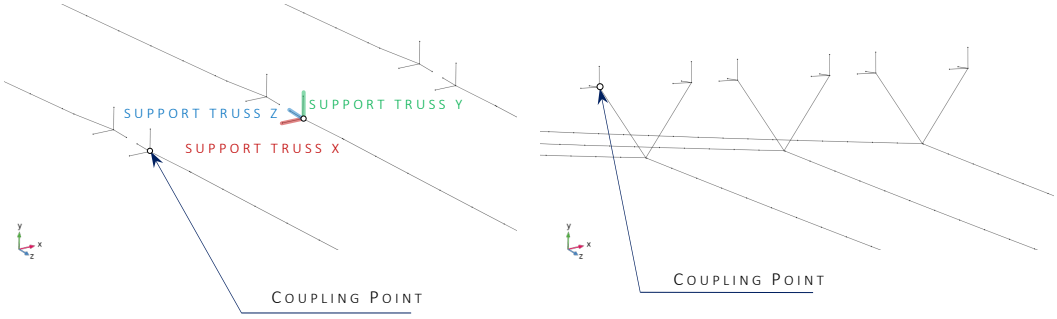

Figure 6.16. Coupling point – geometry of conductors

V-string insulators modeled as *truss* elements has prescribed symmetry in individual coordinate system. This reflects the physical conditions, where one of the insulators under compression (see Figure 2.7) transfer little force to the tower (Figure 6.17).

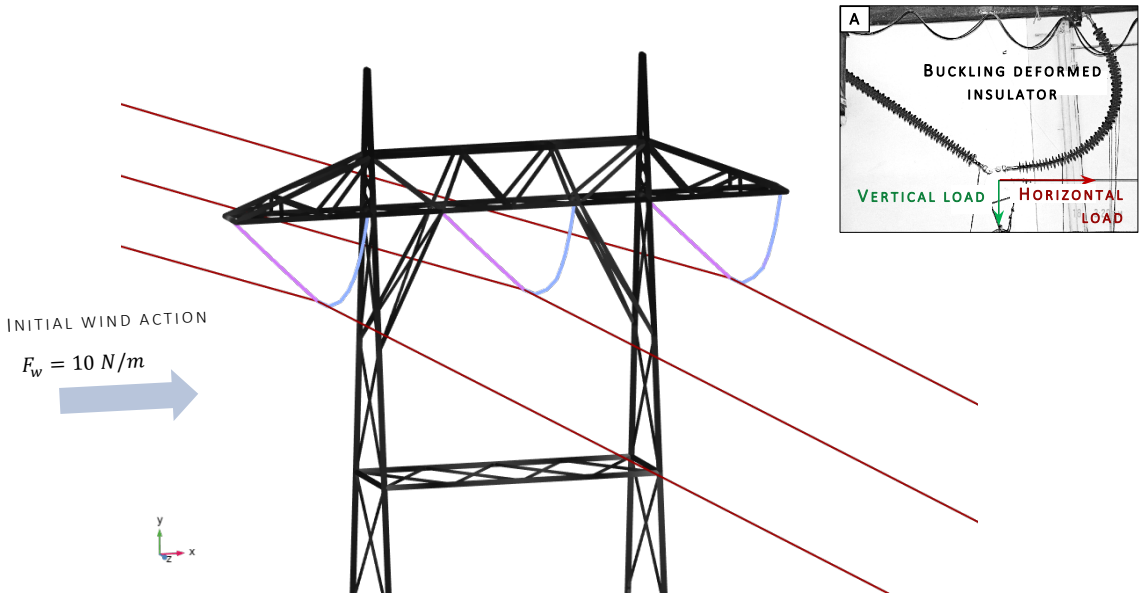

FIGURE 6.17. BOUNDARY CONDITIONS OF *SYMMETRY* APPLIED ON V-STRING INSULATOR REFLECTING ITS PHYSICAL BEHAVIOR. **(A)** REFERENCE DEFLECTION OF V-STRING INSULATOR (EXPERIMENTAL TESTING) [102]

Conductors were pretensioned with initial stress corresponding catenary tension from MATLAB calculations. *Edge mass* was applied on conductors to include weight of conductors in addition to FRP rod. End points of tower legs are fully constrained. The initial conditions assume dead-load of all components and initial wind load $F_w = 10\ N/m$.

6.7.3. COMPUTATIONAL MESH

The computational mesh consists of line segments (1D elements) that is presented in Figure 6.18. Considering 1D elements, mesh quality is merely function of element size.

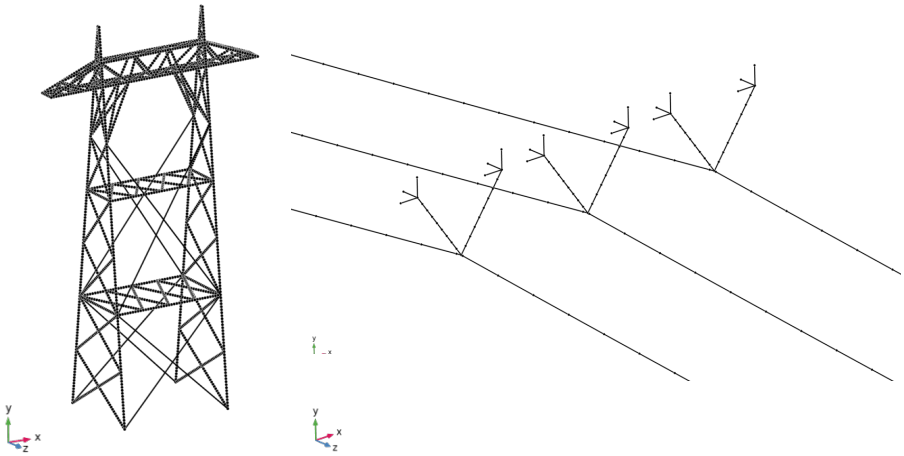

FIGURE 6.18. COMPUTATIONAL MESH ON BEAM (TOWER) AND TRUSS (CONDUCTORS)

6.7.4. Dead-load and initial wind load case

Visualization of the pre-processed model of the power line under the gravitational load, and the deflected model under test wind load (*edge load*) acting perpendicularly to power line direction, are presented in the Figure 6.19. The reference model assumed equal tension of conductors for all spans, except of the longest span, where due to ground collision, the tension was modified (see Figure 6.4). The difference in the tension distribution was compensated with the swing of the V-string insulators, so that the tension was again equalized (see Figure 6.19).

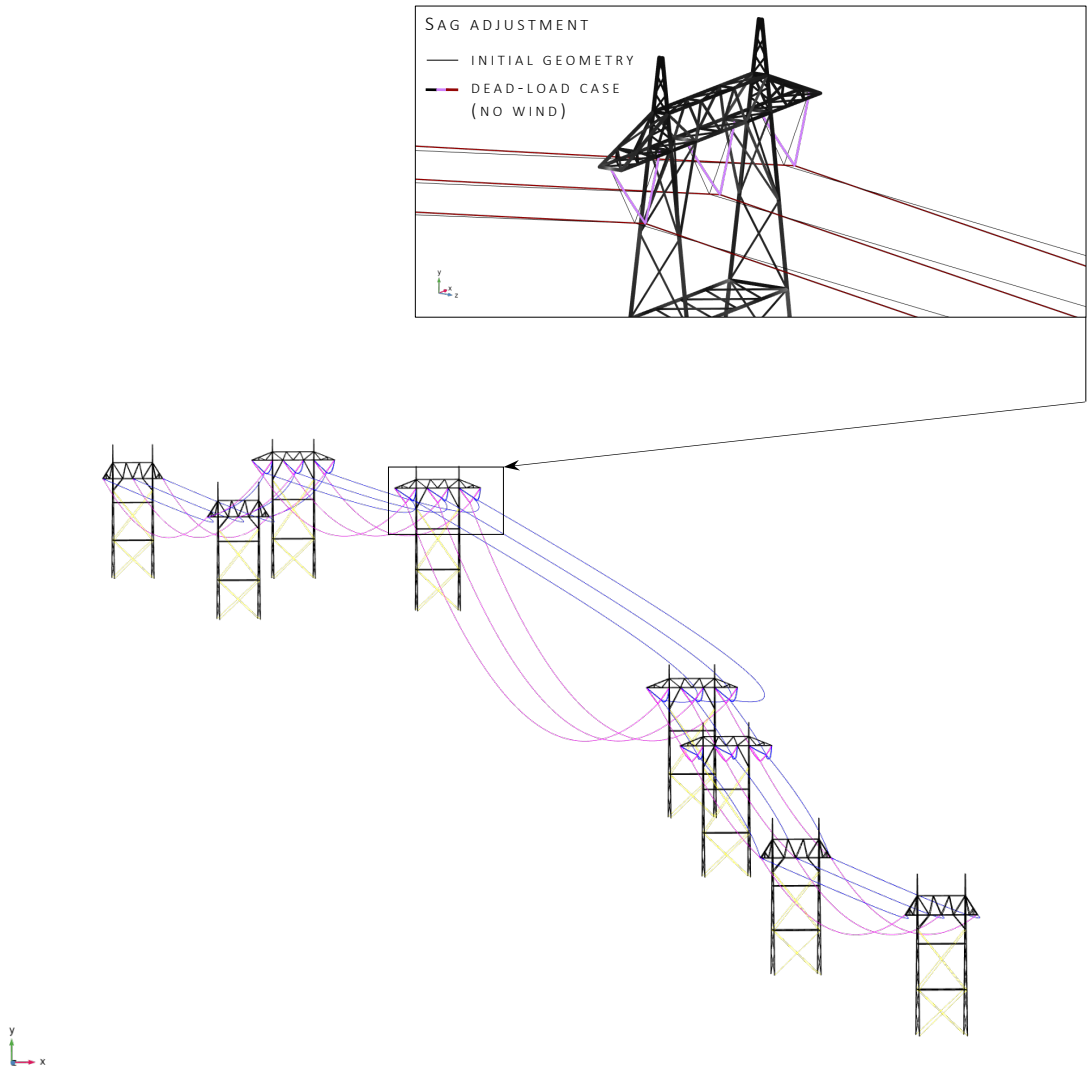

FIGURE 6.19. POWER LINE FOR ( ) DEAD-LOAD CASE AND ( ) INITIAL WIND APPLIED AS *EDGE LOAD* ON CONDUCTORS (DEFORMATION FACTOR FOR WIND LOAD $\kappa = 10$)

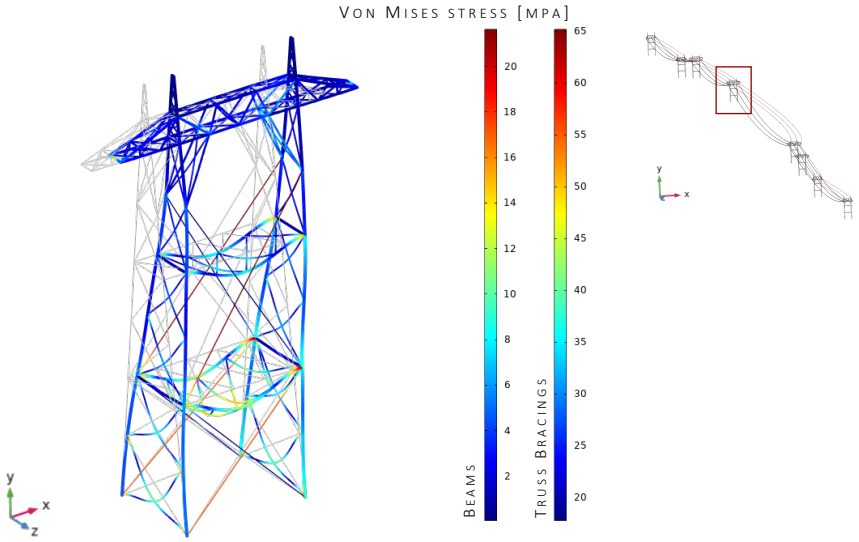

Figure 6.20. Von Mises stress distribution on suspension tower for initial wind load case (Deformation factor $\kappa = 200$)

6.8. Eigenfrequency of conductors

COMSOL Multiphysics has built-in module to analyze eigenfrequencies of the input system. Since the conductors has little damping capabilities (see section 1.2.1) it is required to analyze the power lines in terms of those certain frequencies for which the conductor may resonate and affect severely towers. As described earlier in this thesis, low frequency (0.1 - 1 Hz) and high in amplitude galloping impacts towers with dynamic overloading and in case of fatigue breakage of conductors, results in unbalanced loading on towers.

Considering the FEM analysis in the frequency domain, the system oscillating closer to its natural frequencies would approach infinite amplitude, that in a real case is not physical, due to presence of some fraction of damping in the mechanical system. The energy of oscillating conductors dissipates through the internal friction and relative slips between aluminum strands and steel core. Furthermore, damping results from interaction of conductors with other components of power line, i.e. clamps or insulators, as well as from drag force and air-structure interactions [5]. Damping should be thus included in the analysis. The conductor´s damping characteristics can be obtained through laboratory testing, such as these performed by Malwande et al. [103]. In this master thesis damping coefficient ξ was assumed constant with a value 0.02 [104] (Load case 1). Later, the damping coefficient was increased to the value 0.08 to investigate its contribution to frequency response (Load case 2). Ice accretions in the form of edge load equal to 2.5 kg/m (Load case 3) and 2.5 kg/m (Load case 4) were considered as well with damping coefficient $\xi = 0.02$.

The analysis in frequency domain is preceded with reference steady-state solution that includes gravity load on power line. Laterally, for frequency analysis, the gravity is excluded and wind load is applied as the harmonic perturbation load. Due to introduced damping, the eigenfrequencies will have a complex formula with imaginary part representing damping of the modes.

Several eigenfrequencies and eigenmodes for the example power line, under dead load and initial wind load, are presented in the Figures 6.21-6.22. The amplitude of displacement in XY plane for selected points on the conductors in a function of frequency is presented in the Figures 6.23-24.

The resulting eigenfrequencies serves as input for calculating the response of the structure with a frequency domain module available in COMSOL. The coupling between conductors and tower must include parametric sweep in order to calculate multiple solutions. This is done as follows:

C.GC1(withsol('sol', C.CP(C.conductor geometry tag.Nxl),setval(freq,freq)))

where:

C	tag of conductor *component,*
GC1	*Nonlocal coupling* (general extrusion) tag for conductor geometry,
CP	Nonlocal coupling (Integration) tag for coupling node,
sol	solution of frequency domain analysis of conductors,
withsol	operator,
Nxl	local axial force tag,
setval	sweep value operator,
freq	frequencies for which the solution is swept.

The structure is excited with harmonic force with the eigenfrequencies obtained in the preceding simulation. The oscillations of conductor results in reaction forces with high amplitudes in points of conductors' support that are laterally applied as input for analysis of towers. The reaction forces in example point of support are presented in the Figure 6.25,28,29.

The "picks" in the frequency response (see Figures 6.23-24 and Figures 6.26-27) indicate the frequencies for which the structures approaches resonance. For *Load case 1* visualizations of full harmonic oscillations for selected frequencies (0.172, 0.235, 0.337, 0.515 and 0.554 [Hz]) are presented in Figures 6.31-35. The deformation of towers due to galloping is presented in Figure 6.36 (for frequency 0.515 Hz) and deformation of insulators on suspension tower 4 for harmonic cycle is presented in Figure 6.37 (for frequency 0.515 Hz).

Modified damping coefficient does not change the systems´ eigenmodes, however reduce amplitude of oscillations, that led to reduction of the reaction loads on towers (see Figure 6.25). For suspension towers, reaction forces in x and y direction dominates over the reaction longitudinal to power line (z-axis). Whilst for strain pylons the force in z direction dominates (see Figure 6.30).

The additional mass on conductors changes the frequency response of the system, i.e. different eigenmodes are observed (see Figure 6.26 and 6.27). This was expected as the equation of motion of each node is a function of mass. For the case of edge load on conductor equal to 2.5 kg/m (Load Case 3), the reaction on towers increases with reference to the Load case 1 (see Figure 6.28). However, for edge load on conductor equal to 7.5 kg/m

(Load Case 4) the reduction of reaction forces is considerable (see Figure 6.29). The increasing accretion on conductors, i.e. mass, reduces oscillation amplitude of conductors in the investigated spectrum of frequencies. With increasing mass of the system, the higher live load is required to excite the conductors. This is consistent with reference observations of *Edison Electric Institute* [5], where most of the galloping incidents were observed for ice cover less than 6 mm. Hard rime and glaze accretions are sufficiently adhesive and elastic to persist on conductors even for galloping motions [68].

The galloping is although not merely the function of mass of conductors. The considerable ice deposit introduces damping that would have to be included in the analysis. Furthermore, conductor with ice accretions with high thicknesses, oscillating with high amplitudes would probably lead to ice shedding or tower collapse, rather than resonance, although, galloping events for ice thicknesses up to 32 mm were reported as well [5].

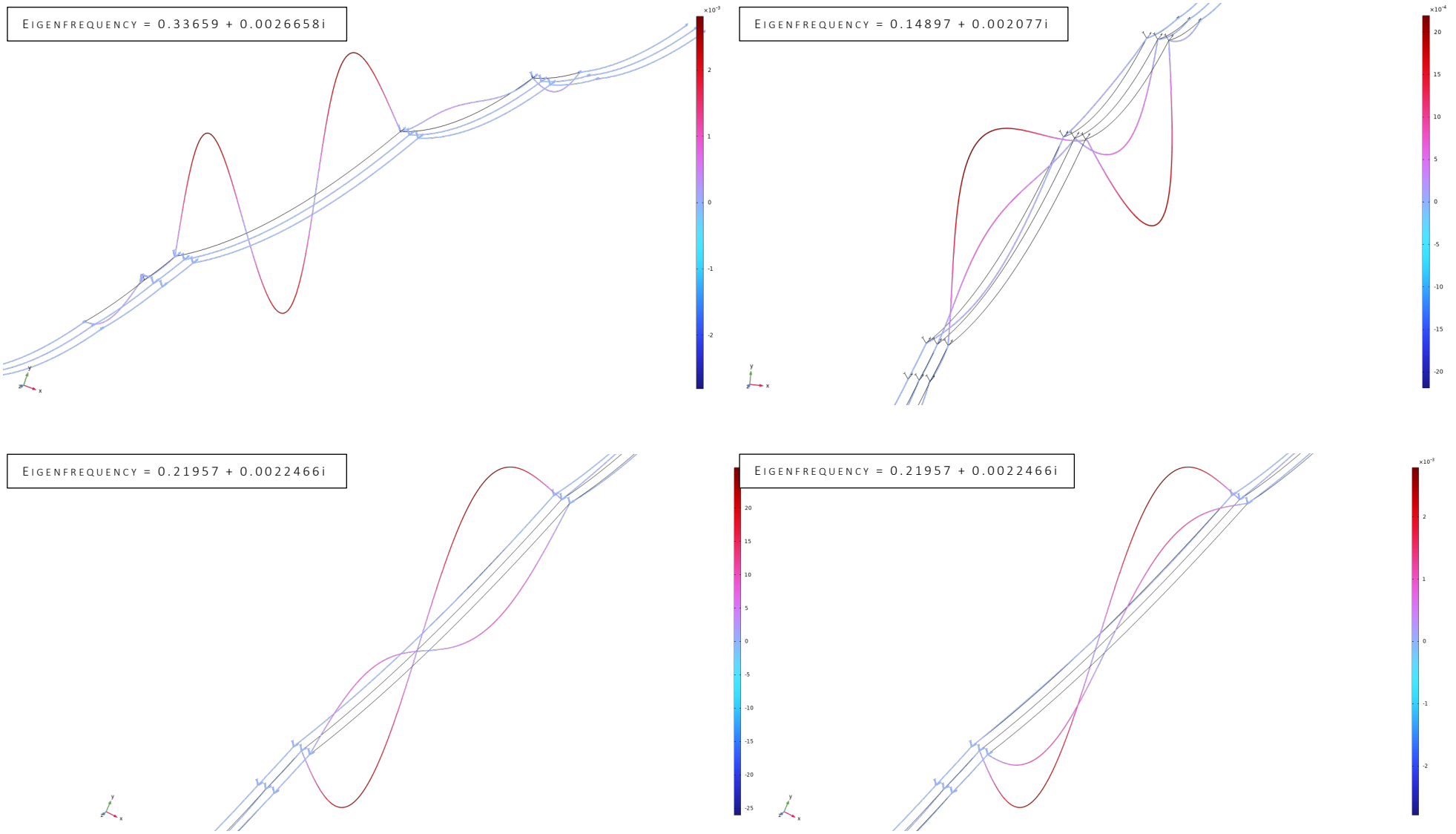

Figure 6.21. Eigenmodes of the conductors displayed in a function of *displacement magnitude [m]*

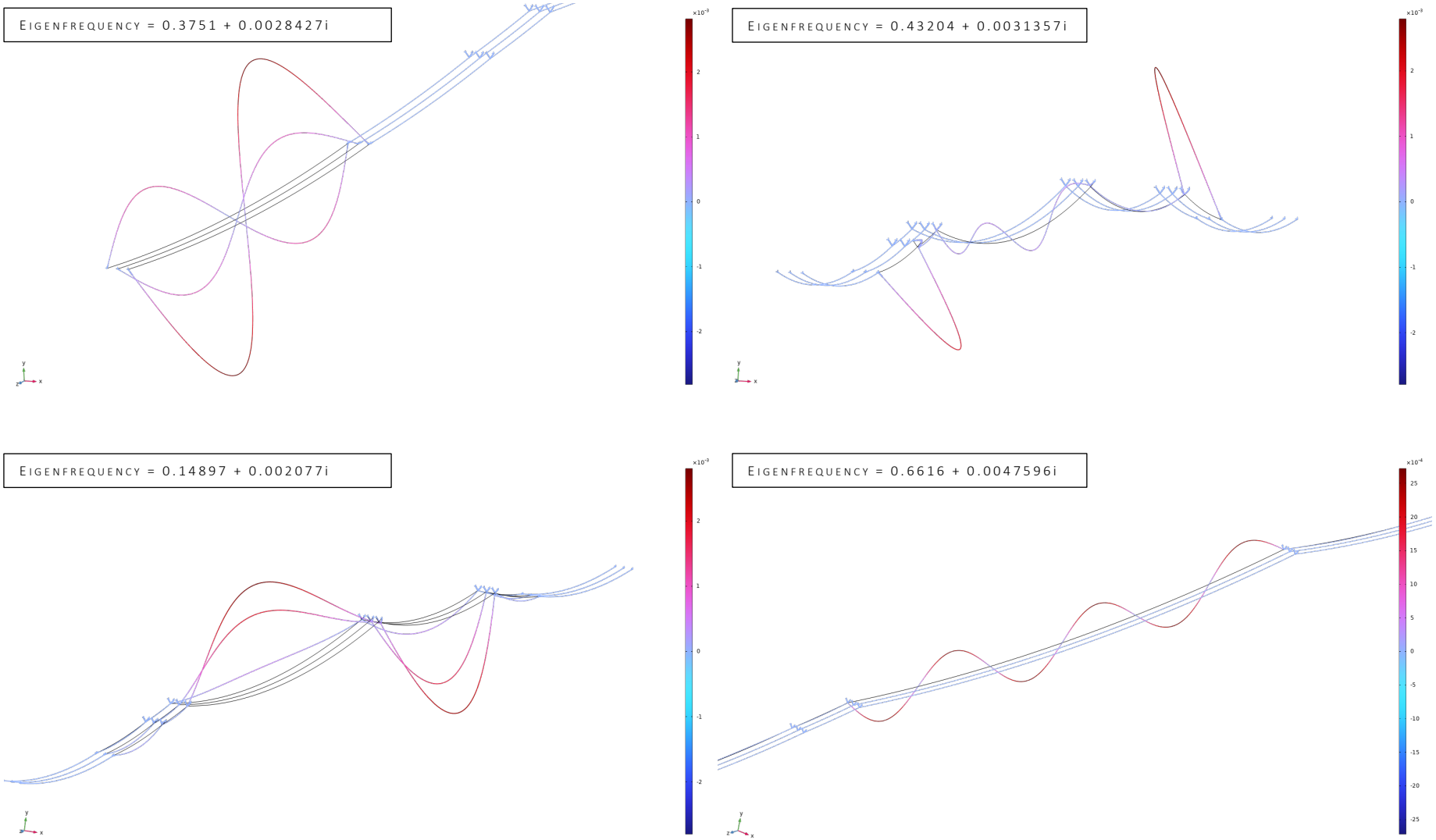

Figure 6.22. Eigenmodes of the conductors displayed in a function of *displacement magnitude [m]*

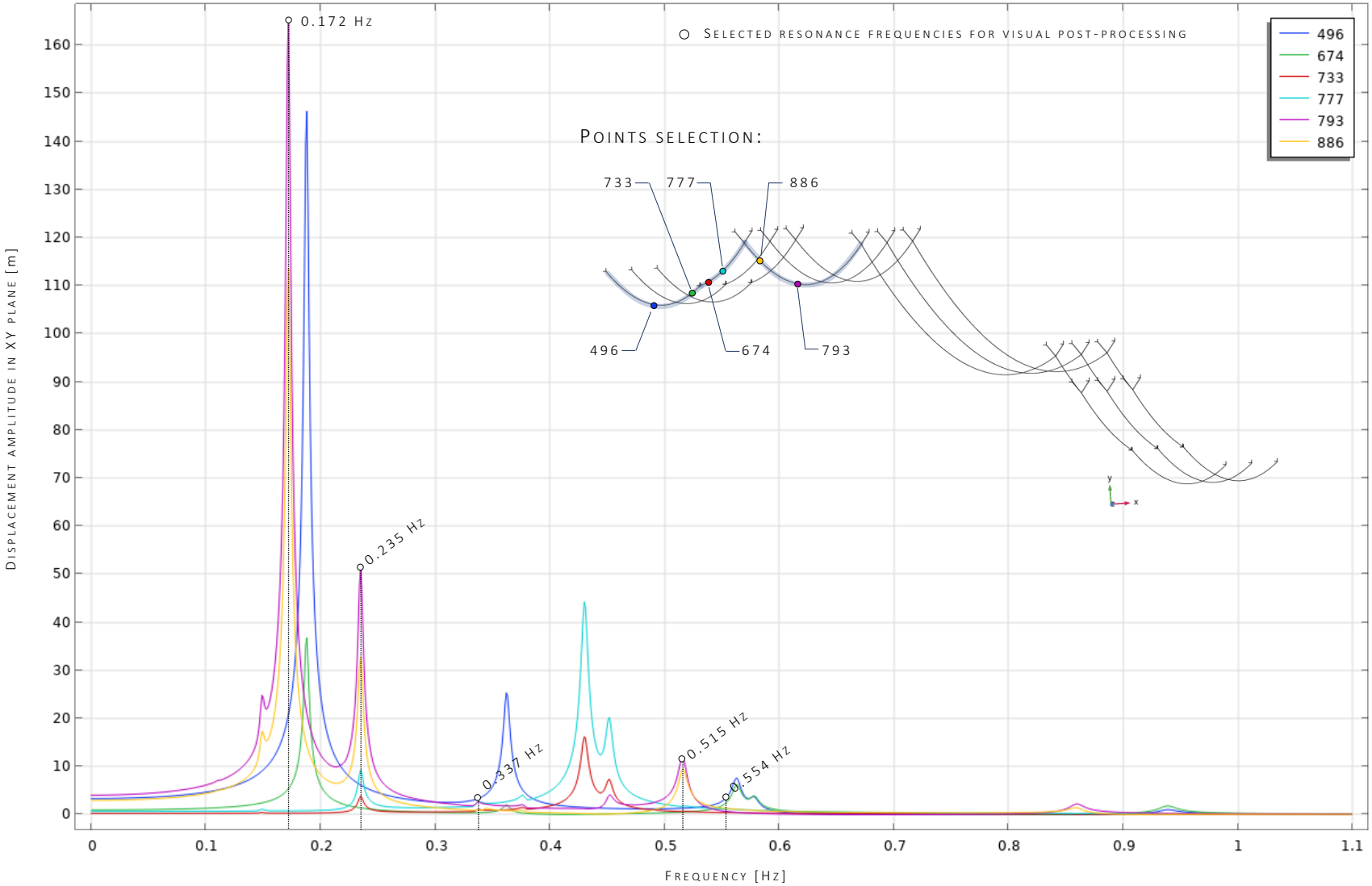

Figure 6.23. Frequency response of selected points for *displacement amplitude in XY plane [m]* with damping factor of conductors $\xi = 0.02$

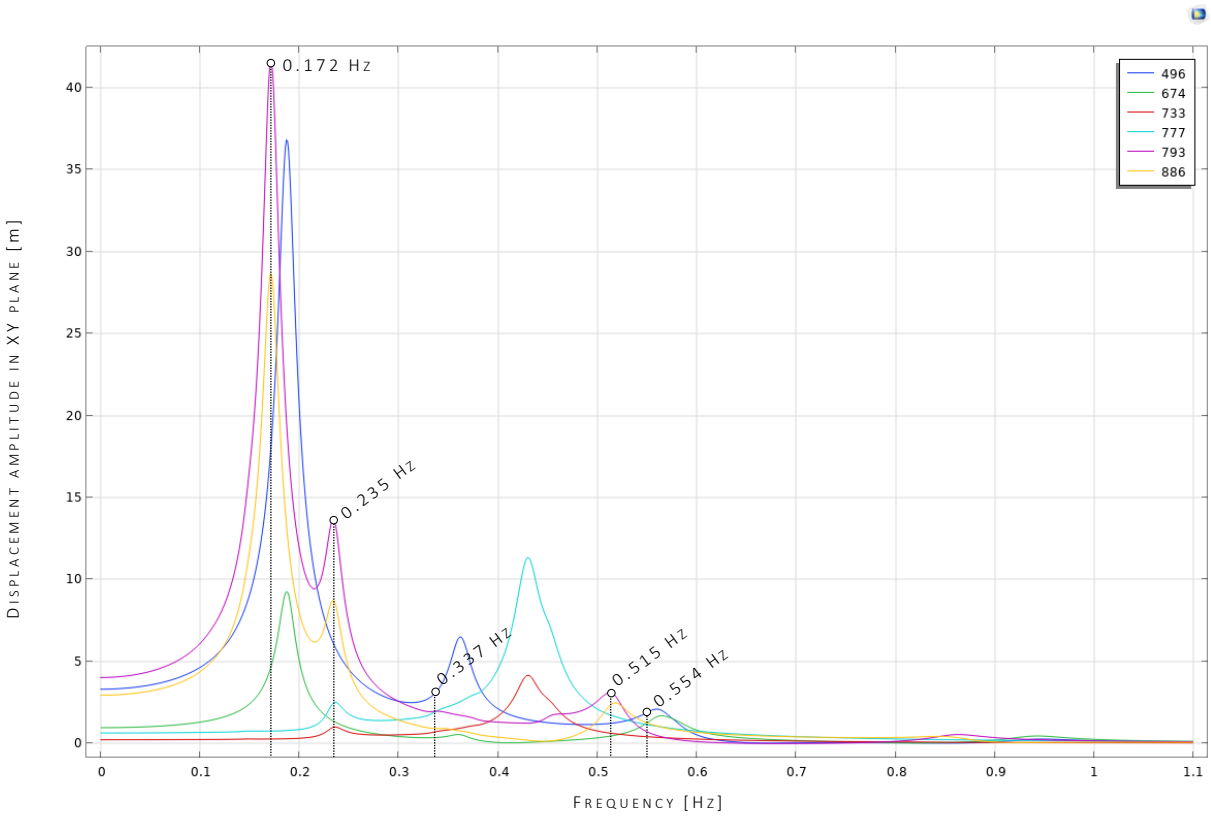

FIGURE 6.24. FREQUENCY RESPONSE OF SELECTED POINTS (SEE FIGURE 6.22) FOR *DISPLACEMENT AMPLITUDE IN XY PLANE [M]* WITH DAMPING FACTOR OF CONDUCTORS $\xi = 0.08$

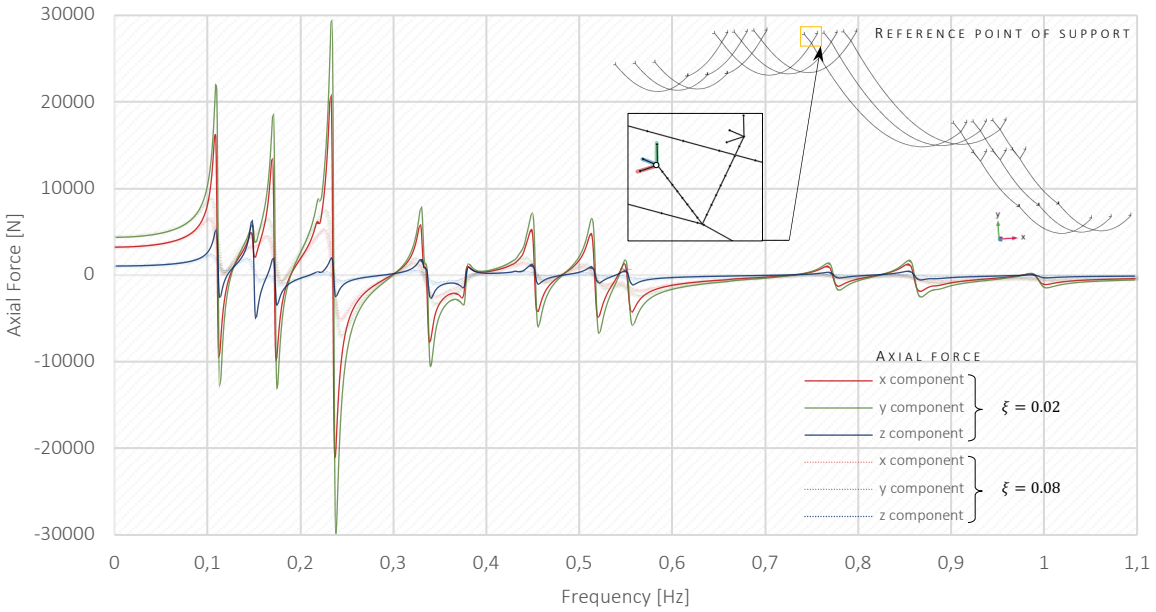

FIGURE 6.25. COMPARISON OF REACTION FORCES ON EXAMPLE COUPLING POINT ON SUSPENSION TOWER DUE TO GALLOPING OF CONDUCTORS FOR DAMPING FACTOR OF CONDUCTORS $\xi = 0.02$ AND $\xi = 0.08$

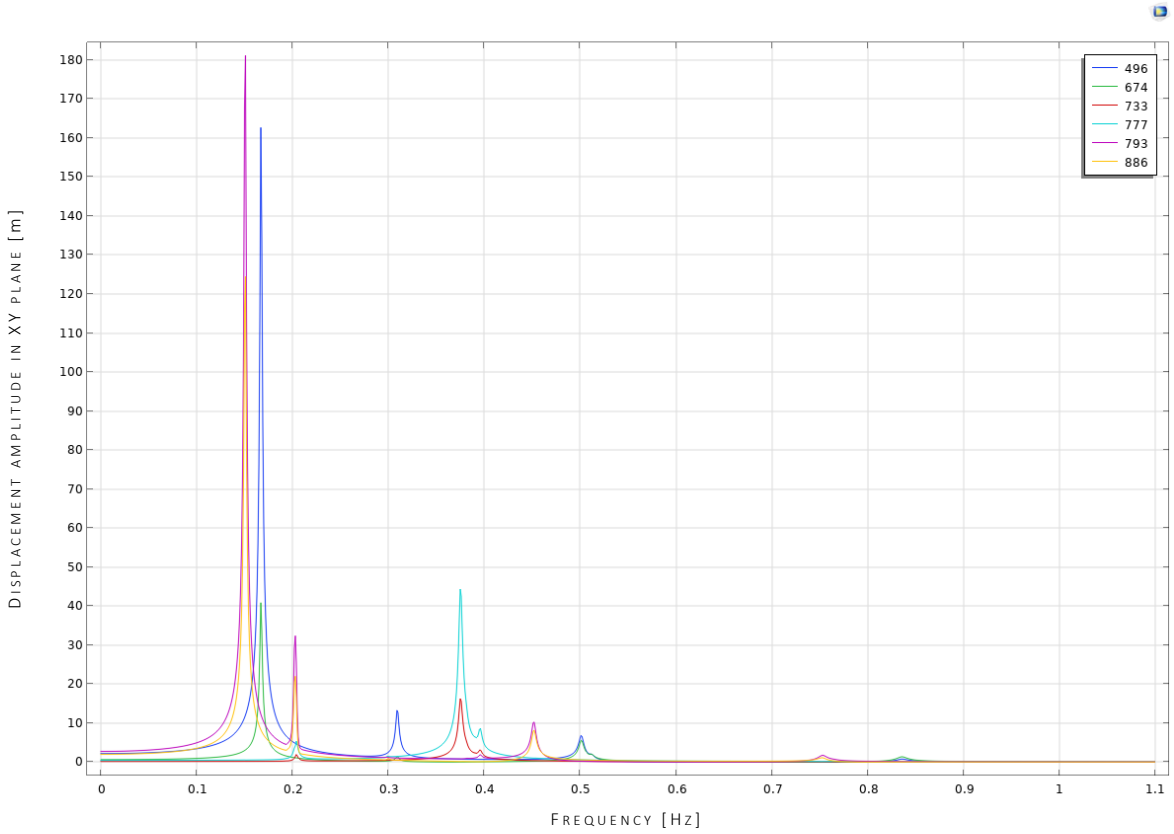

Figure 6.26. Frequency response of selected points (see Figure 6.22) for displacement amplitude in XY plane [m] with damping factor of conductors $\xi = 0.02$ and uniform edge load on conductors 2,5 kg/m

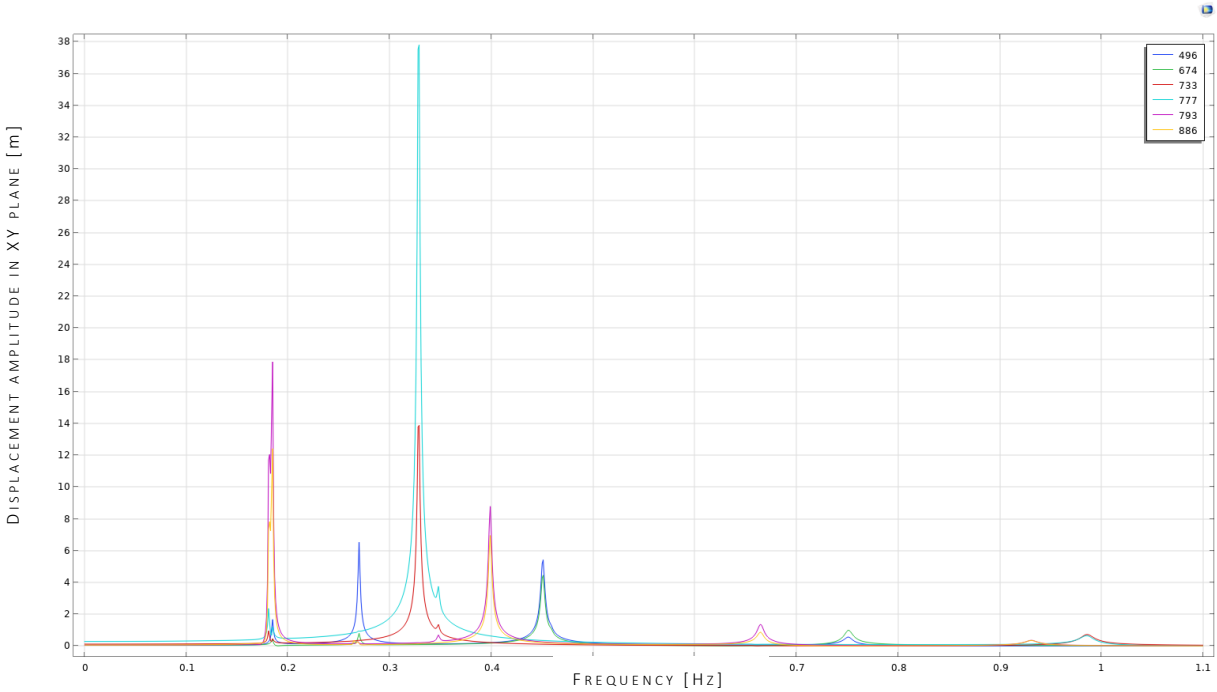

Figure 6.27. Frequency response of selected points (see Figure 6.22) for displacement amplitude in XY plane [m] with damping factor of conductors $\xi = 0.02$ and uniform edge load on conductors 7,5 kg/m

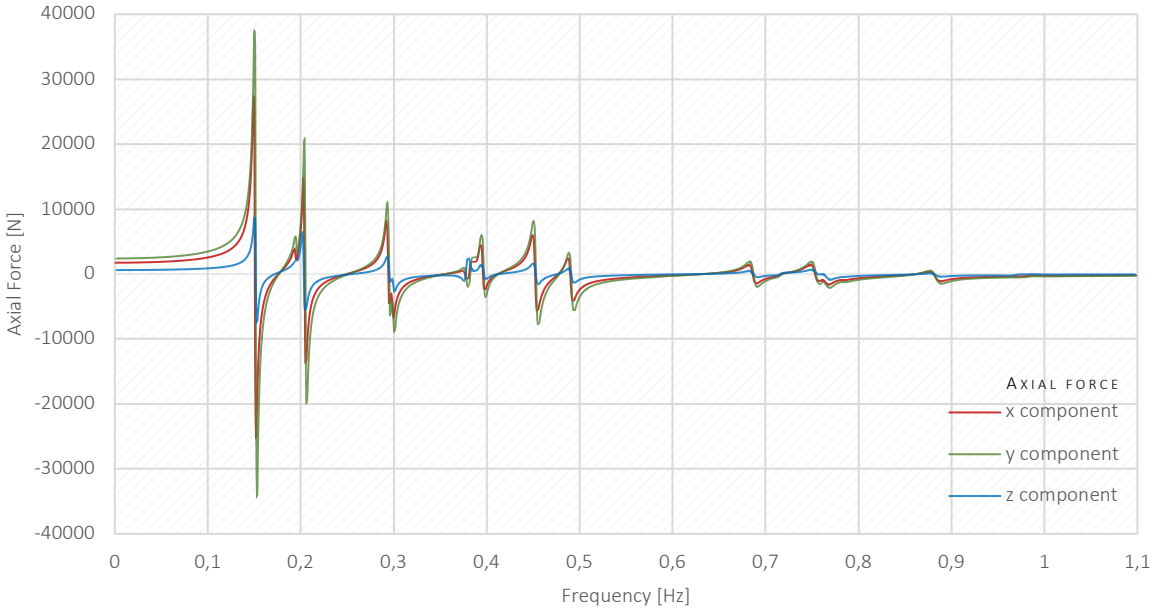

Figure 6.28. Reaction forces on example coupling point (see Figure 6.25) on suspension tower due to galloping of conductors for damping factor of conductors $\xi = 0.02$ and uniform edge load on conductors 2,5 kg/m

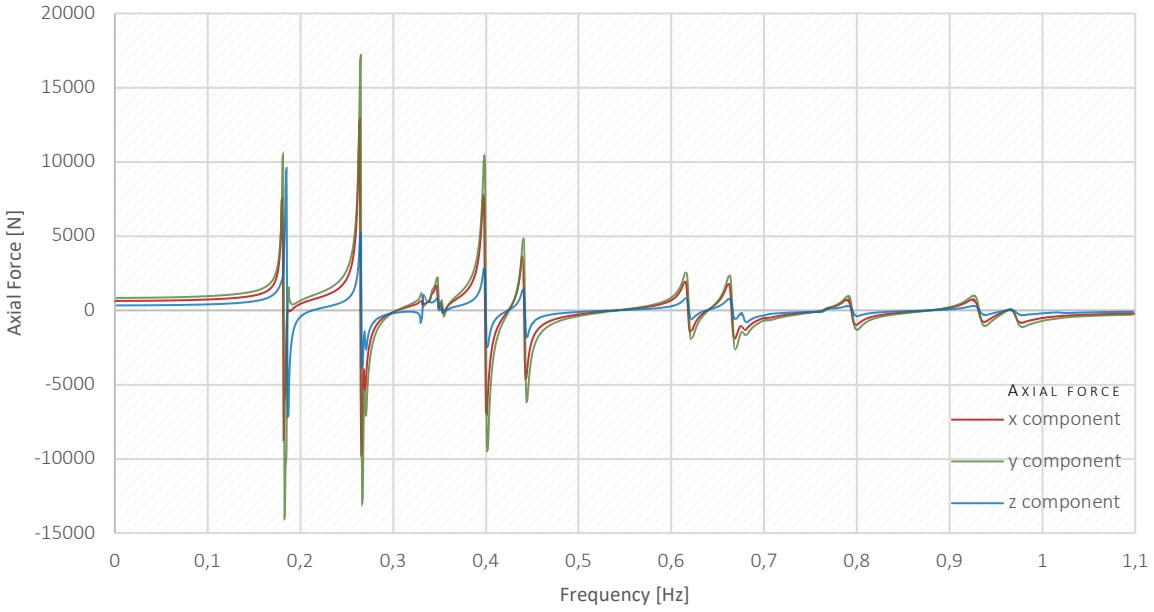

Figure 6.29. Reaction forces on example coupling point (see Figure 6.25) on suspension tower due to galloping of conductors for damping factor of conductors $\xi = 0.02$ and uniform edge load on conductors 7,5 kg/m

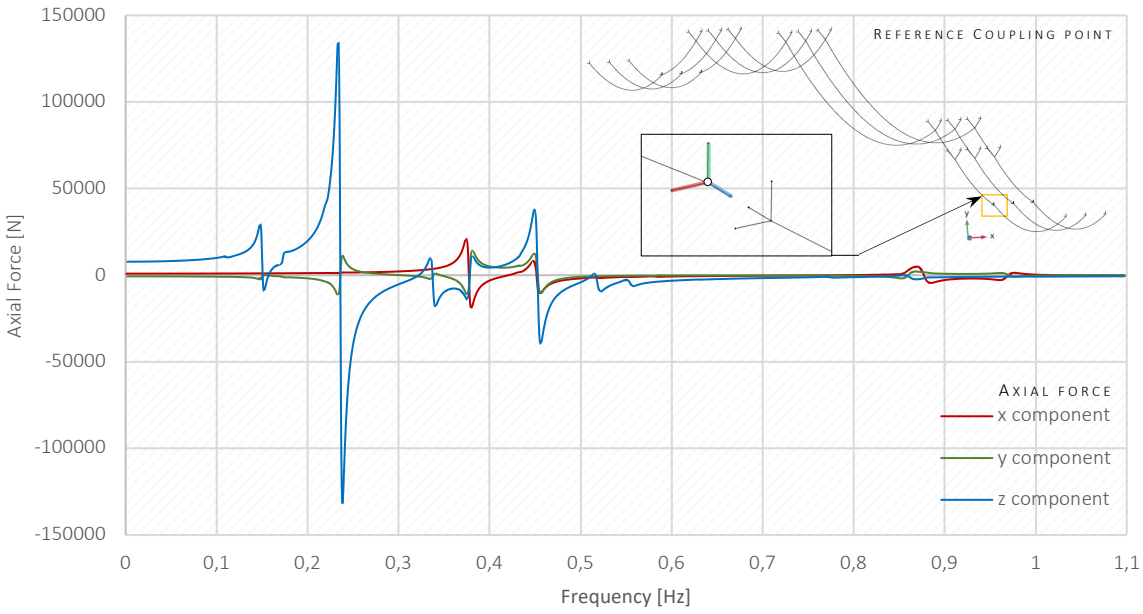

FIGURE 6.30. REACTION FORCES ON EXAMPLE COUPLING POINT ON STRAIN PYLON DUE TO GALLOPING OF CONDUCTORS FOR DAMPING FACTOR OF CONDUCTORS $\xi = 0.02$

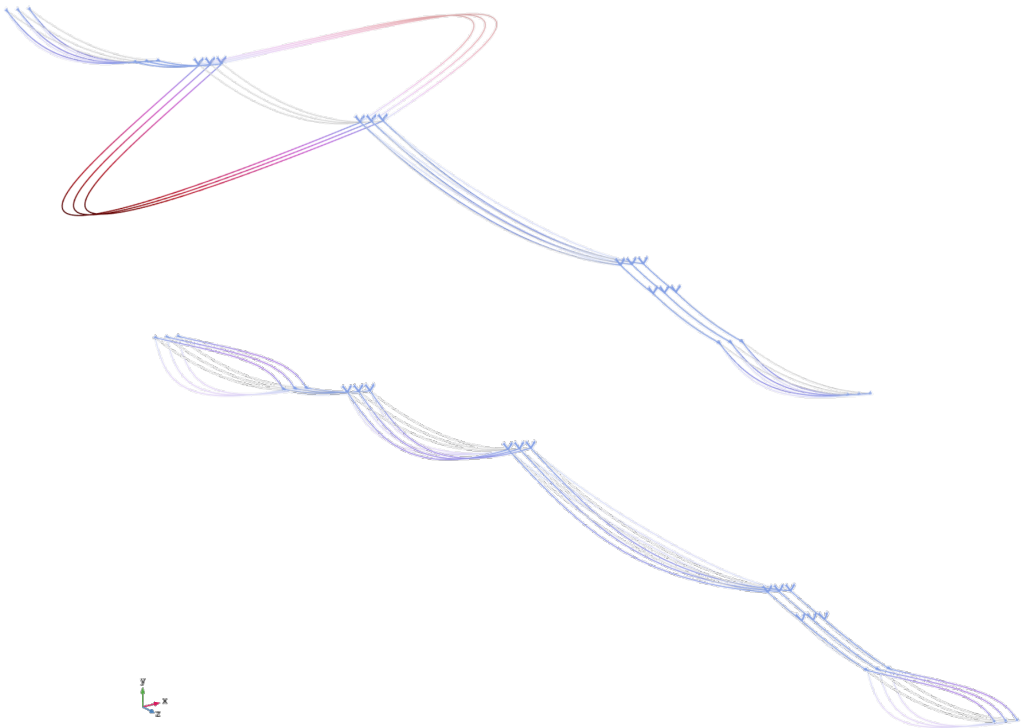

FIGURE 6.31. VISUALIZATIONS OF FULL HARMONIC OSCILLATIONS OF CONDUCTORS SUBJECTED TO WIND LOADING WITH FREQUENCY 0.172 HZ – *LOAD CASE 1* (SCALE FACTOR K=1)

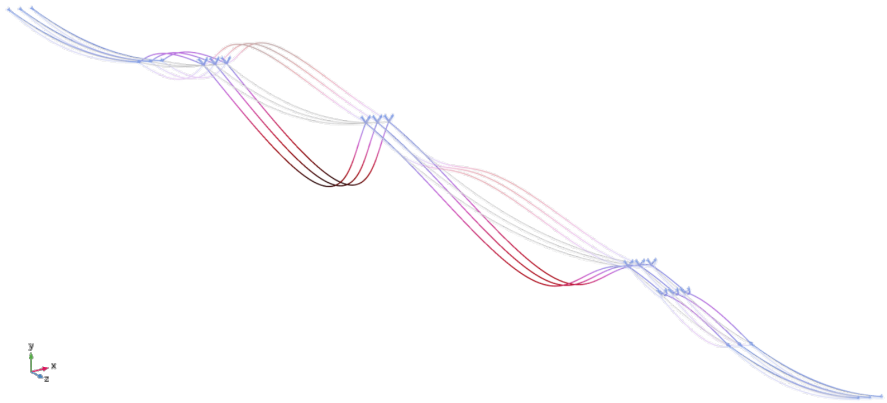

FIGURE 6.32. VISUALIZATIONS OF FULL HARMONIC OSCILLATIONS OF CONDUCTORS SUBJECTED TO WIND LOADING WITH FREQUENCY 0.235 HZ – *LOAD CASE 1* (SCALE FACTOR K=1)

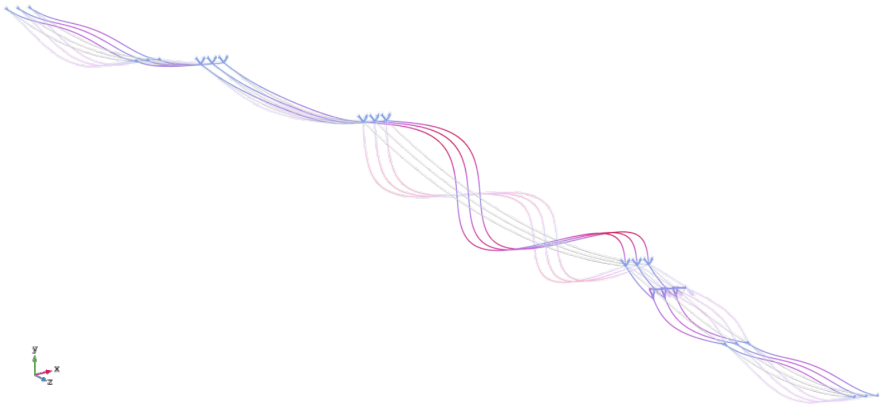

FIGURE 6.33. VISUALIZATIONS OF FULL HARMONIC OSCILLATIONS OF CONDUCTORS SUBJECTED TO WIND LOADING WITH FREQUENCY 0.337 HZ – *LOAD CASE 1* (SCALE FACTOR K=3)

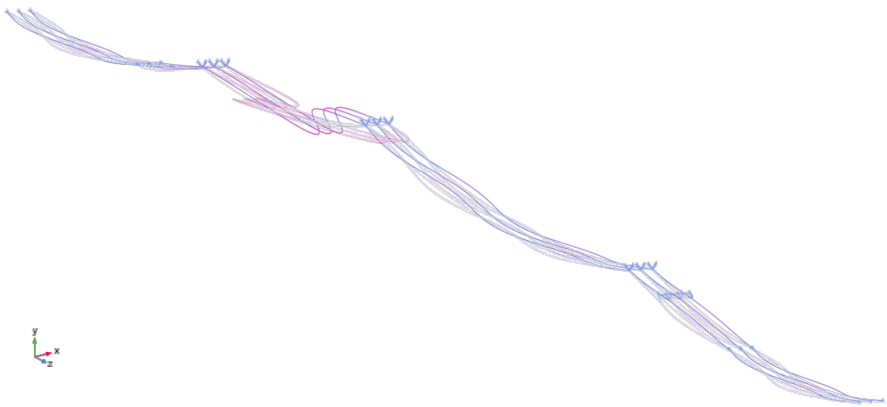

FIGURE 6.34. VISUALIZATIONS OF FULL HARMONIC OSCILLATIONS OF CONDUCTORS SUBJECTED TO WIND LOADING WITH FREQUENCY 0.515 HZ – *LOAD CASE 1* (SCALE FACTOR K=5)

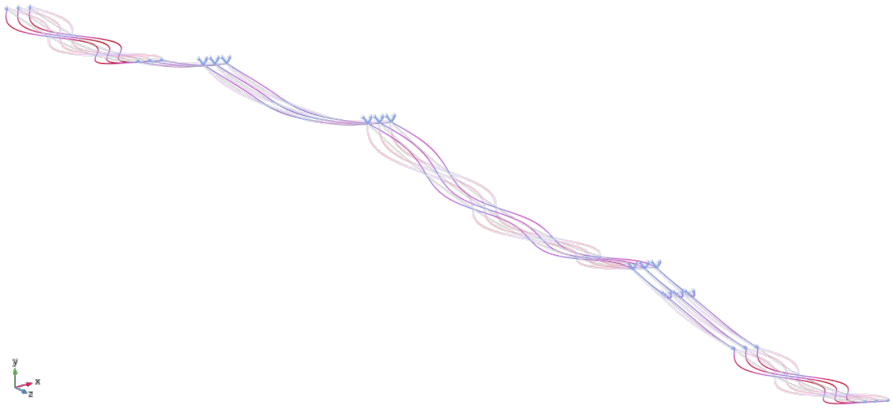

FIGURE 6.35. VISUALIZATIONS OF FULL HARMONIC OSCILLATIONS OF CONDUCTORS SUBJECTED TO WIND LOADING WITH FREQUENCY 0.554 HZ – *LOAD CASE 1* (SCALE FACTOR K=3)

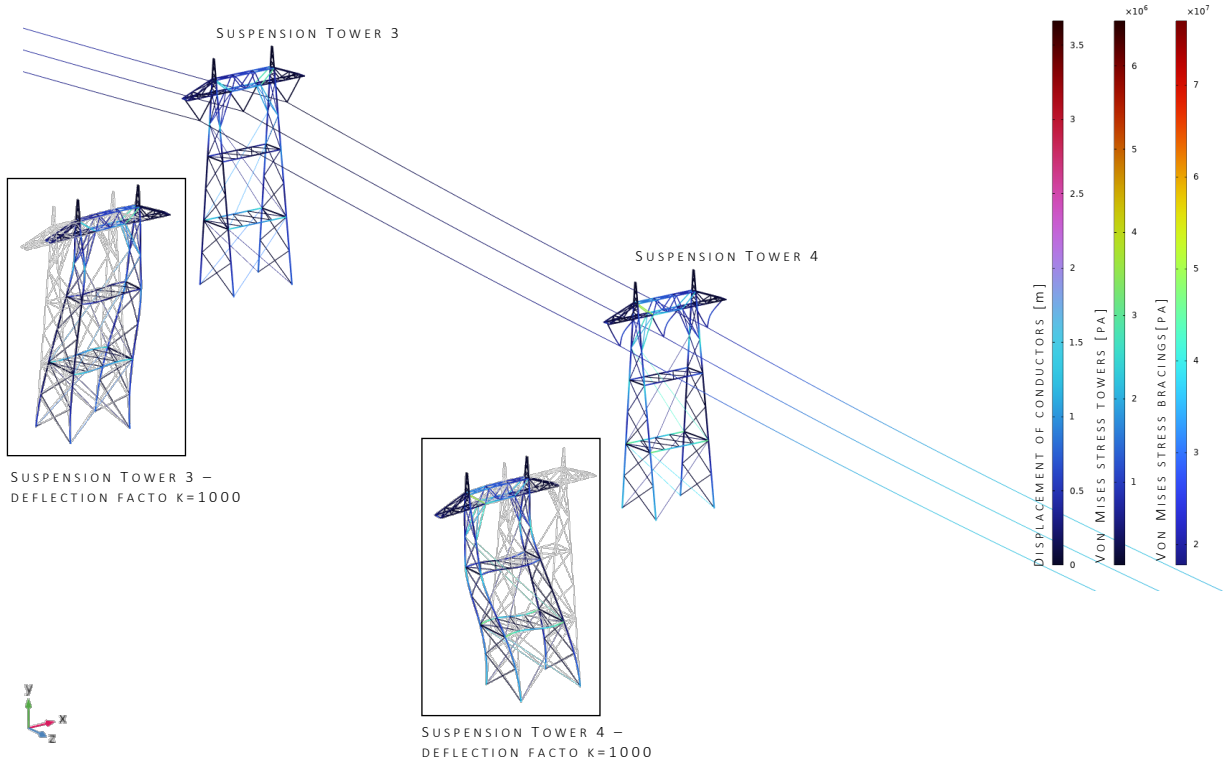

FIGURE 6.36. VISUALIZATION OF DEFORMATION OF TOWERS DUE TO GALLOPING WITH FREQUENCY 0.515 HZ

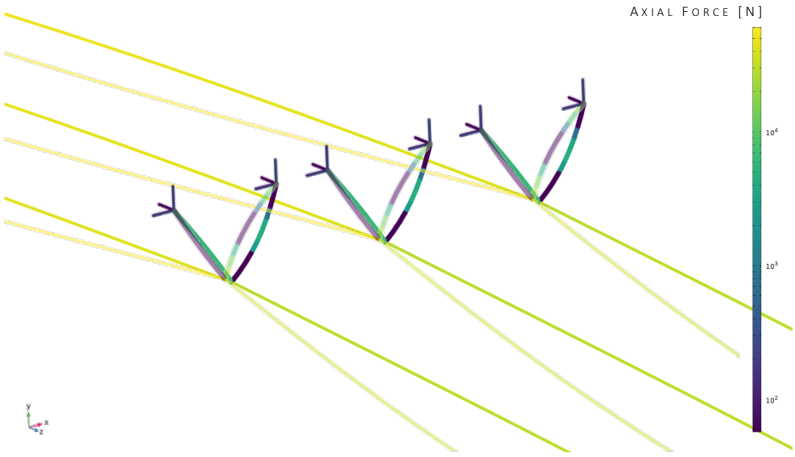

Figure 6.37. Visualizations of full harmonic oscillations of insulators on *suspension tower 3* subjected to wind loading with frequency 0.515 Hz – *Load Case 1* (scale factor k=30)

6.9. Buckling analysis of towers

Based on stress state of structure for predefined loading conditions, the *critical load factor* together with *buckling shapes* are calculated with *linear buckling module* in COMSOL. The factor is the number by which the applied loading has to be multiplied in order to reach the buckling load. This may be taken as the factor of safety against buckling. It must be although emphasize that COMSOL results with Euler´s buckling approach, thus in order to comply the requirements set by standards (Eurocode 3 [99]), the verification with the corresponding buckling curve should be performed. The resulting buckling modes shape for one of the selected towers from the reference power line section (suspension tower 2) are presented in the Figure 6.38.

6.10. Unbalanced load

The unbalanced loading on towers due to uneven ice accretions on conductors is simply modelled with additional mass applied on conductor geometry and performed as steady-state analysis. In case of ice shedding or conductor breakage the force imbalance must be analyzed with time dependent solver. The dynamics of those actions would result in the sudden changes of equilibrium of the computational model with peak values of reactions on coupling points exceeding those that would be obtained with steady state analysis.

The simulation of conductor breakage (see Figure 6.39) under wind loading was performed in time dependent implicit solver for solution time $t_{analysis} = 3\ s$ and time step $t_{step} = 1e\text{-}04\ s$. The breakage of conductor is simulated with sudden exclusion of considered conductor from analysis, with preceding steady-state simulations that considers dead and wind loads. The reaction forces on the coupling points are displayed in time that presents Figures 6.40.1-3. Based on this simulation, the relevance of analyzing the whole section of power line is evident. The breakage of one span contributes indeed to considerable reaction forces on all the towers. The peaks of reaction forces due to dynamic loading exceeds the values for converged solution for resulting unbalanced loading, that is represented with the dotted lines on the Figures 6.40.1-3.

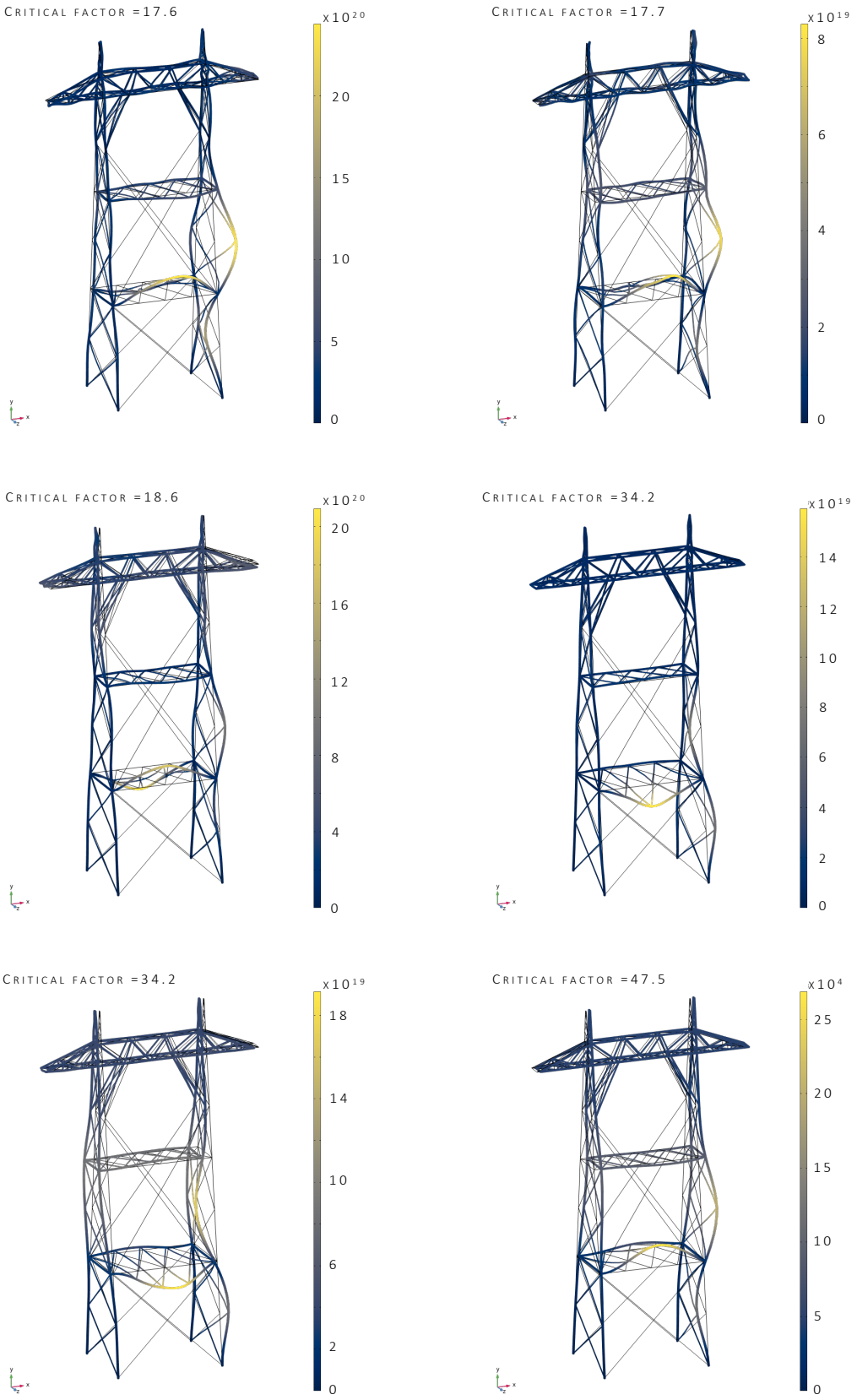

FIGURE 6.38. BUCKLING MODE SHAPES FOR SUSPENSION TOWER 2 DUE TO DEAD LOAD AND INITIAL WIND LOAD CASE

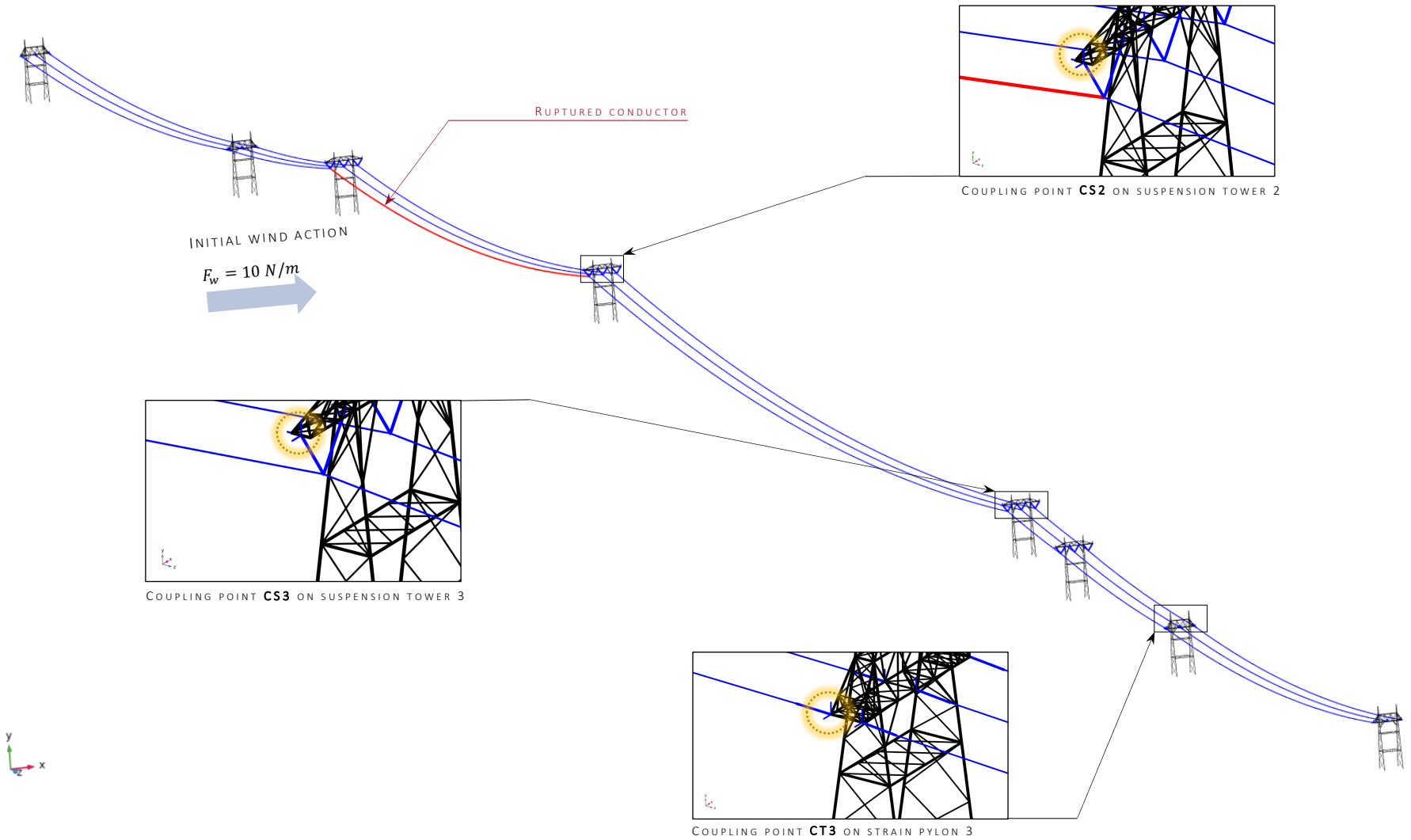

Figure 6.39. Conductor rupture load case setup – coupling points for which reaction forces are displayed

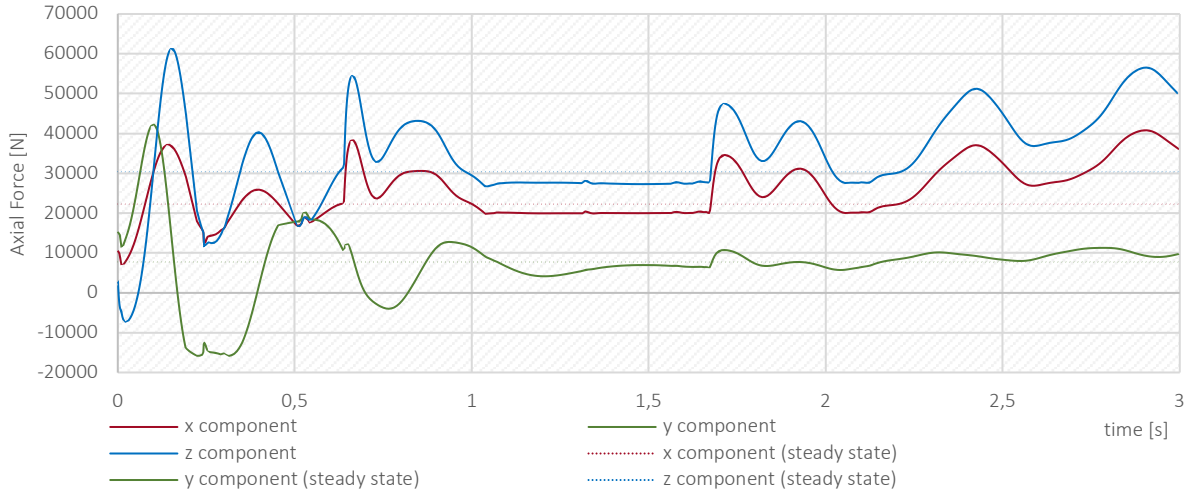

FIGURE 6.40.1. RESULTING REACTION FORCES FOR COUPLING POINT **CS2** DUE TO CONDUCTOR RUPTURE

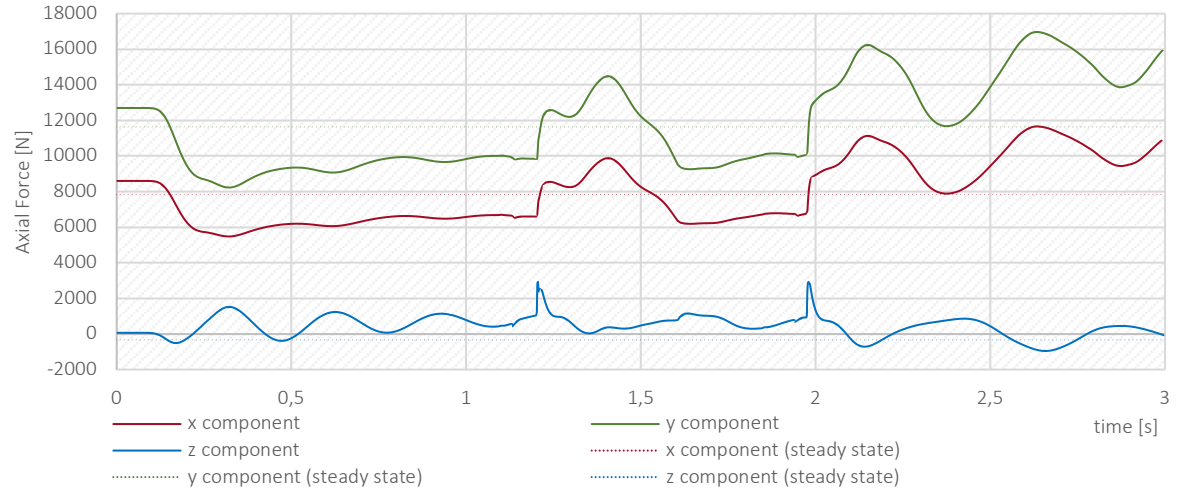

FIGURE 6.40.2. RESULTING REACTION FORCES FOR COUPLING POINT **CS3** DUE TO CONDUCTOR RUPTURE

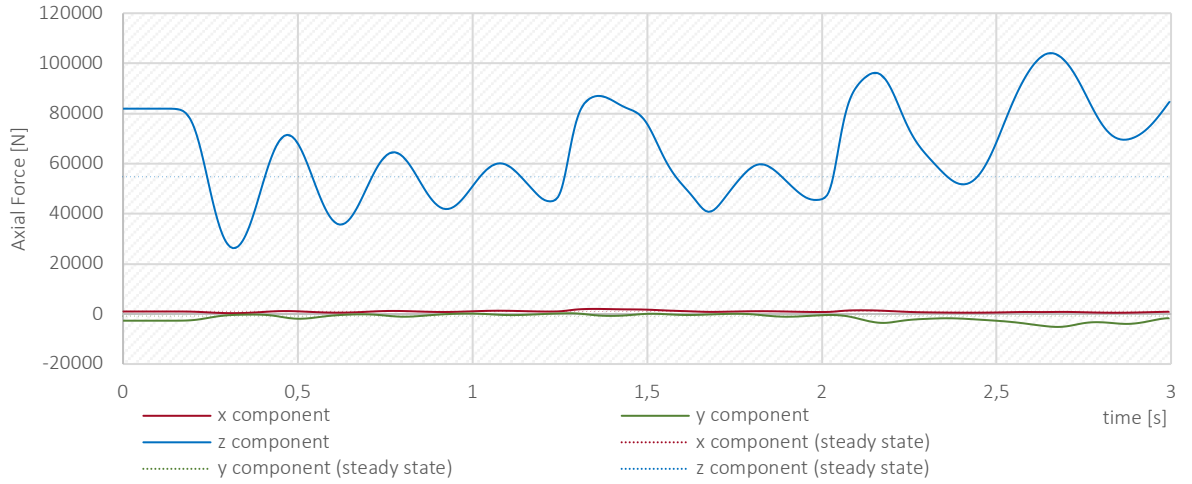

FIGURE 6.40.3. RESULTING REACTION FORCES FOR COUPLING POINT **CT3** DUE TO CONDUCTOR RUPTURE

7. DISCUSSION

Overhead transmission lines exposed to combination of wind and ice loads were found the major design and operational concern for electric distribution networks, especially in sub-arctic terrains such as Norway. Wind loads acting on conductors and earth wires create tensile and compression forces, as well as bending and torsional moments in associated suspension structures, such as poles and towers. Not with significance remains wind loads acting directly on those structures. Among quasi-static interactions of aerodynamic effects, the suspension structures are additionally subjected to wind-induced vibrations of conductors, i.e.: aeolian vibrations and galloping. Such slender constructions may lose stability due to buckle loads of structural members. Icing of powerlines may amplify the vibrations of conductors. The excess weight added to the structure due to accumulating frost and snow contributes to hazardous events and under severe wind conditions the structures might collapse.

MATLAB SCRIPT

The literature study revealed importance of analyzing the power line as the system composed of interdependent components, i.e. power line section consisting of several towers and conductors, instead of analyzing towers individually. Hence, parametrized geometry of power line section consisting of strain and suspension pylons, as well as conductors, was designed with the use of MATLAB, in order to automatize the design process. User-defined geometry was laterally exported to COMSOL Multiphysics software. The set of static and dynamic analysis were performed in order to assess the software´s efficiency to create commercial application for analyzing the powerline with finite element method.

The algorithms that generate the geometry of the power line based on user´s input could be improved in order to reduce solution time of the iterative sequences. For system composed of many towers, placed on different heights, the algorithms may loop for several minutes. The attempt to simplify the adjustment of the catenary curves between towers should be considered.

COMPUTATIONAL MODEL SETUP

With regards to pre-processing of power-line model, different element definitions were assigned to conductors and towers, i.e. respectively truss and beams, thus it was necessary to divide the power line into two separate models coupled with displacements and reaction forces. COMSOL Multiphysics allows to connect trusses and beams, although predefined geometrical nonlinearity of conductors would exert the same conditions for beams, that would result in inefficient time of analysis. Hence, loads applied on model of conductors (and insulator) results in reaction forces in the node connecting conductors to towers. Those forces are laterally applied as the input for analysis of towers. Resulting deflections of towers, i.e. points of conductor-tower connection, serves as boundary condition for conductor analysis.

The work-around of abovementioned coupling, is to design the whole power line as truss structure, that on the one hand would considerably simplify the computation model, however on the other hand would introduce less realistic solution and would limit the application merely to lattice towers.

On the other hand, division of the computational model introduces limitations in interactions between conductors and towers. The oscillations characterized with high amplitude of displacements will results with small but noticeable swings of towers that contributes to oscitation modes. If it would not be included in the model, this may cause inconsistencies with physical results. The dummy lattice structure corresponding to the one modelled with beam elements shall be implemented into model of conductors in order to reflect the system´s degrees of freedom accurately. Laterally, the reaction forces and displacement of conductor model would be applied to model of beam towers.

Frequency domain analysis

The modal analysis module in COMSOL Multiphysics has been found useful to analyze the structure in the frequency domain. Although no straightforward requirement is set by discussed design codes in terms of resonance of power lines, the galloping phenomena may severely affect the power lines due to dynamic loading and shall be thus taken into consideration. For eigenfrequency analysis the damping coefficient of conductors should be obtained as prerequisite in order to prevent the resonance reaching the infinity and obtain computational model which responses are closest to those in the physical state. Establishing of damping is important as the amount of energy dissipated from the system is mainly dependent on conductors and further defines the system of dampers.

Time dependent solution of conductor breakage

In terms of dynamics of unbalanced load, the time-dependent solution requires small time step to relatively large analysis time. Solution time of dynamic calculations such as sudden breakage of pretensioned conductor may takes several hours. The equilibrium would not be reached since it is just a short fraction of sudden response of the system, where the breakage introduces the considerable imbalance. Solver resolves the problem of energy dissipated from conductors and furthermore from the ruptured conductor that falls due to gravitational force, thus obtaining the reaction forces on the coupling points is not straightforward. The simplification for the case of conductor breakage is to calculate the initial loading for steady state solver, i.e. dead and live load, and continuation of the calculations in time dependent solver without the geometry of conductor for which the rupture is aimed to simulate. For the analysis performed in the master thesis it took appx. 100 minutes to simulate the abovementioned conductor rupture for simulation time $t_{analysis} = 3\ s$ with average time step to $t_{step} \approx 1e\text{-}04$ (Processor AMD FX™ - 9590 Eight-Core Processor 4.72 GHz, 32.0 GB RAM). The postprocessing of imbalance of conductors and reaction on coupling points, gives the evident results although might be questioned without model validation. The reaction forces have violent oscillating characteristic with peak values that stabilize over time, however it should not be used as input data for the model of towers

since the interaction between conductors and towers in the same analysis was neglected, i.e. coupling point are independent from each other. The breakage of conductors represents time-consuming solutions and based on performed calculations, the simulation time $t_{analysis} = 3\ s$ was no sufficient to determine the maximum loading acting on towers due to continuous oscillations. Nevertheless, the finite element method gives better understanding of dynamic phenomena and was found useful for further development and optimization of the dynamic interactions.

Ice shedding

In case of ice shedding the solution similar to the above mentioned may be applied. Instead of excluding the conductor form the analysis the solver introduces sudden reduction of mass applied on the edge of conductor.

Buckling of structural members

For the buckling analysis the COMSOL Multiphysics does not provide built-in setup that allows to distinguish between live and dead loads. The magnifying factor is thus related to both gravitational load acting on towers, as well as loads representing atmospheric actions. Such solution verifies efficiently the risk of buckling as long as the critical load factor remains ≤ 1. From the optimalization point of view this limitation shall be addressed with a solution provided by COMSOL [105] that relates the critical load factor directly to live loads. This was not done yet in the scope of master thesis.

8. CONCLUSIONS

This master thesis addresses the structural aspect of transmission towers subjected to atmospheric loading with insight into possibilities to facilitate the design process in commercial software COMSOL Multiphysics. Key aspects and engineering practices of structural design of overhead power lines were first discussed, followed by the finite element analysis of the example power line section in COMSOL Multiphysics software.

The design codes related to structural analysis of power lines, i.e. EN 50341-1:20212 [7], EN 50341-2-16:2016 , NEK IEC 60826:2017 [56] and Eurocode 3 [87], were studied, that led to straightforward summary and guideline for analyzing the supporting structures subjected to different arrangements of atmospheric loading. It does not cover the fatigue analysis of the structures. The considerations related to limitations of the design codes were discussed in the summary of section 4 of this thesis. Furthermore, buckling of the towers' members as the design load was discussed.

A major part of this work is establishing the parametrized geometry of power line section that includes strain and suspension towers, conductors in a form of catenaries and insulators with MATLAB script, proceeded with set of static and dynamic analysis in COMOSL Multiphysics. The workarounds of difficulties and limitations of the software that were encountered, such as modelling of coupling, were discussed.

The final conclusion is that the performed work is just a tip of an iceberg of the considerations over structural analysis of power lines, although it gives good understanding of significance with which structural engineers have to face up. The complexity of interactions between conductors and tower generates numerous of uncertainties that are considered for the analysis of the structure, thus understanding of physics behind structural aspect of power line is crucial. Furthermore, although obtained computational model is characterized with flexibility of performing different types of structural analysis with adjustable boundary conditions, the results shall be validated with physical reference.

9. FURTHER WORK

(1) Primarily, the validations of the model with physical reference must be done.

(2) Furthermore, *COMSOL Multiphysics Compiler* would allow to create interface for parametrized modeling and user-oriented FEM analysis with predefined input data, i.e. type of structure, loading, automatically applied boundary conditions, etc. The desired solution would integrate loads on structure either from standardized requirements or from subsystem application for power line design. The solution could take advantage of up-to date atmospheric database to incorporate wind and icing loads and increase the reliability of power lines, as well as reduce a risk of failure due to the hazardous events.

(3) The buckling curves that represents inelasticity should be incorporated into the software in order to comply safety requirements set by design codes (Eurocode 3 [99]),

(4) The investigation of aeolian vibration with possibilities of implementation model of dampers that would limit its impact on conductors and fittings should be considered.

(5) Model of conductors must be developed with *dummy* towers in order to accurately reflect degrees of freedom of the model.

(6) The procedure of analyzing conductor failure and ice shedding is going to be further investigated.

APPENDIX 1 POWER LINE DESIGN CODE FOR MATLAB

```
clear all
clc

syms H mc g x x_prim xA xB yA yB ae fe


% Sample parameters of power line

    mc  =   1.5;        % weight of conductor kg/m
    g   =   9.81;       % gravity acceleration m/s^2

    condition = 1;
    while condition == 1
        nt  = input(['Enter number of suspension towers in a section (between 1 and 10):\n']);
        if nt>=1 && nt<=10
            condition=0;
            else    condition=1;
                    fprintf('WARNING! Number of towers must be in a range <1;10>:\n')
        end
    end

      condition = 1;
    while condition == 1
        ht  = input(['Enter elevation of supsension point for conductors above the ground (between 20 m
and 40 m):\n']);
        if ht>=20 && ht<=40
            condition=0;
            else    condition=1;
                    fprintf('WARNING! Elevation must be in a range <20;40> [m]:\n')
        end
    end
   condition = 1;
    while condition == 1
        insL  = input(['Enter length of strain elevator (between 1.5 m and 4.5 m):\n']);
        if insL>=1.5 && insL<=4.5
            condition=0;
            else    condition=1;
                    fprintf('WARNING! Length of the insulators must be in a range <1.5;4.5> [m]:\n')
        end
    end

    % matrix with length of spans ae
    ae              =  zeros(nt+3,1);
    ae(1)           =  400;
    ae(nt+3)        =  400;
    h               =  zeros(nt+4,1);


    % matrix with hirizontal tension H
    H             =  zeros(nt+3,1)+30338;

     % matrix with strain insulators coordinates
    insLm             =  zeros(6,6);

    % User defined spans
    n=2;
    while nt+2 >= n
        condition=1;
        while condition == 1

        ae(n) = input(['Enter length [m] of span no.: '  num2str(n) ' between 100 m and 800 m\n']);
            if ae(n)>=100 && ae(n)<=800
            condition=0;
            n=n+1;
            else    condition=1;
                    fprintf('WARNING! Length of span must be in a range <100 m;800 m>\n')
            end
        end
    end

% User defined elevation
    n=2;
    fprintf (['Designed power line consist of ' num2str(nt+2) ' towers,\n i.e.: 2 strain towers on each
end of designed section and ' num2str(nt) ' suspension towers\n\n']);
    while nt+3 >= n
        condition=1;
        while condition == 1
        h(n) = input(['Enter elevation of tower no.:' num2str(n-1) ' between value 0 m and 50 m from
reference level 0 m\n']);
            if h(n)>=0 && h(n)<=50
            condition=0;
            n=n+1;
            else    condition=1;
                    fprintf('WARNING! Choose elevation in a range of <0;50>:\n')
            end
        end
    end

    h(1)=h(2);
    h(nt+4)=h(nt+3);

% Matrix for coordinates of points of support
    co=zeros(nt+4,4);
    co

% Matrix for sag
    sags=zeros(nt+3,4);

% Matrix for values of difference in elevation between consequitive supports eldif
    n=1;
    eldif = zeros(nt+3,1);
    while nt+3 >= n
        eldif(n)=h(n+1)-h(n);
        n=n+1;
    end

% Sag calculations for each span TENSION ADJUSTMENT
n=1;
while nt+3 >= n
    fprintf(['Creating span no. ' num2str(n) '\n'])
    % adjust tension
    condition = 1;
    while condition == 1
        co(n,1) =   -ae(n)/2;
        co(n,2) =   (H(n)/(mc*g))*((cosh(mc*g*ae(n)/(2*H(n))))-1);
        xB      =   co(n,1)+ae(n);
        yB      =   co(n,2)+eldif(n);

        y           =       @(x) (H(n)/(mc*g))*((cosh((mc*g/H(n))*x))-1);
        ytriangle   =       @(x) (((yB-co(n,2))/(xB-co(n,1)))*x)+co(n,2)+(co(n,1)*(co(n,2)-yB)/(xB-
co(n,1)));
        ytriangle1  =       diff(ytriangle,x);
        Lfunction   =       sqrt(1+((ytriangle1)^2));
        LAB         =       int(Lfunction,x,'IgnoreAnalyticConstraints',true,co(n,1),xB);


        cross               =         fzero(@(x) (y(x))-ytriangle(x), 2*xB);

        if co(n,2)>yB && (isnan(cross) || cross <=0.99*co(n,1)) && n>1 && n<nt+3
            H(n,1)=H(n,1)-50;
            condition = 1;
        elseif (co(n,2)<yB && n>1 && n<nt+3) || (co(n,2)<yB && n>1 && n<nt+3 && (isnan(cross) || cross
<=0.99*co(n,1)))
                ymirror             =         @(x) -y(x)+(2*(co(n,2)));
                cross               =         fzero(@(x) ymirror(x)-ytriangle(x), 2*xB);
                if cross <=0.99*co(n,1) || (cross <=0.99*co(n,1) || isnan(cross))
                     H(n,1)=H(n,1)-50;
                     condition = 1;
                else
                    condition = 0;
                end
        else
            condition = 0;
        end


    end

   fprintf(['Tension of span no. ' num2str(n) ' = .\n' num2str(H(n,1)) ' [N]\n']);
   fprintf(['Span no. ' num2str(n) ' numerical adjustment.\n']);
    dx=1e-1;
    xAS=co(n,1);
    if eldif(n)<=0
        length=0;
        while length<LAB
            if eldif(n)<0
            xAS           =         xAS-dx;
            else
```

(a)

```
        length = LAB;
                    co(n,3)       =        xB;
                    co(n,4)       =        yB;
                    sags(n,1)     =        0;
                    sags(n,2)     =        yB;
                    sags(n,3)     =        0;
                    sags(n,4)     =        yB;
                    break
            end

             yAS           =         (H(n)/(mc*g))*((cosh((mc*g/H(n))*xAS))-1);
             ytriangle2    =         @(x) ((((yAS+eldif(n))-yAS)/((xAS+ae(n))-xAS))*x)+yAS+(xAS*(yAS-
(yAS+eldif(n)))/((xAS+ae(n))-xAS));
             co(n,3)       =         fzero(@(x) y(x)-ytriangle2(x), xB);
             co(n,4)       =         (H(n)/(mc*g))*((cosh((mc*g/H(n))*co(n,3)))-1);
             ytriangle21   =         diff(ytriangle2,x);
             Lfunction     =         sqrt(1+((ytriangle21)^2));
             length        =         int(Lfunction,x,'IgnoreAnalyticConstraints',true,xAS,co(n,3));
             co(n,1)=xAS;
             co(n,2)=yAS;


        end
    elseif  eldif(n)>0
            length=LAB+1;
            while     length>LAB
                      xAS           =         xAS+dx;
                      yAS           =         (H(n)/(mc*g))*((cosh((mc*g/H(n))*xAS))-1);
                      ytriangle2    =         @(x) ((((yAS+eldif(n))-yAS)/((xAS+ae(n))-
xAS))*x)+yAS+(xAS*(yAS-(yAS+eldif(n)))/((xAS+ae(n))-xAS));
                      co(n,3)       =         fzero(@(x) y(x)-ytriangle2(x), 2*xB);
                      co(n,4)       =         (H(n)/(mc*g))*((cosh((mc*g/H(n))*co(n,3)))-1);
                      ytriangle21   =         diff(ytriangle2,x);
                      Lfunction     =         sqrt(1+((ytriangle21)^2));
                      length        =
int(Lfunction,x,'IgnoreAnalyticConstraints',true,xAS,co(n,3));
                      co(n,1)=xAS;
                      co(n,2)=yAS;
            end

     end

     fprintf(['Span no. ' num2str(n) ' sag calculations.\n']);

             if eldif(n)<0 || eldif(n)>0
             sagi=xAS;
             sagcondition=0;
             sagcondition2=1;

                while sagcondition<=sagcondition2
                 sags(n,2)=ytriangle2(sagi);
                 sags(n,3)=y(sagi);
                 sagcondition=sags(n,2)-sags(n,3);

                 sagi=sagi+0.01;

                 sags(n,2)=ytriangle2(sagi);
                 sags(n,3)=y(sagi);
                 sags(n,1)=sagi;

                 sagcondition2=sags(n,2)-sags(n,3);

                 end
                fx=sagcalc(ae(n),H(n),mc,g,xAS,eldif(n),sagi);
                sags(n,4)=fx;
             end

             if sags(n,4)>=0.75*ht
                 H(n,1)=H(n,1)+3500;
                 n=n;
                 fprintf(['Sag of span no. ' num2str(n) ' colides with ground. Tension adjustmen is
performed \n']);
             else n=n+1;

             end

end

vector=zeros(nt+3,2);

vector(1,2)=-co(1,2)+ht+h(1);

n=2;
while n<=nt+3
   vector(n,1) = co(n-1,3)-co(n,1)+vector(n-1,1);
   vector(n,2) = co(n-1,4)-co(n,2)+vector(n-1,2);
   n=n+1;
```

```
end

n=1;

tiledlayout(2,1)
nexttile

while n<=nt+3
   y          =       @(x) (H(n)/(mc*g))*((cosh((mc*g/H(n))*x))-1);
   ytriangle2   =         @(x) ((((co(n,2)+eldif(n))-co(n,2))/((co(n,1)+ae(n))-
co(n,1)))*x)+co(n,2)+(co(n,1)*(co(n,2)-(co(n,2)+eldif(n)))/((co(n,1)+ae(n))-co(n,1)));
   fplot(@(x) y(x-vector(n,1))+vector(n,2), [co(n,1)+vector(n,1) co(n,3)+vector(n,1)],'Color','#0072BD')
   hold on
   plottriangle(co(n,1)+vector(n,1),co(n,2)+vector(n,2),ht)
   hold on
   fplot(@(x) ytriangle2(x-vector(n,1))+vector(n,2), [co(n,1)+vector(n,1) co(n,3)+vector(n,1)],':k')
   hold on
   plot([sags(n,1)+vector(n,1) sags(n,1)+vector(n,1)],[sags(n,2)+vector(n,2)
sags(n,3)+vector(n,2)],'Color','#D95319')
   hold on
   txt = [' f = ' num2str(sags(n,4)) ' m '];
   text(sags(n,1)+vector(n,1),sags(n,2)-(0.5*sags(n,4))+vector(n,2),txt)
   hold on
   txt2 = [' H = ' num2str(H(n)) ' N '];
   text(sags(n,1)+vector(n,1),sags(n,3)-2+vector(n,2),txt2)
   hold on
   ytr=[co(n,2)+vector(n,2)-ht co(n,4)+vector(n,2)-ht];
   xtr=[co(n,1)+vector(n,1)+ht*tand(15) co(n,3)+vector(n,1)-ht*tand(15)];
   plot(xtr,ytr,'Color','#77AC30')
   hold on
   n=n+1;

end

plottriangle(co(n,1)+vector(n-1,1)+200,co(n-1,2)+vector(n-1,2),ht)
hold on

ylim padded
xlabel('Horizontal distance [m]')
ylabel('Height above reference level 0 [m]')
hold off
grid on

%space alocation for matrixes with XY data for each catenary
fprintf(['Space allocation for 3D data of spans\n']);
n=1;
while n<=nt+3
        i=0.1;
        size=2;
       while (co(n,1)+i)<(co(n,3)-0.05)
           size=size+1;
           i=i+0.1;

       end
    A{n} = zeros(size, 6);
    n=n+1;
end

%Write xy data of each catenary into array of matrixes in the same coordinate system
n=1;
fprintf(['Extracting series of points to create 3D representation of catenary\n']);
while n<=nt+3
        i=0.1;
        k=1;
        A{n}(k,1)=co(n,1);
        A{n}(k,2)=co(n,2);
        while (A{n}(k,1)+i)<(co(n,3)-0.05)
            k=k+1;
            A{n}(k,1)=A{n}(k-1,1)+i;
            A{n}(k,2)=(H(n)/(mc*g))*((cosh((mc*g/H(n))*(A{n}(k,1))))-1);
            A{n}(k-1,4)=A{n}(k,1);
            A{n}(k-1,5)=A{n}(k,2);

        end

       A{n}(k+1,1)=co(n,3);
       A{n}(k+1,2)=co(n,4);
       A{n}(k,4)=A{n}(k+1,1);
       A{n}(k,5)=A{n}(k+1,2);



    n=n+1;
end
```

```
%single curve representation of catenary
fprintf(['Creating single catenary curve\n']);
n=1;
while n<=nt+3

   k=1;
   while k<=height(A{n})
   A{n}(k,1)=A{n}(k,1)+vector(n,1);
   A{n}(k,2)=A{n}(k,2)+vector(n,2);
   A{n}(k,4)=A{n}(k,4)+vector(n,1);
   A{n}(k,5)=A{n}(k,5)+vector(n,2);
   k=k+1;
   end
   n=n+1;
end

%Add insulator
fprintf(['Adjustment of insulators to catenary tension\n']);
n=1;
k=1;
while n<=nt+3

    if n<=2 || n>=nt+2

        length=0;
        xl1=A{n}(1,1);
        yl1=A{n}(1,2);
        insLm(k,1)=xl1;
        insLm(k,2)=yl1;
        p=0;
        while length<insL && (n<=2 || n==nt+3)


             A{n}(1,:)=[];

             xl2=A{n}(1,1);
             yl2=A{n}(1,2);
             yconductor   =       @(x) (((yl2-yl1)/(xl2-xl1))*x)+yl1+(xl1*(yl1-yl2)/(xl2-xl1));
             yconductor1  =       diff(yconductor,x);
             Lconductor   =       sqrt(1+((yconductor1)^2));
             length        =         int(Lconductor,x,'IgnoreAnalyticConstraints',true,xl1,xl2);

             insLm(k,4)=xl2;
             insLm(k,5)=yl2;


         p=1;
        end
             if p==1
                k=k+1;
             end

        length=0;
        [s1 s2]=cellfun(@size,A(n),'UniformOutput',false);
        size=cell2mat(s1);
        xl1=A{n}(size,1);
        yl1=A{n}(size,2);
        insLm(k,1)=xl1;
        insLm(k,2)=yl1;
        p=0;
        while length<insL && (n==1 || n>=nt+2)


             A{n}(size,:)=[];

            [s1 s2]=cellfun(@size,A(n),'UniformOutput',false);
             size=cell2mat(s1);
             xl2=A{n}(size,1);
             yl2=A{n}(size,2);

             yconductor   =       @(x) (((yl2-yl1)/(xl2-xl1))*x)+yl1+(xl1*(yl1-yl2)/(xl2-xl1));
             yconductor1  =       diff(yconductor,x);
             Lconductor   =       sqrt(1+((yconductor1)^2));
             length        =         int(Lconductor,x,'IgnoreAnalyticConstraints',true,xl2,xl1);



             insLm(k,4)=xl2;
             insLm(k,5)=yl2;
             p=1;
        end
            if p==1
                k=k+1;
            end

    end
```

```
    [s1 s2]=cellfun(@size,A(n),'UniformOutput',false);
    size=cell2mat(s1);
    A{n}(size,:)=[];
    n=n+1;
end

fprintf(['Creating section of 3 parallell conductors\n']);
nexttile
AL=repmat(A,1);
AR=repmat(A,1);

fprintf(['Draw conductors\n']);
k2=1;
while k2<=nt+3
     [k p]=cellfun(@size,A(k2),'UniformOutput',false);
     size=cell2mat(k);
     n=1;
     while n<=size

     p1=[A{k2}(n,1) A{k2}(n,4)];
     p2=[A{k2}(n,2) A{k2}(n,5)];
     p3=[A{k2}(n,3) A{k2}(n,6)];
     plot3(p1,p2,p3,'Color','#0072BD')
     hold on
     p1=[AL{k2}(n,1) AL{k2}(n,4)];
     p2=[AL{k2}(n,2) AL{k2}(n,5)];
     p3=[AL{k2}(n,3)+7.5 AL{k2}(n,6)+7.5];
     AL{k2}(n,3)=AL{k2}(n,3)+7.5;
     AL{k2}(n,6)=AL{k2}(n,6)+7.5;
     plot3(p1,p2,p3,'Color','#0072BD')
     hold on
     p1=[AR{k2}(n,1) AR{k2}(n,4)];
     p2=[AR{k2}(n,2) AR{k2}(n,5)];
     p3=[AR{k2}(n,3)-7.5 AR{k2}(n,6)-7.5];
     AR{k2}(n,3)=AR{k2}(n,3)-7.5;
     AR{k2}(n,6)=AR{k2}(n,6)-7.5;
     plot3(p1,p2,p3,'Color','#0072BD')
     hold on
     n=n+1;

     end
    k2=k2+1;
end

%writing catenaries into file

i=1;
while i<=nt+3
COMSOLconductors('Conductor M of span no.', A{i}, i);
COMSOLconductors('Conductor L of span no.', AL{i}, i);
COMSOLconductors('Conductor R of span no.', AR{i}, i);
i=i+1;
end

n=3;
name=1;
while n<=nt+2

fprintf(['Draw towers and conductors\n']);
hpylon22(ht,A{
end n}(1,1),A{n}(1,2),name);
hold on
n=n+1;
name=name+1;


n=1;
name=1;
strainpylon22(ht,insLm(n,1),insLm(n,2),insLm,n,name);
hold on
n=n+1;
name=name+1;
while n<=6

strainpylon22(ht,insLm(n,1),insLm(n,2),insLm,n,name);
hold on

name=name+1;
n=n+2;
end
```

```
zlim([-20 20])
view([-89.5 2])
daspect([1 1 1])
xlabel('Z')
ylabel('Y')
zlabel('X')
camup([0 1 0])
hold off
grid on

function plottriangle(x,y,ht)

   ytr=[y y-ht y-ht y];
   xtr=[x x-ht*tand(15) x+ht*tand(15) x];
   plot(xtr,ytr,'Color','#EDB120')
   hold on
   plot(x,y,'ok')

end

function fx=sagcalc(ae,H,mc,g,xAS,eldif,x)

fx=((eldif/ae)*(x-xAS))+((H/(mc*g))*(cosh(((mc*g)/H)*xAS)-cosh(((mc*g)/H)*x)));

end
```

(b)

```
% Sag calculations for each span NO TENSION ADJUSTMENT
n=1;
while nt+3 >= n
    fprintf(['Creating span no. ' num2str(n) '\n'])

        co(n,1) =   -ae(n)/2;
        co(n,2) =   (H(n)/(mc*g))*((cosh(mc*g*ae(n)/(2*H(n))))-1);
        xB      =   co(n,1)+ae(n);
        yB      =   co(n,2)+eldif(n);

        y           =       @(x) (H(n)/(mc*g))*((cosh((mc*g/H(n))*x))-1);
        ytriangle   =       @(x) (((yB-co(n,2))/(xB-co(n,1)))*x)+co(n,2)+(co(n,1)*(co(n,2)-yB)/(xB-
co(n,1)));
        ytriangle1  =       diff(ytriangle,x);
        Lfunction   =       sqrt(1+((ytriangle1)^2));
        LAB         =       int(Lfunction,x,'IgnoreAnalyticConstraints',true,co(n,1),xB);


   fprintf(['Tension of span no. ' num2str(n) ' = .\n' num2str(H(n,1)) ' [N]\n']);
   fprintf(['Span no. ' num2str(n) ' numerical adjustment.\n']);

            xAS=co(n,1)
            yAS         =       (H(n)/(mc*g))*((cosh((mc*g/H(n))*xAS))-1);
            ytriangle2  =       @(x) ((((yAS+eldif(n))-yAS)/((xAS+ae(n))-xAS))*x)+yAS+(xAS*(yAS-
(yAS+eldif(n)))/((xAS+ae(n))-xAS));
            fun= @(x) ((H(n)/(mc*g))*((cosh((mc*g/H(n))*x))-1))-(((((yAS+eldif(n))-yAS)/((xAS+ae(n))-
xAS))*x)+yAS+(xAS*(yAS-(yAS+eldif(n)))/((xAS+ae(n))-xAS)));
            x0=[-1000 1000];
            X_int=fsolve(fun,x0,opts)
            Y_int=subs(ytriangle2,X_int)
            xAS=X_int(1,1);
            yAS=Y_int(1,1);
            co(n,3)     =       X_int(1,2);
            co(n,4)     =       Y_int(1,2);
            ytriangle21 =       diff(ytriangle2,x);
            Lfunction   =       sqrt(1+((ytriangle21)^2));
            length      =       int(Lfunction,x,'IgnoreAnalyticConstraints',true,xAS,co(n,3));

       if eldif(n)<0
           if length > LAB
                dx=-(1e-1);
            else
               dx=1e-1;
           end

           while (length<LAB && dx==1e-1) || (length>LAB && dx==-(1e-1))

                xAS         =       xAS-dx;
                yAS         =       (H(n)/(mc*g))*((cosh((mc*g/H(n))*xAS))-1);
                ytriangle2  =       @(x) ((((yAS+eldif(n))-yAS)/((xAS+ae(n))-xAS))*x)+yAS+(xAS*(yAS-
(yAS+eldif(n)))/((xAS+ae(n))-xAS));
                fun= @(x) ((H(n)/(mc*g))*((cosh((mc*g/H(n))*x))-1))-(((((yAS+eldif(n))-
yAS)/((xAS+ae(n))-xAS))*x)+yAS+(xAS*(yAS-(yAS+eldif(n)))/((xAS+ae(n))-xAS)));
                x0=[-1000 1000];
                X_int=fsolve(fun,x0,opts);
                Y_int=subs(ytriangle2,X_int);
                xAS=X_int(1,1);
                yAS=Y_int(1,1);
                co(n,3)     =       X_int(1,2);
                co(n,4)     =       Y_int(1,2);
                ytriangle21 =       diff(ytriangle2,x);
                Lfunction   =       sqrt(1+((ytriangle21)^2));
                length      =       int(Lfunction,x,'IgnoreAnalyticConstraints',true,xAS,co(n,3));
                eval(length)


                co(n,1)=xAS;
                co(n,2)=yAS;

           end
       elseif  eldif(n)>0

               dx=1e-1;

           while length>LAB

                xAS         =       xAS+dx;
                yAS         =       (H(n)/(mc*g))*((cosh((mc*g/H(n))*xAS))-1);
                ytriangle2  =       @(x) ((((yAS+eldif(n))-yAS)/((xAS+ae(n))-xAS))*x)+yAS+(xAS*(yAS-
(yAS+eldif(n)))/((xAS+ae(n))-xAS));
                fun= @(x) ((H(n)/(mc*g))*((cosh((mc*g/H(n))*x))-1))-(((((yAS+eldif(n))-
yAS)/((xAS+ae(n))-xAS))*x)+yAS+(xAS*(yAS-(yAS+eldif(n)))/((xAS+ae(n))-xAS)));
                x0=[-1000 1000];
                X_int=fsolve(fun,x0,opts);
                Y_int=subs(ytriangle2,X_int);

                xAS=X_int(1,1);
                yAS=Y_int(1,1);
                co(n,3)     =       X_int(1,2);
                co(n,4)     =       Y_int(1,2);
                ytriangle21 =       diff(ytriangle2,x);
                Lfunction   =       sqrt(1+((ytriangle21)^2));
                length      =       int(Lfunction,x,'IgnoreAnalyticConstraints',true,xAS,co(n,3));
               eval(length)

                co(n,1)=xAS;
                co(n,2)=yAS;
           end
         elseif eldif(n)==0
                    length = LAB;
                    co(n,3)     =       xB;
                    co(n,4)     =       yB;
                    sags(n,1)   =       0;
                    sags(n,2)   =       yB;
                    sags(n,3)   =       0;
                    sags(n,4)   =       yB;
       end
```

Two solutions are proposed – (a) the one with sag adjustment in case of catenary approaching straight line, and (b) no sag adjustment.

```
function strainpylon22(ht,vector,vector2,insLm,ops,name)

fprintf(['Creating strain pylon no.' num2str(name) '\n'])

P=zeros(100,3);
Pn=zeros(100,3);

P(1,:)=[5      -ht              (5/25)*ht];
P(2,:)=[5      (-15.5/25)*ht    0];
P(3,:)=[5      (-6/25)*ht       0];
P(4,:)=[5      0                0];
P(5,:)=[5      (4.0/25)*ht      0];
P(6,:)=[5      (8.5/25)*ht      (0.2/25)*ht];

atang=atan(((P(6,2)-P(1,2))/P(1,3)))*180/pi;
tg=tand(atang);
hr=(P(6,2)-P(1,2))+((P(6,3)*(P(6,2)-P(1,2)))/(P(1,3)-P(6,3)));

P(2,3)=((hr-(ht-abs(P(2,2))))/hr)*P(1,3);
P(3,3)=((hr-(ht-abs(P(3,2))))/hr)*P(1,3);
P(4,3)=((hr-ht-abs(P(4,2)))/hr)*P(1,3);
P(5,3)=((hr-ht-abs(P(5,2)))/hr)*P(1,3);

P(7,:)=[7.5      P(4,2)              P(4,3)];
Pn(7,:)=[7.5      P(4,2)              P(4,3)];

P(8,:)=[(P(4,1)+(((P(7,1)-P(4,1))/3)))     P(4,2)              P(4,3)];
P(9,:)=[(P(4,1)+2*(((P(7,1)-P(4,1))/3)))     P(4,2)              P(4,3)];

a=P(5,2)-P(4,2);
b=sqrt(((P(7,1)-P(4,1))^2)+((P(7,2)-P(4,2))^2)+((P(7,3)-P(5,3))^2));
c=b*(P(7,1)-P(9,1))/(P(7,1)-P(4,1));

e=sqrt(((P(5,1)-P(4,1))^2)+((P(5,2)-P(4,2))^2)+((P(5,3)-P(4,3))^2));
f=P(7,1)-P(4,1);
g=P(7,1)-P(9,1);
d=e*g/f;


P(10,:)=[P(9,1)     (P(9,2)+(a*c/b))             (P(9,3)-(sqrt((d^2)-((a*c/b)^2))))];
P(11,:)=[5          -ht+((P(2,2)-P(1,2))/2)            0];
P(11,3)=((hr-(ht-abs(P(11,2))))/hr)*P(1,3);
P(12,:)=[5          P(2,2)+((P(3,2)-P(2,2))/2)             0];
P(12,3)=((hr-(ht-abs(P(12,2))))/hr)*P(1,3);
P(13,:)=[5          P(3,2)+((P(4,2)-P(3,2))/2)           0];
P(13,3)=((hr-(ht-abs(P(13,2))))/hr)*P(1,3);
P(14,:)=[5          P(4,2)+((P(5,2)-P(4,2))/3)           0];
P(14,3)=((hr-ht-abs(P(14,2)))/hr)*P(1,3);
P(15,:)=[5          P(4,2)+(2*((P(5,2)-P(4,2))/3))          0];
P(15,3)=((hr-ht-abs(P(15,2)))/hr)*P(1,3);
P(16,:)=[5          P(5,2)+((P(6,2)-P(5,2))/3)           0];
P(16,3)=((hr-ht-abs(P(16,2)))/hr)*P(1,3);
P(17,:)=[5          P(5,2)+(2*((P(6,2)-P(5,2))/3))          0];
P(17,3)=((hr-ht-abs(P(17,2)))/hr)*P(1,3);

P(18,:)=[0         P(2,2)  P(2,3)];
P(19,:)=[P(2,1)/2  P(2,2)  P(2,3)];
P(20,:)=[P(3,1)/2  P(3,2)  P(3,3)];
P(21,:)=[P(4,1)/2  P(4,2)  P(4,3)];
P(22,:)=[P(5,1)/3  P(5,2)  P(5,3)];
P(23,:)=[0         P(4,2)  P(4,3)];
P(24,:)=[0         P(3,2)  P(3,3)];
P(25,:)=[P(7,1)    P(7,2)  0     ];
P(26,:)=[P(21,1)   P(21,2) 0     ];
P(27,:)=[P(4,1)    P(4,2)  0     ];

P2=zeros(size(P,1), size(P,2));
n=1;
while n<=size(P,1)
P2(n,1)=P(n,1).* (-1);
P2(n,2)=P(n,2);
P2(n,3)=P(n,3);
n=n+1;
end

P3=zeros(size(P,1), size(P,2));
n=1;
while n<=size(P,1)
P3(n,1)=P(n,1);
P3(n,2)=P(n,2);
P3(n,3)=P(n,3).* (-1);
n=n+1;
end

P4=zeros(size(P,1), size(P,2));
n=1;
while n<=size(P,1)
P4(n,1)=P2(n,1);
P4(n,2)=P2(n,2);
P4(n,3)=P2(n,3).* (-1);
n=n+1;
end


P5=zeros(100,3);
P5(1,:)=[7.5 0 0];
P5(2,:)=[0 0 0];
P5(3,:)=[-7.5 0 0];

n=1;
while n<=100

   P(n,3)=P(n,3)+vector;
   P2(n,3)=P2(n,3)+vector;
   P3(n,3)=P3(n,3)+vector;
   P4(n,3)=P4(n,3)+vector;
   P5(n,3)=P5(n,3)+vector;

   P(n,2)=P(n,2)+vector2;
   P2(n,2)=P2(n,2)+vector2;
   P3(n,2)=P3(n,2)+vector2;
   P4(n,2)=P4(n,2)+vector2;
   P5(n,2)=P5(n,2)+vector2;

   n=n+1;
end

A=[1 11;11 2;2 12;12 3;3 13;13 4;4 14;14 15;15 5;5 16;16 17;17 6]

A1=[4 8;8 9;9 7;7 10;10 5;23 21;21 4;22 5;18 19;19 2;24 20;20 3]

A2=[5 8;8 10;10 9;5 21;21 22;22 23;21 13];

%rectangular cross section RCS
n=1;
k=1;
while n<=size(A,1)

n1=A(n,1);
n2=A(n,2);
x1=[P(n1,1) P(n2,1)];
y1=[P(n1,2) P(n2,2)];
z1=[P(n1,3) P(n2,3)];
plot3(z1,y1,x1, 'Color','#808080')
RCS(k,:)=[x1(1,1) y1(1,1) z1(1,1) x1(1,2) y1(1,2) z1(1,2)];

hold on
k=k+1;
x2=[P2(n1,1) P2(n2,1)];
y2=[P2(n1,2) P2(n2,2)];
z2=[P2(n1,3) P2(n2,3)];
plot3(z2,y2,x2, 'Color','#808080')
RCS(k,:)=[x2(1,1) y2(1,1) z2(1,1) x2(1,2) y2(1,2) z2(1,2)];
hold on
k=k+1;
x3=[P3(n1,1) P3(n2,1)];
y3=[P3(n1,2) P3(n2,2)];
z3=[P3(n1,3) P3(n2,3)];
plot3(z3,y3,x3, 'Color','#808080')
RCS(k,:)=[x3(1,1) y3(1,1) z3(1,1) x3(1,2) y3(1,2) z3(1,2)];
hold on
k=k+1;
x4=[P4(n1,1) P4(n2,1)];
y4=[P4(n1,2) P4(n2,2)];
z4=[P4(n1,3) P4(n2,3)];
plot3(z4,y4,x4, 'Color','#808080')
RCS(k,:)=[x4(1,1) y4(1,1) z4(1,1) x4(1,2) y4(1,2) z4(1,2)];
hold on
k=k+1;
n=n+1;
end

%L cross section size LL
n=1;
k=1;
while n<=size(A1,1)

n1=A1(n,1);
n2=A1(n,2);
x1=[P(n1,1) P(n2,1)];
y1=[P(n1,2) P(n2,2)];
z1=[P(n1,3) P(n2,3)];
plot3(z1,y1,x1, 'Color','#A2142F')
```

```
LL(k,:)=[x1(1,1) y1(1,1) z1(1,1) x1(1,2) y1(1,2) z1(1,2)];

hold on
k=k+1;
x2=[P2(n1,1) P2(n2,1)];
y2=[P2(n1,2) P2(n2,2)];
z2=[P2(n1,3) P2(n2,3)];
plot3(z2,y2,x2, 'Color','#A2142F')
LL(k,:)=[x2(1,1) y2(1,1) z2(1,1) x2(1,2) y2(1,2) z2(1,2)];

hold on
k=k+1;
x3=[P3(n1,1) P3(n2,1)];
y3=[P3(n1,2) P3(n2,2)];
z3=[P3(n1,3) P3(n2,3)];
plot3(z3,y3,x3, 'Color','#A2142F')
LL(k,:)=[x3(1,1) y3(1,1) z3(1,1) x3(1,2) y3(1,2) z3(1,2)];

hold on
k=k+1;
x4=[P4(n1,1) P4(n2,1)];
y4=[P4(n1,2) P4(n2,2)];
z4=[P4(n1,3) P4(n2,3)];
plot3(z4,y4,x4, 'Color','#A2142F')
LL(k,:)=[x4(1,1) y4(1,1) z4(1,1) x4(1,2) y4(1,2) z4(1,2)];
hold on
k=k+1;
n=n+1;
end


B3=[4 4;5 5;6 6;3 3;2 2;7 7]

n=1;
while n<=size(B3,1)

n1=B3(n,1);
n2=B3(n,2);
x1=[P(n1,1) P3(n2,1)];
y1=[P(n1,2) P3(n2,2)];
z1=[P(n1,3) P3(n2,3)];
LL(k,:)=[x1(1,1) y1(1,1) z1(1,1) x1(1,2) y1(1,2) z1(1,2)];
k=k+1;
plot3(z1,y1,x1, 'Color','#A2142F')
hold on
x2=[P2(n1,1) P4(n2,1)];
y2=[P2(n1,2) P4(n2,2)];
z2=[P2(n1,3) P4(n2,3)];
plot3(z2,y2,x2, 'Color','#A2142F')
LL(k,:)=[x2(1,1) y2(1,1) z2(1,1) x2(1,2) y2(1,2) z2(1,2)];
k=k+1;
hold on

n=n+1;
end

C=[22 22];
n1=C(1,1);
n2=C(1,2);
x1=[P(n1,1) P2(n2,1)];
y1=[P(n1,2) P2(n2,2)];
z1=[P(n1,3) P2(n2,3)];
LL(k,:)=[x1(1,1) y1(1,1) z1(1,1) x1(1,2) y1(1,2) z1(1,2)];
k=k+1;
plot3(z1,y1,x1, 'Color','#A2142F')
hold on
x2=[P3(n1,1) P4(n2,1)];
y2=[P3(n1,2) P4(n2,2)];
z2=[P3(n1,3) P4(n2,3)];
LL(k,:)=[x2(1,1) y2(1,1) z2(1,1) x2(1,2) y2(1,2) z2(1,2)];
k=k+1;
plot3(z2,y2,x2, 'Color','#A2142F')
hold on


%L cross section size M LM

n=1;
k=1;
while n<=size(A2,1)

n1=A2(n,1);
n2=A2(n,2);
x1=[P(n1,1) P(n2,1)];
y1=[P(n1,2) P(n2,2)];
z1=[P(n1,3) P(n2,3)];
plot3(z1,y1,x1, 'Color','#00FF80')
```

```
LM(k,:)=[x1(1,1) y1(1,1) z1(1,1) x1(1,2) y1(1,2) z1(1,2)];

hold on
k=k+1;
x2=[P2(n1,1) P2(n2,1)];
y2=[P2(n1,2) P2(n2,2)];
z2=[P2(n1,3) P2(n2,3)];
plot3(z2,y2,x2, 'Color','#00FF80')
LM(k,:)=[x2(1,1) y2(1,1) z2(1,1) x2(1,2) y2(1,2) z2(1,2)];
hold on
k=k+1;
x3=[P3(n1,1) P3(n2,1)];
y3=[P3(n1,2) P3(n2,2)];
z3=[P3(n1,3) P3(n2,3)];
plot3(z3,y3,x3, 'Color','#00FF80')
LM(k,:)=[x3(1,1) y3(1,1) z3(1,1) x3(1,2) y3(1,2) z3(1,2)];
hold on
k=k+1;
x4=[P4(n1,1) P4(n2,1)];
y4=[P4(n1,2) P4(n2,2)];
z4=[P4(n1,3) P4(n2,3)];
plot3(z4,y4,x4, 'Color','#00FF80')
LM(k,:)=[x4(1,1) y4(1,1) z4(1,1) x4(1,2) y4(1,2) z4(1,2)];
hold on
k=k+1;
n=n+1;
end

C=[21 21;22 22;23 23;10 10];
n1=C(1,1);
n2=C(1,2);
n3=C(2,1);
n4=C(2,2);
n5=C(3,1);
n6=C(3,2);
n7=C(4,1);
n8=C(4,2);


x1=[P(n1,1) P3(n2,1)];
y1=[P(n1,2) P3(n2,2)];
z1=[P(n1,3) P3(n2,3)];
plot3(z1,y1,x1, 'Color','#00FF80')
LM(k,:)=[x1(1,1) y1(1,1) z1(1,1) x1(1,2) y1(1,2) z1(1,2)];
k=k+1;
hold on

x1=[P2(n1,1) P4(n2,1)];
y1=[P2(n1,2) P4(n2,2)];
z1=[P2(n1,3) P4(n2,3)];
plot3(z1,y1,x1, 'Color','#00FF80')
LM(k,:)=[x1(1,1) y1(1,1) z1(1,1) x1(1,2) y1(1,2) z1(1,2)];
k=k+1;
hold on

x1=[P(n3,1) P3(n4,1)];
y1=[P(n3,2) P3(n4,2)];
z1=[P(n3,3) P3(n4,3)];
plot3(z1,y1,x1, 'Color','#00FF80')
LM(k,:)=[x1(1,1) y1(1,1) z1(1,1) x1(1,2) y1(1,2) z1(1,2)];
k=k+1;
hold on

x1=[P2(n3,1) P4(n4,1)];
y1=[P2(n3,2) P4(n4,2)];
z1=[P2(n3,3) P4(n4,3)];
plot3(z1,y1,x1, 'Color','#00FF80')
LM(k,:)=[x1(1,1) y1(1,1) z1(1,1) x1(1,2) y1(1,2) z1(1,2)];
k=k+1;
hold on

x1=[P(n5,1) P3(n6,1)];
y1=[P(n5,2) P3(n6,2)];
z1=[P(n5,3) P3(n6,3)];
plot3(z1,y1,x1, 'Color','#00FF80')
LM(k,:)=[x1(1,1) y1(1,1) z1(1,1) x1(1,2) y1(1,2) z1(1,2)];
k=k+1;
hold on

x1=[P(n7,1) P3(n8,1)];
y1=[P(n7,2) P3(n8,2)];
z1=[P(n7,3) P3(n8,3)];
plot3(z1,y1,x1, 'Color','#00FF80')
LM(k,:)=[x1(1,1) y1(1,1) z1(1,1) x1(1,2) y1(1,2) z1(1,2)];
k=k+1;
hold on
```

```
x1=[P2(n7,1) P4(n8,1)];
y1=[P2(n7,2) P4(n8,2)];
z1=[P2(n7,3) P4(n8,3)];
plot3(z1,y1,x1, 'Color','#00FF80')
LM(k,:)=[x1(1,1) y1(1,1) z1(1,1) x1(1,2) y1(1,2) z1(1,2)];
k=k+1;
hold on

%L cross section size S LS

B=[4 8;8 4;8 9;9 8;9 7;7 9;
   21 4;4 21;21 23;23 21;
   24 20;20 24;20 3;3 20;
   18 19;19 18;19 2;2 19;
   13 21;21 13;
   7 10;10 7;10 5;5 10;
   1 11;11 1;11 2;2 11;2 12;12 2;12 3;3 12;3 13;13 3;
   13 4;4 13;4 14;14 4;14 15;15 14;15 5;5 15;5 16;16 5;16 17;17 16;17 6;6 17;
    22 5;5 22];
k=1;
n=1;
while n<=size(B,1)

n1=B(n,1);
n2=B(n,2);
x1=[P(n1,1) P3(n2,1)];
y1=[P(n1,2) P3(n2,2)];
z1=[P(n1,3) P3(n2,3)];
LS(k,:)=[x1(1,1) y1(1,1) z1(1,1) x1(1,2) y1(1,2) z1(1,2)];
k=k+1;
plot3(z1,y1,x1, 'Color','#808080')
hold on
x2=[P2(n1,1) P4(n2,1)];
y2=[P2(n1,2) P4(n2,2)]
z2=[P2(n1,3) P4(n2,3)];
plot3(z2,y2,x2, 'Color','#808080')
LS(k,:)=[x2(1,1) y2(1,1) z2(1,1) x2(1,2) y2(1,2) z2(1,2)];
k=k+1;
hold on

n=n+1;
end

C2=[22 22];
n1=C2(1,1);
n2=C2(1,2);
x3=[P(n1,1) P4(n2,1)];
y3=[P(n1,2) P4(n2,2)];
z3=[P(n1,3) P4(n2,3)];
LS(k,:)=[x3(1,1) y3(1,1) z3(1,1) x3(1,2) y3(1,2) z3(1,2)];
k=k+1;
plot3(z3,y3,x3, 'Color','#808080')
hold on
x4=[P2(n1,1) P3(n2,1)];
y4=[P2(n1,2) P3(n2,2)];
z4=[P2(n1,3) P3(n2,3)];
LS(k,:)=[x4(1,1) y4(1,1) z4(1,1) x4(1,2) y4(1,2) z4(1,2)];
k=k+1;
plot3(z4,y4,x4, 'Color','#808080')
hold on


%Bracing BRACING
 D=[1 2;2 1;2 13;13 2];
n=1;
k=1;
while n<=size(D,1)

n1=D(n,1);
n2=D(n,2);
x1=[P(n1,1) P2(n2,1)];
y1=[P(n1,2) P2(n2,2)];
z1=[P(n1,3) P2(n2,3)];
plot3(z1,y1,x1, 'Color','#008080')
BRACING(k,:)=[x1(1,1) y1(1,1) z1(1,1) x1(1,2) y1(1,2) z1(1,2)];
k=k+1;
hold on
x2=[P3(n1,1) P4(n2,1)];
y2=[P3(n1,2) P4(n2,2)];
z2=[P3(n1,3) P4(n2,3)];
plot3(z2,y2,x2, 'Color','#008080')
BRACING(k,:)=[x2(1,1) y2(1,1) z2(1,1) x2(1,2) y2(1,2) z2(1,2)];
hold on
n=n+1;
k=k+1;
end
```

```
%Insulators CON
k=1;
if ops==1
    x1=[P(7,1) insLm(ops,6)+Pn(7,1)];
    y1=[P(7,2) insLm(ops,5)];
    z1=[P(7,3) insLm(ops,4)];
    plot3(z1,y1,x1, 'Color','#D95319')
    CON(k,:)=[x1(1,1) y1(1,1) z1(1,1) x1(1,2) y1(1,2) z1(1,2)];
    k=k+1;
    hold on

    x2=[P(23,1) insLm(ops,6)];
    y2=[P(23,2) insLm(ops,5)];
    z2=[P(23,3) insLm(ops,4)];
    plot3(z2,y2,x2, 'Color','#D95319')
    CON(k,:)=[x2(1,1) y2(1,1) z2(1,1) x2(1,2) y2(1,2) z2(1,2)];
    k=k+1;
    hold on

    x3=[P2(7,1) insLm(ops,6)-Pn(7,1)];
    y3=[P2(7,2) insLm(ops,5)];
    z3=[P2(7,3) insLm(ops,4)];
    plot3(z3,y3,x3, 'Color','#D95319')
    CON(k,:)=[x3(1,1) y3(1,1) z3(1,1) x3(1,2) y3(1,2) z3(1,2)];
    k=k+1;
    hold on
end
k=1;
if ops==2 || ops==4

    x4=[P3(7,1) insLm(ops,6)+Pn(7,1)];
    y4=[P3(7,2) insLm(ops,5)];
    z4=[P3(7,3) insLm(ops,4)];
    plot3(z4,y4,x4, 'Color','#D95319')
    CON(k,:)=[x4(1,1) y4(1,1) z4(1,1) x4(1,2) y4(1,2) z4(1,2)];
    k=k+1;
    hold on

    x5=[P3(23,1) insLm(ops,6)];
    y5=[P3(23,2) insLm(ops,5)];
    z5=[P3(23,3) insLm(ops,4)];
    plot3(z5,y5,x5, 'Color','#D95319')
    CON(k,:)=[x5(1,1) y5(1,1) z5(1,1) x5(1,2) y5(1,2) z5(1,2)];
    k=k+1;
    hold on

    x6=[P4(7,1) insLm(ops,6)-Pn(7,1)];
    y6=[P4(7,2) insLm(ops,5)];
    z6=[P4(7,3) insLm(ops,4)];
    plot3(z6,y6,x6, 'Color','#D95319')
    CON(k,:)=[x6(1,1) y6(1,1) z6(1,1) x6(1,2) y6(1,2) z6(1,2)];
    k=k+1;
    hold on

    x1=[P(7,1) insLm(ops+1,6)+Pn(7,1)];
    y1=[P(7,2) insLm(ops+1,5)];
    z1=[P(7,3) insLm(ops+1,4)];
    plot3(z1,y1,x1, 'Color','#D95319')
    CON(k,:)=[x1(1,1) y1(1,1) z1(1,1) x1(1,2) y1(1,2) z1(1,2)];
    k=k+1;
    hold on

    x2=[P(23,1) insLm(ops+1,6)];
    y2=[P(23,2) insLm(ops+1,5)];
    z2=[P(23,3) insLm(ops+1,4)];
    plot3(z2,y2,x2, 'Color','#D95319')
    CON(k,:)=[x2(1,1) y2(1,1) z2(1,1) x2(1,2) y2(1,2) z2(1,2)];
    k=k+1;
    hold on

    x3=[P2(7,1) insLm(ops+1,6)-Pn(7,1)];
    y3=[P2(7,2) insLm(ops+1,5)];
    z3=[P2(7,3) insLm(ops+1,4)];
    plot3(z3,y3,x3, 'Color','#D95319')
    CON(k,:)=[x3(1,1) y3(1,1) z3(1,1) x3(1,2) y3(1,2) z3(1,2)];
    k=k+1;
    hold on
end
k=1;
if ops==6
    x4=[P3(7,1) insLm(ops,6)+Pn(7,1)];
    y4=[P3(7,2) insLm(ops,5)];
    z4=[P3(7,3) insLm(ops,4)];
    plot3(z4,y4,x4, 'Color','#D95319')
    CON(k,:)=[x4(1,1) y4(1,1) z4(1,1) x4(1,2) y4(1,2) z4(1,2)];
    k=k+1;
    hold on
```

```
    x5=[P3(23,1) insLm(ops,6)];
    y5=[P3(23,2) insLm(ops,5)];
    z5=[P3(23,3) insLm(ops,4)];
    plot3(z5,y5,x5, 'Color','#D95319')
    CON(k,:)=[x5(1,1) y5(1,1) z5(1,1) x5(1,2) y5(1,2) z5(1,2)];
    k=k+1;
    hold on

    x6=[P4(7,1) insLm(ops,6)-Pn(7,1)];
    y6=[P4(7,2) insLm(ops,5)];
    z6=[P4(7,3) insLm(ops,4)];
    plot3(z6,y6,x6, 'Color','#D95319')
    CON(k,:)=[x6(1,1) y6(1,1) z6(1,1) x6(1,2) y6(1,2) z6(1,2)];
    k=k+1;
    hold on
end

%Supports SP
k=1;
if ops==1 || ops==2 || ops==4

    x1=[P(7,1) P(7,1)-1];
    y1=[P(7,2) P(7,2)];
    z1=[P(7,3) P(7,3)];
    SP(k,:)=[x1(1,1) y1(1,1) z1(1,1) x1(1,2) y1(1,2) z1(1,2)];
    k=k+1;

    x2=[P(7,1) P(7,1)];
    y2=[P(7,2) P(7,2)+1];
    z2=[P(7,3) P(7,3)];
    SP(k,:)=[x2(1,1) y2(1,1) z2(1,1) x2(1,2) y2(1,2) z2(1,2)];
    k=k+1;

    x3=[P(7,1) P(7,1)];
    y3=[P(7,2) P(7,2)];
    z3=[P(7,3) P(7,3)-1];
    SP(k,:)=[x3(1,1) y3(1,1) z3(1,1) x3(1,2) y3(1,2) z3(1,2)];
    k=k+1;

    x4=[P(23,1) P(23,1)-1];
    y4=[P(23,2) P(23,2)];
    z4=[P(23,3) P(23,3)];
    SP(k,:)=[x4(1,1) y4(1,1) z4(1,1) x4(1,2) y4(1,2) z4(1,2)];
    k=k+1;

    x5=[P(23,1) P(23,1)];
    y5=[P(23,2) P(23,2)+1];
    z5=[P(23,3) P(23,3)];
    SP(k,:)=[x5(1,1) y5(1,1) z5(1,1) x5(1,2) y5(1,2) z5(1,2)];
    k=k+1;

    x6=[P(23,1) P(23,1)];
    y6=[P(23,2) P(23,2)];
    z6=[P(23,3) P(23,3)-1];
    SP(k,:)=[x6(1,1) y6(1,1) z6(1,1) x6(1,2) y6(1,2) z6(1,2)];
    k=k+1;

    x7=[P2(7,1) P2(7,1)-1];
    y7=[P2(7,2) P2(7,2)];
    z7=[P2(7,3) P2(7,3)];
    SP(k,:)=[x7(1,1) y7(1,1) z7(1,1) x7(1,2) y7(1,2) z7(1,2)];
    k=k+1;

    x8=[P2(7,1) P2(7,1)];
    y8=[P2(7,2) P2(7,2)+1];
    z8=[P2(7,3) P2(7,3)];
    SP(k,:)=[x8(1,1) y8(1,1) z8(1,1) x8(1,2) y8(1,2) z8(1,2)];
    k=k+1;

    x9=[P2(7,1) P2(7,1)];
    y9=[P2(7,2) P2(7,2)];
    z9=[P2(7,3) P2(7,3)-1];
    SP(k,:)=[x9(1,1) y9(1,1) z9(1,1) x9(1,2) y9(1,2) z9(1,2)];
    k=k+1;

end

if ops==2 || ops==4 || ops==6
    x1=[P3(7,1) P3(7,1)-1];
    y1=[P3(7,2) P3(7,2)];
    z1=[P3(7,3) P3(7,3)];
    SP(k,:)=[x1(1,1) y1(1,1) z1(1,1) x1(1,2) y1(1,2) z1(1,2)];
    k=k+1;

    x2=[P3(7,1) P3(7,1)];
    y2=[P3(7,2) P3(7,2)+1];
    z2=[P3(7,3) P3(7,3)];
    SP(k,:)=[x2(1,1) y2(1,1) z2(1,1) x2(1,2) y2(1,2) z2(1,2)];
    k=k+1;
```

```
    x3=[P3(7,1) P3(7,1)];
    y3=[P3(7,2) P3(7,2)];
    z3=[P3(7,3) P3(7,3)+1];
    SP(k,:)=[x3(1,1) y3(1,1) z3(1,1) x3(1,2) y3(1,2) z3(1,2)];
    k=k+1;

    x4=[P3(23,1) P3(23,1)-1];
    y4=[P3(23,2) P3(23,2)];
    z4=[P3(23,3) P3(23,3)];
    SP(k,:)=[x4(1,1) y4(1,1) z4(1,1) x4(1,2) y4(1,2) z4(1,2)];
    k=k+1;

    x5=[P3(23,1) P3(23,1)];
    y5=[P3(23,2) P3(23,2)+1];
    z5=[P3(23,3) P3(23,3)];
    SP(k,:)=[x5(1,1) y5(1,1) z5(1,1) x5(1,2) y5(1,2) z5(1,2)];
    k=k+1;

    x6=[P3(23,1) P3(23,1)];
    y6=[P3(23,2) P3(23,2)];
    z6=[P3(23,3) P3(23,3)+1];
    SP(k,:)=[x6(1,1) y6(1,1) z6(1,1) x6(1,2) y6(1,2) z6(1,2)];
    k=k+1;

    x7=[P4(7,1) P4(7,1)-1];
    y7=[P4(7,2) P4(7,2)];
    z7=[P4(7,3) P4(7,3)];
    SP(k,:)=[x7(1,1) y7(1,1) z7(1,1) x7(1,2) y7(1,2) z7(1,2)];
    k=k+1;

    x8=[P4(7,1) P4(7,1)];
    y8=[P4(7,2) P4(7,2)+1];
    z8=[P4(7,3) P4(7,3)];
    SP(k,:)=[x8(1,1) y8(1,1) z8(1,1) x8(1,2) y8(1,2) z8(1,2)];
    k=k+1;

    x9=[P4(7,1) P4(7,1)];
    y9=[P4(7,2) P4(7,2)];
    z9=[P4(7,3) P4(7,3)+1];
    SP(k,:)=[x9(1,1) y9(1,1) z9(1,1) x9(1,2) y9(1,2) z9(1,2)];
    k=k+1;
end

COMSOLfile('Strain pylon ', 'elements', 'RCS', RCS, name)

COMSOLfile('Strain pylon ', 'elements', 'LL', LL, name)

COMSOLfile('Strain pylon ', 'elements', 'LM', LM, name)

COMSOLfile('Strain pylon ', 'elements', 'LS', LS, name)

COMSOLfile('Strain pylon ', 'elements', 'BRACING', BRACING, name)

COMSOLfile('Strain pylon ', 'elements', 'INS', INS, name)

COMSOLfile('Strain pylon ', 'elements', 'SUP', SP, name)

daspect([1 1 1])
camup([0 1 0])
grid on
hold off
end
```

```
function hpylon22(ht,vector,vector2,name)

fprintf(['Creating support pylon no.' num2str(name) '\n'])

P=zeros(100,3);
Pn=zeros(100,3);

P(1,:)=[5      -ht              (4/25)*ht];
P(2,:)=[5      (-15.5/25)*ht    0];
P(3,:)=[5      (-6/25)*ht       0];
P(4,:)=[5      (3.5/25)*ht      0];
P(5,:)=[5      (5.5/25)*ht      0];
P(6,:)=[5      (8.5/25)*ht      (0.1/25)*ht];

atang=atan(((P(6,2)-P(1,2))/P(1,3)))*180/pi;
tg=tand(atang);
hr=(P(6,2)-P(1,2))+((P(6,3)*(P(6,2)-P(1,2)))/(P(1,3)-P(6,3)));

P(2,3)=((hr-(ht-abs(P(2,2))))/hr)*P(1,3);
P(3,3)=((hr-(ht-abs(P(3,2))))/hr)*P(1,3);
P(4,3)=((hr-ht-abs(P(4,2)))/hr)*P(1,3);
P(5,3)=((hr-ht-abs(P(5,2)))/hr)*P(1,3);

P(7,:)=[10      P(4,2)              P(4,3)];
Pn(7,:)=[7.5      P(4,2)              P(4,3)];

P(8,:)=[(P(4,1)+(((P(7,1)-P(4,1))/3)))     P(4,2)              P(4,3)];
P(9,:)=[(P(4,1)+2*(((P(7,1)-P(4,1))/3)))     P(4,2)              P(4,3)];

a=P(5,2)-P(4,2);
b=sqrt(((P(7,1)-P(4,1))^2)+((P(7,2)-P(4,2))^2)+((P(7,3)-P(5,3))^2));
c=b*(P(7,1)-P(9,1))/(P(7,1)-P(4,1));

e=sqrt(((P(5,1)-P(4,1))^2)+((P(5,2)-P(4,2))^2)+((P(5,3)-P(4,3))^2));
f=P(7,1)-P(4,1);
g=P(7,1)-P(9,1);
d=e*g/f;


P(10,:)=[P(9,1)     (P(9,2)+(a*c/b))             (P(9,3)-(sqrt((d^2)-((a*c/b)^2))))];
P(11,:)=[5          -ht+((P(2,2)-P(1,2))/2)             0];
P(11,3)=((hr-(ht-abs(P(11,2))))/hr)*P(1,3);
P(12,:)=[5          P(2,2)+((P(3,2)-P(2,2))/2)             0];
P(12,3)=((hr-(ht-abs(P(12,2))))/hr)*P(1,3);

P(13,:)=[5          P(3,2)+((P(4,2)-P(3,2))/2)             0];
P(13,3)=((hr-(ht-abs(P(13,2))))/hr)*P(1,3);
P(14,:)=[5          P(4,2)+((P(5,2)-P(4,2))/3)             0];
P(14,3)=((hr-ht-abs(P(14,2)))/hr)*P(1,3);
P(15,:)=[5          P(4,2)+(2*((P(5,2)-P(4,2))/3))            0];
P(15,3)=((hr-ht-abs(P(15,2)))/hr)*P(1,3);
P(16,:)=[5          P(5,2)+((P(6,2)-P(5,2))/3)             0];
P(16,3)=((hr-ht-abs(P(16,2)))/hr)*P(1,3);
P(17,:)=[5          P(5,2)+(2*((P(6,2)-P(5,2))/3))            0];
P(17,3)=((hr-ht-abs(P(17,2)))/hr)*P(1,3);

P(18,:)=[0         P(2,2)  P(2,3)];
P(19,:)=[P(2,1)/2  P(2,2)  P(2,3)];
P(20,:)=[P(3,1)/2  P(3,2)  P(3,3)];
P(21,:)=[P(4,1)/2  P(4,2)  P(4,3)];
P(22,:)=[P(5,1)/3  P(5,2)  P(5,3)];
P(23,:)=[0         P(4,2)  P(4,3)];
P(24,:)=[0         P(3,2)  P(3,3)];
P(25,:)=[P(7,1)    P(7,2)  0     ];
P(26,:)=[P(21,1)   P(21,2) 0     ];
P(27,:)=[P(4,1)    P(4,2)  0     ];

P2=zeros(size(P,1), size(P,2));
n=1;
while n<=size(P,1)
P2(n,1)=P(n,1).* (-1);
P2(n,2)=P(n,2);
P2(n,3)=P(n,3);
n=n+1;
end

P3=zeros(size(P,1), size(P,2));
n=1;
while n<=size(P,1)
P3(n,1)=P(n,1);
P3(n,2)=P(n,2);
P3(n,3)=P(n,3).* (-1);
n=n+1;
end
```

```
P4=zeros(size(P,1), size(P,2));
n=1;
while n<=size(P,1)
P4(n,1)=P2(n,1);
P4(n,2)=P2(n,2);
P4(n,3)=P2(n,3).* (-1);
n=n+1;
end


P5=zeros(100,3);
P5(1,:)=[7.5 0 0];
P5(2,:)=[0 0 0];
P5(3,:)=[-7.5 0 0];

n=1;
while n<=100

   P(n,3)=P(n,3)+vector;
   P2(n,3)=P2(n,3)+vector;
   P3(n,3)=P3(n,3)+vector;
   P4(n,3)=P4(n,3)+vector;
   P5(n,3)=P5(n,3)+vector;

   P(n,2)=P(n,2)+vector2;
   P2(n,2)=P2(n,2)+vector2;
   P3(n,2)=P3(n,2)+vector2;
   P4(n,2)=P4(n,2)+vector2;
   P5(n,2)=P5(n,2)+vector2;

   n=n+1;
end

A=[1 11;11 2;2 12;12 3;3 13;13 4;4 14;14 15;15 5;5 16;16 17;17 6];

A1=[4 8;8 9;9 7;7 10;10 5;23 21;21 4;22 5;18 19;19 2;24 20;20 3];

A2=[5 8;8 10;10 9;5 21;21 22;22 23;21 13];

%rectangular cross section RCS

n=1;
k=1;
while n<=size(A,1)

n1=A(n,1);
n2=A(n,2);
x1=[P(n1,1) P(n2,1)];
y1=[P(n1,2) P(n2,2)];
z1=[P(n1,3) P(n2,3)];
plot3(z1,y1,x1, 'Color','#EDB120')
RCS(k,:)=[x1(1,1) y1(1,1) z1(1,1) x1(1,2) y1(1,2) z1(1,2)];

hold on
k=k+1;
x2=[P2(n1,1) P2(n2,1)];
y2=[P2(n1,2) P2(n2,2)];
z2=[P2(n1,3) P2(n2,3)];
plot3(z2,y2,x2, 'Color','#EDB120')
RCS(k,:)=[x2(1,1) y2(1,1) z2(1,1) x2(1,2) y2(1,2) z2(1,2)];

hold on
k=k+1;
x3=[P3(n1,1) P3(n2,1)];
y3=[P3(n1,2) P3(n2,2)];
z3=[P3(n1,3) P3(n2,3)];
plot3(z3,y3,x3, 'Color','#EDB120')
RCS(k,:)=[x3(1,1) y3(1,1) z3(1,1) x3(1,2) y3(1,2) z3(1,2)];

hold on
k=k+1;
x4=[P4(n1,1) P4(n2,1)];
y4=[P4(n1,2) P4(n2,2)];
z4=[P4(n1,3) P4(n2,3)];
plot3(z4,y4,x4, 'Color','#EDB120')
RCS(k,:)=[x4(1,1) y4(1,1) z4(1,1) x4(1,2) y4(1,2) z4(1,2)];

hold on
k=k+1;
n=n+1;
end
```

```
%L cross section size LL
n=1;
k=1;
while n<=size(A1,1)

n1=A1(n,1);
n2=A1(n,2);
x1=[P(n1,1) P(n2,1)];
y1=[P(n1,2) P(n2,2)];
z1=[P(n1,3) P(n2,3)];
plot3(z1,y1,x1, 'Color','#77AC30')
LL(k,:)=[x1(1,1) y1(1,1) z1(1,1) x1(1,2) y1(1,2) z1(1,2)];

hold on
k=k+1;
x2=[P2(n1,1) P2(n2,1)];
y2=[P2(n1,2) P2(n2,2)];
z2=[P2(n1,3) P2(n2,3)];
plot3(z2,y2,x2, 'Color','#77AC30')
LL(k,:)=[x2(1,1) y2(1,1) z2(1,1) x2(1,2) y2(1,2) z2(1,2)];

hold on
k=k+1;
x3=[P3(n1,1) P3(n2,1)];
y3=[P3(n1,2) P3(n2,2)];
z3=[P3(n1,3) P3(n2,3)];
plot3(z3,y3,x3, 'Color','#77AC30')
LL(k,:)=[x3(1,1) y3(1,1) z3(1,1) x3(1,2) y3(1,2) z3(1,2)];

hold on
k=k+1;
x4=[P4(n1,1) P4(n2,1)];
y4=[P4(n1,2) P4(n2,2)];
z4=[P4(n1,3) P4(n2,3)];
plot3(z4,y4,x4, 'Color','#77AC30')
LL(k,:)=[x4(1,1) y4(1,1) z4(1,1) x4(1,2) y4(1,2) z4(1,2)];
hold on
k=k+1;
n=n+1;
end


B3=[4 4;5 5;6 6;3 3;2 2;7 25;21 26;4 27]

n=1;
while n<=size(B3,1)

n1=B3(n,1);
n2=B3(n,2);
x1=[P(n1,1) P3(n2,1)];
y1=[P(n1,2) P3(n2,2)];
z1=[P(n1,3) P3(n2,3)];
LL(k,:)=[x1(1,1) y1(1,1) z1(1,1) x1(1,2) y1(1,2) z1(1,2)];
k=k+1;
plot3(z1,y1,x1, 'Color','#77AC30')
hold on
x2=[P2(n1,1) P4(n2,1)];
y2=[P2(n1,2) P4(n2,2)];
z2=[P2(n1,3) P4(n2,3)];
plot3(z2,y2,x2, 'Color','#77AC30')

LL(k,:)=[x2(1,1) y2(1,1) z2(1,1) x2(1,2) y2(1,2) z2(1,2)];
k=k+1;
hold on

n=n+1;
end

C=[22 22];
n1=C(1,1);
n2=C(1,2);
x1=[P(n1,1) P2(n2,1)];
y1=[P(n1,2) P2(n2,2)];
z1=[P(n1,3) P2(n2,3)];
LL(k,:)=[x1(1,1) y1(1,1) z1(1,1) x1(1,2) y1(1,2) z1(1,2)];
k=k+1;
plot3(z1,y1,x1, 'Color','#77AC30')
hold on
x2=[P3(n1,1) P4(n2,1)];
y2=[P3(n1,2) P4(n2,2)];
z2=[P3(n1,3) P4(n2,3)];
LL(k,:)=[x2(1,1) y2(1,1) z2(1,1) x2(1,2) y2(1,2) z2(1,2)];
k=k+1;
plot3(z2,y2,x2, 'Color','#77AC30')
hold on

B4=[7 25;21 26;4 27]
```

```
n=1;
while n<=size(B4,1)

n1=B4(n,1);
n2=B4(n,2);
x1=[P3(n1,1) P(n2,1)];
y1=[P3(n1,2) P(n2,2)];
z1=[P3(n1,3) P(n2,3)];
LL(k,:)=[x1(1,1) y1(1,1) z1(1,1) x1(1,2) y1(1,2) z1(1,2)];
k=k+1;
plot3(z1,y1,x1, 'Color','#77AC30')
hold on
x2=[P4(n1,1) P2(n2,1)];
y2=[P4(n1,2) P2(n2,2)];
z2=[P4(n1,3) P2(n2,3)];
plot3(z2,y2,x2, 'Color','#77AC30')
LL(k,:)=[x2(1,1) y2(1,1) z2(1,1) x2(1,2) y2(1,2) z2(1,2)];
k=k+1;
hold on

n=n+1;
end

%L cross section size M LM

n=1;
k=1;
while n<=size(A2,1)

n1=A2(n,1);
n2=A2(n,2);
x1=[P(n1,1) P(n2,1)];
y1=[P(n1,2) P(n2,2)];
z1=[P(n1,3) P(n2,3)];
plot3(z1,y1,x1, 'Color','#7E2F8E')
LM(k,:)=[x1(1,1) y1(1,1) z1(1,1) x1(1,2) y1(1,2) z1(1,2)];

hold on
k=k+1;
x2=[P2(n1,1) P2(n2,1)];
y2=[P2(n1,2) P2(n2,2)];
z2=[P2(n1,3) P2(n2,3)];
plot3(z2,y2,x2, 'Color','#7E2F8E')
LM(k,:)=[x2(1,1) y2(1,1) z2(1,1) x2(1,2) y2(1,2) z2(1,2)];
hold on
k=k+1;
x3=[P3(n1,1) P3(n2,1)];
y3=[P3(n1,2) P3(n2,2)];
z3=[P3(n1,3) P3(n2,3)];
plot3(z3,y3,x3, 'Color','#7E2F8E')
LM(k,:)=[x3(1,1) y3(1,1) z3(1,1) x3(1,2) y3(1,2) z3(1,2)];
hold on
k=k+1;
x4=[P4(n1,1) P4(n2,1)];
y4=[P4(n1,2) P4(n2,2)];
z4=[P4(n1,3) P4(n2,3)];
plot3(z4,y4,x4, 'Color','#7E2F8E')
LM(k,:)=[x4(1,1) y4(1,1) z4(1,1) x4(1,2) y4(1,2) z4(1,2)];
hold on
k=k+1;
n=n+1;
end

C=[22 22;10 10;23 23];
n1=C(1,1);
n2=C(1,2);
n3=C(2,1);
n4=C(2,2);
n5=C(3,1);
n6=C(3,2);


x1=[P(n1,1) P3(n2,1)];
y1=[P(n1,2) P3(n2,2)];
z1=[P(n1,3) P3(n2,3)];
plot3(z1,y1,x1, 'Color','#7E2F8E')
LM(k,:)=[x1(1,1) y1(1,1) z1(1,1) x1(1,2) y1(1,2) z1(1,2)];
k=k+1;
hold on

x1=[P2(n1,1) P4(n2,1)];
y1=[P2(n1,2) P4(n2,2)];
z1=[P2(n1,3) P4(n2,3)];
plot3(z1,y1,x1, 'Color','#7E2F8E')
LM(k,:)=[x1(1,1) y1(1,1) z1(1,1) x1(1,2) y1(1,2) z1(1,2)];
k=k+1;
hold on
```

```
x1=[P(n3,1) P3(n4,1)];
y1=[P(n3,2) P3(n4,2)];
z1=[P(n3,3) P3(n4,3)];
plot3(z1,y1,x1, 'Color','#7E2F8E')
LM(k,:)=[x1(1,1) y1(1,1) z1(1,1) x1(1,2) y1(1,2) z1(1,2)];
k=k+1;
hold on

x1=[P2(n3,1) P4(n4,1)];
y1=[P2(n3,2) P4(n4,2)];
z1=[P2(n3,3) P4(n4,3)];
plot3(z1,y1,x1, 'Color','#7E2F8E')
LM(k,:)=[x1(1,1) y1(1,1) z1(1,1) x1(1,2) y1(1,2) z1(1,2)];
k=k+1;
hold on

x1=[P(n5,1) P3(n6,1)];
y1=[P(n5,2) P3(n6,2)];
z1=[P(n5,3) P3(n6,3)];
plot3(z1,y1,x1, 'Color','#7E2F8E')
LM(k,:)=[x1(1,1) y1(1,1) z1(1,1) x1(1,2) y1(1,2) z1(1,2)];
k=k+1;
hold on



%L cross section size S LS

B=[4 8;8 4;8 9;9 8;9 7;7 9;
   21 4;4 21;21 23;23 21;
   24 20;20 24;20 3;3 20;
   18 19;19 18;19 2;2 19;
   13 21;21 13;
   7 10;10 7;10 5;5 10;
   1 11;11 1;11 2;2 11;2 12;12 2;12 3;3 12;3 13;13 3;
   13 4;4 13;4 14;14 4;14 15;15 14;15 5;5 15;5 16;16 5;16 17;17 16;17 6;6 17;
    22 5;5 22];
k=1;
n=1;
while n<=size(B,1)

n1=B(n,1);
n2=B(n,2);
x1=[P(n1,1) P3(n2,1)];
y1=[P(n1,2) P3(n2,2)];
z1=[P(n1,3) P3(n2,3)];
LS(k,:)=[x1(1,1) y1(1,1) z1(1,1) x1(1,2) y1(1,2) z1(1,2)];
k=k+1;
plot3(z1,y1,x1, 'Color','#00C0C0')
hold on
x2=[P2(n1,1) P4(n2,1)];
y2=[P2(n1,2) P4(n2,2)]
z2=[P2(n1,3) P4(n2,3)];
plot3(z2,y2,x2, 'Color','#00C0C0')
LS(k,:)=[x2(1,1) y2(1,1) z2(1,1) x2(1,2) y2(1,2) z2(1,2)];
k=k+1;
hold on

n=n+1;
end

C2=[22 22];
n1=C2(1,1);
n2=C2(1,2);

x3=[P(n1,1) P4(n2,1)];
y3=[P(n1,2) P4(n2,2)];
z3=[P(n1,3) P4(n2,3)];
LS(k,:)=[x3(1,1) y3(1,1) z3(1,1) x3(1,2) y3(1,2) z3(1,2)];
k=k+1;
plot3(z3,y3,x3, 'Color','#00C0C0')
hold on
x4=[P2(n1,1) P3(n2,1)];
y4=[P2(n1,2) P3(n2,2)];
z4=[P2(n1,3) P3(n2,3)];
LS(k,:)=[x4(1,1) y4(1,1) z4(1,1) x4(1,2) y4(1,2) z4(1,2)];
k=k+1;
plot3(z4,y4,x4, 'Color','#00C0C0')
hold on

%Bracing BRACING
D=[1 2;2 1;2 13;13 2];
n=1;
k=1;
while n<=size(D,1)
```

```
n1=D(n,1);
n2=D(n,2);
x1=[P(n1,1) P2(n2,1)];
y1=[P(n1,2) P2(n2,2)];
z1=[P(n1,3) P2(n2,3)];
plot3(z1,y1,x1, 'Color','#808080')
BRACING(k,:)=[x1(1,1) y1(1,1) z1(1,1) x1(1,2) y1(1,2) z1(1,2)];
k=k+1;
hold on
x2=[P3(n1,1) P4(n2,1)];
y2=[P3(n1,2) P4(n2,2)];
z2=[P3(n1,3) P4(n2,3)];
plot3(z2,y2,x2, 'Color','#808080')
BRACING(k,:)=[x2(1,1) y2(1,1) z2(1,1) x2(1,2) y2(1,2) z2(1,2)];

hold on
k=k+1;
n=n+1;
end

%Insulators
k=1;
x1=[P5(1,1) P(25,1)];
y1=[P5(1,2) P(25,2)];
z1=[P5(1,3) P(25,3)];
plot3(z1,y1,x1, 'Color','#D95319')
CON(k,:)=[x1(1,1) y1(1,1) z1(1,1) x1(1,2) y1(1,2) z1(1,2)];
k=k+1;
hold on
x2=[P5(1,1) P(27,1)];
y2=[P5(1,2) P(27,2)];
z2=[P5(1,3) P(27,3)];
plot3(z2,y2,x2, 'Color','#D95319')
CON(k,:)=[x2(1,1) y2(1,1) z2(1,1) x2(1,2) y2(1,2) z2(1,2)];
k=k+1;
hold on

x3=[P5(2,1) P(26,1)];
y3=[P5(2,2) P(26,2)];
z3=[P5(2,3) P(26,3)];
plot3(z3,y3,x3, 'Color','#D95319')
CON(k,:)=[x3(1,1) y3(1,1) z3(1,1) x3(1,2) y3(1,2) z3(1,2)];
k=k+1;
hold on
x4=[P5(2,1) P2(26,1)];
y4=[P5(2,2) P2(26,2)];
z4=[P5(2,3) P2(26,3)];
plot3(z4,y4,x4, 'Color','#D95319')
CON(k,:)=[x4(1,1) y4(1,1) z4(1,1) x4(1,2) y4(1,2) z4(1,2)];
k=k+1;
hold on
x5=[P5(3,1) P2(27,1)];
y5=[P5(3,2) P2(27,2)];
z5=[P5(3,3) P2(27,3)];
plot3(z5,y5,x5, 'Color','#D95319')
CON(k,:)=[x5(1,1) y5(1,1) z5(1,1) x5(1,2) y5(1,2) z5(1,2)];
k=k+1;
hold on
x6=[P5(3,1) P2(25,1)];
y6=[P5(3,2) P2(25,2)];
z6=[P5(3,3) P2(25,3)];
plot3(z6,y6,x6, 'Color','#D95319')
CON(k,:)=[x6(1,1) y6(1,1) z6(1,1) x6(1,2) y6(1,2) z6(1,2)];
k=k+1;
hold on

%Supports SP

  S=[25;26;27];

k=1;
n=1;
while n<=size(S,1)
n1=S(n,1);

    x1=[P(n1,1) P(n1,1)-1];
    y1=[P(n1,2) P(n1,2)];
    z1=[P(n1,3) P(n1,3)];
    SP(k,:)=[x1(1,1) y1(1,1) z1(1,1) x1(1,2) y1(1,2) z1(1,2)];
    k=k+1;

    x2=[P(n1,1) P(n1,1)];
    y2=[P(n1,2) P(n1,2)+1];
    z2=[P(n1,3) P(n1,3)];
    SP(k,:)=[x2(1,1) y2(1,1) z2(1,1) x2(1,2) y2(1,2) z2(1,2)];
    k=k+1;
```

```
    x3=[P(n1,1) P(n1,1)];
    y3=[P(n1,2) P(n1,2)];
    z3=[P(n1,3) P(n1,3)-1];
    SP(k,:)=[x3(1,1) y3(1,1) z3(1,1) x3(1,2) y3(1,2) z3(1,2)];
    k=k+1;

    x4=[P2(n1,1) P2(n1,1)-1];
    y4=[P2(n1,2) P2(n1,2)];
    z4=[P2(n1,3) P2(n1,3)];
    SP(k,:)=[x4(1,1) y4(1,1) z4(1,1) x4(1,2) y4(1,2) z4(1,2)];
    k=k+1;

    x5=[P2(n1,1) P2(n1,1)];
    y5=[P2(n1,2) P2(n1,2)+1];
    z5=[P2(n1,3) P2(n1,3)];
    SP(k,:)=[x5(1,1) y5(1,1) z5(1,1) x5(1,2) y5(1,2) z5(1,2)];
    k=k+1;

    x6=[P2(n1,1) P2(n1,1)];
    y6=[P2(n1,2) P2(n1,2)];
    z6=[P2(n1,3) P2(n1,3)-1];
    SP(k,:)=[x6(1,1) y6(1,1) z6(1,1) x6(1,2) y6(1,2) z6(1,2)];
    k=k+1;
    n=n+1;
end

COMSOLfile('Suspension pylon ', 'elements', 'RCS', RCS, name)
COMSOLfile('Suspension pylon ', 'elements', 'LL', LL, name)
COMSOLfile('Suspension pylon ', 'elements', 'LM', LM, name)
COMSOLfile('Suspension pylon ', 'elements', 'LS', LS, name)
COMSOLfile('Suspension pylon ', 'elements', 'BRACING', BRACING, name)
COMSOLfile('Suspension pylon ', 'elements', 'INS', INS, name)
COMSOLfile('Suspension pylon ', 'elements', 'SUP', SP, name)

daspect([1 1 1])
camup([0 1 0])
grid on
hold off

end
```

```
function COMSOLconductors(name1, MATRIX, number)

directorypath = '/Users/wojciech.poradowski/Documents/Master thesis/CatenaryCurve/COMSOL_files/';

fnm = sprintf([directorypath num2str(name1) ' ' num2str(number) '.mphtxt']);
fid = fopen (fnm,'w');

i=1;
fprintf(fid, [num2str(MATRIX(i,3)) ' ' num2str(MATRIX(i,2)) ' ' num2str(MATRIX(i,1)) '\n']);
while i<size(MATRIX,1)
    fprintf(fid, [num2str(MATRIX(i,6)) ' ' num2str(MATRIX(i,5)) ' ' num2str(MATRIX(i,4)) '\n']);
    i=i+25;
end

last=size(MATRIX,1);

fprintf(fid, [num2str(MATRIX(last,6)) ' ' num2str(MATRIX(last,5)) ' ' num2str(MATRIX(last,4)) '\n']);
fclose(fid);

end

function COMSOLfile(name1, name2, name3, MATRIX, number)

directorypath = '/Users/wojciech.poradowski/Documents/Master thesis/CatenaryCurve/COMSOL_files/';

fnm = sprintf([directorypath num2str(name1) ' ' num2str(number) ' ' num2str(name2) ' ' num2str(name3)
'.mphtxt']);
fid = fopen (fnm,'w');
fprintf(fid,['# Created by COMSOL Multiphysics.\n\n' '# Major & minor version\n' '0 1\n' '1 # number of
tags\n' '# Tags\n' '5 geom1\n'  '1 # number of types\n' '# Types\n' '3 obj\n\n' '# --------- Object 0 ---
-------\n\n' '0 0 1\n' '5 Geom3 # class\n' '3 # version\n' '1 # type\n' '1 # voidsLabeled\n' '1e-10 #
gtol\n' '0.0001 # resTol\n\n']);

%Calculate number of points
    POINTS=zeros(size(MATRIX,1),2);
    i=1;
    k=1;
    POINTS(k,1)=i;
    i=i+1;
    POINTS(k,2)=i;
    i=i+1;
    k=k+1;
    while k<=size(MATRIX,1)

          j=1;
          while j<k

              if MATRIX(k,1)==MATRIX(j,1) && MATRIX(k,2)==MATRIX(j,2) && MATRIX(k,3)==MATRIX(j,3)
              POINTS(k,1)=POINTS(j,1);
               condition=0;
              break
              elseif MATRIX(k,1)==MATRIX(j,4) && MATRIX(k,2)==MATRIX(j,5) && MATRIX(k,3)==MATRIX(j,6)

                  POINTS(k,1)=POINTS(j,2);
                   condition=0;
                  break
              else
                  POINTS(k,1)=i;
                  condition=1;
              end
              j=j+1;
          end

            if condition==1
                i=i+1;
            end

           j=1;

           while j<k
              if MATRIX(k,4)==MATRIX(j,1) && MATRIX(k,5)==MATRIX(j,2) && MATRIX(k,6)==MATRIX(j,3)
              POINTS(k,2)=POINTS(j,1);
              condition=0;
               break
              elseif MATRIX(k,4)==MATRIX(j,4) && MATRIX(k,5)==MATRIX(j,5) && MATRIX(k,6)==MATRIX(j,6)
              POINTS(k,2)=POINTS(j,2);
              condition=0;
               break
              else
                  POINTS(k,2)=i;
               condition=1;
              end
              j=j+1;
           end
           if condition==1
                i=i+1;
            end
    k=k+1;
    end

M = max(POINTS, [], 'all');

fprintf(fid,[num2str(M) ' # number of vertices\n']);

fprintf(fid,['# Vertices\n' '# X Y Z dom tol\n']);

%write down vertices
i=1;
fprintf(fid, [num2str(MATRIX(i,1:3)) ' -1 NAN\n']);
fprintf(fid, [num2str(MATRIX(i,4:6)) ' -1 NAN\n']);
i=i+1;
while i<=size(MATRIX,1)
          j=1;
          condition=0;
          while j<i
              if POINTS(i,1)~=POINTS(j,1) && POINTS(i,1)~=POINTS(j,2)
                  condition=0;
              else
                  condition=1;
                  break
              end
              j=j+1;
          end

        if condition==0
            fprintf(fid, [num2str(MATRIX(i,1:3)) ' -1 NAN\n']);
        end

          j=1;
          condition=0;
          while j<i
              if POINTS(i,2)~=POINTS(j,1) && POINTS(i,2)~=POINTS(j,2)
                  condition=0;
              else
                  condition=1;
                  break
              end
              j=j+1;
          end


        if condition==0
            fprintf(fid, [num2str(MATRIX(i,4:6)) ' -1 NAN\n']);
```

```
        end
        i=i+1;
end

fprintf(fid,['\n0 # number of parameter vertices\n' '# Parameter vertices\n' '# vtx s t fac surf
tol\n\n']);
fprintf(fid,[num2str(size(POINTS,1)) ' # number of edges\n' '# Edges\n' '# vtx1 vtx2 s1 s2 dom curve
tol\n']);

%print edges connection
i=1;
while i<=size(POINTS,1)
fprintf(fid, [num2str(POINTS(i,:)) ' 0 1 0 ' num2str(i) ' NAN\n']);
i=i+1;
end

fprintf(fid,['\n0 # number of parameter edges\n' '# Parameter edges\n' '# edg v1 v2 s1 s2 up down pcurve
surf tol\n\n']);
fprintf(fid,['0 # number of faces\n' '# Faces\n' '# up down surf tol\n\n']);

%print curves connection
fprintf(fid,[num2str(size(POINTS,1)) ' # number of curves\n' '# Curves\n\n']);
i=1;
while i<=size(POINTS,1)
    fprintf(fid,['# Curve ' num2str(i) '\n' '11 BezierCurve # class\n' '1 # version\n' '3 # sdim\n' '1 #
rational?\n' '1 # degree\n' '# homogeneous control points\n']);
    fprintf(fid, [num2str(MATRIX(i,1:3)) ' 1\n']);
    fprintf(fid, [num2str(MATRIX(i,4:6)) ' 1\n']);
    fprintf(fid,'\n');
    i=i+1;
end

fprintf(fid,['0 # number of surfaces\n' '# Surfaces\n\n' '0 # number of parameter curves\n' '# Parameter
curves\n\n']);
fprintf(fid,['# Attributes\n' '0 # nof attributes\n']);
fclose(fid);

end
```

APPENDIX 2 SYMBOLS

CHAPTER 2

α	Coefficient of thermal (linear) expansion
ε	Strain
σ	Stress
σ_b	Bending stress
a	Span length
A	Conductor cross-section area
E	Modulus of elasticity
f	Conductor sag
g	Gravitational acceleration
H	Horizontal component of the conductor tensile force
h	Difference between points of support
L	Length of conductor
L_E	Length of ruling (equivalent) span
L_{H_c}	Length of conductor under horizontal tension H_c
m_c	Weight per unit length
N_f	Number of cycles
S	Conductor tensile force
ΔT_{con}	Temperature change of conductor
x_B, x_A	Geometrical parameters

CHAPTER 3

α	Power law coefficient
γ	Partial factor
δ	Ice density
θ'	Angle formed by the direction of the wind and the cylinder axis
θ	Angle of incidence of wind direction
ν	Kinematic air viscosity
ρ_{ref}	Reference air density
ρ	Air density
τ	Air density correction factor
χ	Solidity ratio
Ψ	Partial factor
Ω	Angle between wind direction and conductor
A_c	Wind load on conductors

A_i	Wind load acting directly on the insulator strings
$A_{t(I)}$, $A_{t(II)}$	Load acting on lattice towers
A_{tc}	Wind load acting on cylindrical members with large diameter
B_{iH}	Reduction factor
B_{iL}	Reduction factor
C	Drag coefficient
c_{alt}	Correction of wind speed
$C_{iH,iL,iH3}$	Drag coefficient
$C_{xt1,2}$	Drag coefficients of each face of lattice tower members
C_{xt}	Drag coefficients of each face of lattice tower members
C_{xtc}	Drag coefficient of cylindrical cross-section
C_{xc}	Drag coefficient of conductor
C_{xi}	Drag coefficient of insulators
d	Diameter of conductor
$D_{L,H,H3}$	Cylindrical ice accretion around conductors
d_{tc}	Diameter of cylinder
E_d	Effect of design actions
$g_{L,H,H3}$	Ice loads corresponding to low and high probabilities of occurrence
G_c	Combined wind factor
G_k	Permanent action
G_L	Span factor
$G_{L,C}$	Combined wind and span factors
G_t	Combined wind factor
H	Altitude considered for power line
H_0	Reference height over which the correction is applied
H_{topp}	The height over sea lever where factor c_{alt} reaches maximum value
K_R	Roughness factor
L	Wind span of the support
l_e	Length of the member
P_n	Designed construction loads
Q_{1K}	Dominant variable action
Q_{nK}	Other variable action
Re	Reynolds number
S_i	Area of insulators string
S_{t1}, S_{t2}	Total area of windward surface of tower members, projected on surface perpendicular/parallel to power line and ground
T	Temperature
t	Radial ice thickness

V_{h_m}	Reference measured velocity on height h_m above the ground
$V_{iH,iL,iL3}$	Wind velocity
V_{RB}	Reference wind speed from meteorological station
V_T	Wind velocity
X_d	Designed resistance
z	Height of the considered element (either insulators or supports) above ground level

CHAPTER 6.1-6.4

α	Linear expansion coefficient
ρ	Density
υ	Poisson ratio
A	Total cross-section Area
A_{Al}	Aluminum corss-section
a_e	Length of span
b_1	Distance to shear center in x direction
d_1	Distance to shear center in y direction
d_{ACSR}	Diameter od conductor
E	Young´s modulus
el_{diff}	Difference of heights between points of support of catenary
E_p	Post yielding tangent Modulus
f_y	Yield strength
h	Elevation of tower
$I_{xx}, I_{yy}, I_{zz}, I_{vv}, I_{uu}$	Moment of inertia
i_{xx}, i_{yy}, i_{vv}	Radius of gyration
J	Torsional constant
m_c	Mass per unit length
$m_c g$	Mass of conductors per meter
w_t	Torsional section modulus

CHAPTER 6.5

α_{LT}	Imperfection factor
α	Imperfection factor
γ_{M1}	Resistance of members to buckling
λ_{eff}	Reduced slenderness
λ	Slenderness ratio
ξ	Factor for torsional-flexural buckling
ρ	Effective widths of the compression elements
σ_{cr}	Critical elastic stress

ϕ	Characteristic value of reduction factor
χ_{LT}	Reduction factor for lateral-torsional buckling
χ	Reduction factor for relevant buckling mode
A_{eff}	Effective are of cross section when subjected to compression
A_{eff}	Effective area
c_{wrap}	Wrapping constant
f_y	Yielding strength
G	Shear modulus
i	Radius of gyration
I_{pol}	Polar moment of inertia about shear center
I_{sv}	St. Venant´s moment of inertia
k_e	Effective length with factor
L_{cr}	Buckling length
L_e	Effective length of structural member
$M_{b,Rd}$	Design buckling resistance moment of the structural member
M_{Ed}	Design value of moment for ULS
$N_{b,Rd}$	Design buckling resistance of the structural member
N_{Ed}	Design value of compression force for ULS

CHAPTER 6.6-6.10

F_w	Wind load
ξ	Damping coefficient

APPENDIX 3 LIST OF FIGURES

APPENDIX 4 LIST OF TABLES

REFERENCES

[1] D. K. O.-o. Energidepartement, "Energi til arbeid – langsiktig verdiskaping fra norske energiressurser," in "Meldt. St. 36 (220-2021)," 11. juni 2021.

[2] N. v.-o. energidirektorat, "Strømforbruk mot 2040," 2019, vol. 22-2019. [Online]. Available: https://www.nve.no/energi/energisystem/energibruk-effektivisering-og-teknologier/samlet-energibruk/

[3] (2019). *Norge Energifakta*. [Online] Available: https://energifaktanorge.no/

[4] Statnett, "Utvikling av nye fjordspennliner," October 10th, 2021. [Online]. Available: https://www.statnett.no/om-statnett/innovasjon-og-teknologiutvikling/vare-sentrale-prosjekter/utvikling-av-nye-fjordspennliner/

[5] E. P. R. Institute, *EPRI The Orange Book 2006 Transmission Line Reference Book - Wind Induced Conductor Motion*. 2008.

[6] B. J. K. Engdahl, B. E. K. Nygaard, G. Thompson, and L. Bengtsson, "Improved predictions of atmospheric icing at MET-
Norway," in *Int. Workshop on Atmospheric Icing of Structures (IWAIS)*, Reykjavík, June 23 – 28 2019.

[7] *EN 50341-1:2012. Overhead electrical lines exceeding AC 1 kV - Part 1: General requirements - Common specifications*, CEN-CENELEC.

[8] I. Gutman, J. Lundengård, V. Naidoo, and B. Adum, "Technologies to reduce and remove ice from phase conductors and shield wires: applicability for
Norwegian conditions," in *Int. Workshop on Atmospheric Icing of Structures (IWAIS)*, Reykjavík, June 23 – 28 2019.

[9] M. Farzaneh, "Advanced monitoring of icing and preventionagainst icing on overhead power lines," *INMR Weekly Technical Review*.

[10] I. Hanssen-Bauer *et al.*, "Climate in Norway 2100 - a knowledge base for climate adaptation" The Norwegian Centre for Climate Services (NCCS) 2017.

[11] Hydro-Québec, "Twenty years ago, Québec was battered by an ice storm," *Hydro Québec* [Online]. Available: http://news.hydroquebec.com/en/press-releases/1313/twenty-years-ago-quebec-was-battered-by-an-ice-storm/

[12] J. Nilsen, "Her henger 1,5 meter is rundt en tynn kraftledning," *Teknisk Ukeblad Media AS*. [Online]. Available: https://www.tu.no/artikler/her-henger-1-5-meter-is-rundt-en-tynn-kraftledning/234878

[13] Ø. Lie, "Sjekk hvordan Statnetts toppliner ises ned om vinteren," *Teknisk Ukeblad Media AS*. [Online]. Available: https://www.tu.no/artikler/sjekk-hvordan-statnetts-toppliner-ises-ned-om-vinteren/230404

[14] J. Nielsen, "Statnett tar i bruk kompositmaster for første gang," *Teknisk Ukeblad Media AS*. [Online]. Available: https://www.tu.no/artikler/utvikler-nye-verktoy-for-a-bli-kvitt-tonnevis-med-is-pa-kraftlinjene/503088

[15] K. Ingvaldsen, B. E. Nygaard, Ø. Byrkjedal, and E. C. Iversen, "Validation of Modelled In-cloud Ice Accretion on Overhead Power Lines at Exposed High Altitude Sites in Norway," in *Int. Workshop on Atmospheric Icing of Structures (IWAIS)*, Reykjavík, June 23 – 28 2019.

[16] J. Thomassen, F. Hanssen, R. May, and K. Bevanger, "Rapport fra dialogseminar 2 - kriterier og kriterieverdier i OPTIPOL-LCP versjon 1.0" Norsk institutt for naturforskning, Trondheim, Januar 2013.

[17] HaroldMcInnes *et al.*, "Klimaendringenes betydning for Statnett sine overføringsanlegg" Norwegian Meteorological Institute, 2016, vol. 27-2015.

[18] B. E. Nygaard and S. Fikke, "Rapport nr 44 Isstorm – Ising på kraftforsyningsnettet," Norges vassdrags- og energidirektorat, November 2012.

[19] J. Lutz, A. Dobler, B. E. Nygaard, H. M. Innes, and J. E. Haugen, "Future Projections of Icing on Power Lines over Norway," in *Int. Workshop on Atmospheric Icing of Structures (IWAIS)*, Reykjavík, June 23 – 28 2019.

[20] M. A. AlAqil and K. Kopsidas, "Modelling the structural-dynamics of electrical overhead line power conductors," 2019.

[21] L. Zhao, X. Huang, Y. Zhang, Y. Zhu, J. Jia, and C. Zhu, "Aeolian vibration-based structural health monitoring system for transmission line conductors," *Structural control and health monitoring,* vol. 27, no. 6, p. n/a, 2020, doi: 10.1002/stc.2538.

[22] C. B. Rawlins, "Research on vibration of overhead ground wires," *IEEE Transactions on Power Delivery,* vol. 3, no. 2, pp. 769-775, 1988, doi: 10.1109/61.4316.

[23] M. Farzaneh, *Atmospheric Icing of Power Networks*. Springer, Dordrecht, 2008.

[24] CIGRE, *Overhead Lines* (CIGRE Green Books). Springer, Cham, 2017.

[25] P. Oberdorfer, "The Beauty of Vortex Streets," *COMSOL Blog*. [Online]. Available: https://www.comsol.com/blogs/the-beauty-of-vortex-streets/

[26] D. Havard, ""Dynamic Loads On Transmission Line Structures During Galloping", by D. G. Havard, IWAIS 2002, Brno, Czech Republic, 17-20 June 2002," 06/10 2002.

[27] J.-l. Lilien, P. Van Dyke, and A. Laneville, *State of the art of conductor galloping* (A complementary document to "Transmission line reference book –Wind-induced conductor motion"). CIGRE, TF B2.11.O6, 2007.

[28] I. Gołębiowska, M. Dutkiewicz, and B. Usewicz, "Galloping of Overhead Power Lines Conductors," in *Engineering Mechanics 2018, 24th International Conference* Svratka, Czech Republic, 2020, no. 239, pp. 257-260, doi: 10.21495/91-8-257.

[29] D. E. S., H. A. R., R. C. B., and I. R., "Transmission line reference book: wind-induced conductor motion," Electric Power Research Institute, Palo Alto, California, 1979.

[30] R. M. Hefny, "Numerical and experimental investigation of the influence of dynamic loads on wet snow shedding from overhead cables," 2013.

[31] G. Huang, B. Yan, J. Liu, C. Wu, and Z. Lv, "Experimental Study on Torsional Behavior of Twin Bundle Conductor Lines," *IEEE transactions on power delivery,* vol. 35, no. 3, pp. 1423-1431, 2020, doi: 10.1109/TPWRD.2019.2944983.

[32] N. O, C. GJ, H. DG, and P. no, "Torsional stability of bundle conductors," *IEEE Paper no F 77 224–9,* January 1977.

[33] C. Wu, B. Yan, G. Huang, B. Zhang, Z. Lv, and Q. Li, "Wake-induced oscillation behaviour of twin bundle conductor transmission lines," *Royal Society Open Science,* vol. 5, p. 180011, 06/01 2018, doi: 10.1098/rsos.180011.

[34] Z.-M. Yang, L. Ding, Q.-Y. Ye, L. Yang, and L. Zhang, "Effect of Gap Flow on the Characteristics of Flow-Around and Flow-Induced Vibration for Two Circular Cylinders with Roughness Strips," *Applied Sciences,* vol. 9, no. 17, p. 3587, 2019. [Online]. Available: https://www.mdpi.com/2076-3417/9/17/3587.

[35] N. Hosseini, M. D. Griffith, and J. S. Leontini, "Vortex Shedding and Flow-Induced Vibration of Two Cylinders in Tandem," in *IUTAM Symposium on Recent Advances in Moving Boundary Problems in Mechanics*, Cham, S. Gutschmidt, J. N. Hewett, and M. Sellier, Eds., 2019// 2019: Springer International Publishing, pp. 41-52.

[36] M. Farzaneh and W. A. Chisholm, *Techniques for Protecting Overhead Lines in Winter Conditions* (CIGRE Study Commitee B2: Oerhead Lines). Springer Nature Switzerland AG, 2022.

[37] M. R. (Statnett). "Icebox." https://www.statnett.no/en/about-statnett/innovation-and-technology-development/our-prioritised-projects/icebox/ (accessed.

[38] K. Pedersen, "Uventet store isproblemer langs Hardangerlinjen," *© Bergens Tidende*. [Online]. Available: https://www.bt.no/nyheter/lokalt/i/1jjXK/uventet-store-isproblemer-langs-hardangerlinjen

[39] H. M. Innes *et al.*, "Wind Ice and Snow Load Impacts on Infrastructure and the Natural Environment (WISLINE)," in *Int. Workshop on Atmospheric Icing of Structures (IWAIS)*, Reykjavík, June 23 – 28 2019.

[40] V. Kul'kov, V. Kuryanov, and R. Fokin, "Methods for dealing with icing of power line wires," *IOP Conference Series: Materials Science and Engineering,* vol. 1035, p. 012042, 01/01 2021, doi: 10.1088/1757-899X/1035/1/012042.

[41] D. Havard, ""Dynamic Loads On Transmission Line Structures During Galloping – Field Data and Elastic Analysis" by D. G. Havard, Fifth International Symposium on Cable Dynamics, Santa Margherita, Italy, 15-18 Sept, 2003," 09/10 2003.

[42] Y. Yu, L. Chen, J. Wang, and G. Liu, "Dynamic Characteristics Analysis of Ice-Adhesion Transmission Tower-Line System under Effect of Wind-Induced Ice Shedding," *Computer modeling in engineering & sciences,* vol. 125, no. 2, pp. 647-670, 2020, doi: 10.32604/cmes.2020.011067.

[43] I. ANSYS. https://www.ansys.com (accessed.

[44] M. Zhang, G. Zhao, L. Wang, and J. Li, "Wind-Induced Coupling Vibration Effects of High-Voltage Transmission Tower-Line Systems," *Shock and Vibration,* vol. 2017, pp. 1-34, 12/10 2017, doi: 10.1155/2017/1205976.

[45] F. Mirshafiei, "Modelling the dynamic response of overhead line conductors subjected to shock-induced ice shedding," ProQuest Dissertations Publishing, 2011.

[46] T. Kálmán, M. Farzaneh, and G. McClure, "Numerical analysis of the dynamic effects of shock-load-induced ice shedding on overhead ground wires," *Computers & Structures,* vol. 85, no. 7, pp. 375-384, 2007/04/01/ 2007, doi: https://doi.org/10.1016/j.compstruc.2006.11.026.

[47] I. ADINA R & D. https://adina.com (accessed.

[48] Y. Fengli, Y. Jingbo, H. Junke, and F. Dongjie, "Dynamic responses of transmission tower-line system under ice shedding," *International Journal of Structural Stability and Dynamics,* vol. 10, no. 3, pp. 461-481, 2010, doi: DOI: 10.1142/S0219455410003579.

[49] F. Yang, J. Yang, and Z. Zhang, "Unbalanced tension analysis for UHV transmission towers in heavy icing areas," *Cold Regions Science and Technology - COLD REG SCI TECHNOL,* vol. 70, 01/31 2012, doi: 10.1016/j.coldregions.2011.07.008.

[50] W. Zhou, X. Zhang, X. Li, and Y. Jiang, "Computational analysis on unbalanced tension in overhead power lines under non-uniform accreted ice," *Electric Power Systems Research,* vol. 202, p. 107606, 2022/01/01/ 2022, doi: https://doi.org/10.1016/j.epsr.2021.107606.

[51] "The Norwegian power system. Grid connection and licensingn" Norwegian water resources and energy directorate, 2018.

[52] K. Harker, *High Voltage Power Network Construction* (Energy engineering). Stevenage: Stevenage: The Institution of Engineering and Technology, 2018.

[53] E. Widenoja and H. Hemstad, "Estetiske hensyn ved valg av kraftledningsmaster," in "Rapport 16/98," 1998.

[54] T. Witzøe, "Estetiske hensyn ved valg av kraftledningsmaster." [Online]. Available: https://www.fvn.no/nyheter/lokalt/i/R992X8/skal-rive-over-200-hoeyspentmaster

[55] https://en-academic.com/dic.nsf/enwiki/1039058 (accessed.

[56] *IEC 60826:2017. Design criteria of overhead transmission lines*, I. E. Commission.

[57] *NEK EN 50341-2-16:2016 Overhead electrical lines exceeding AC 1 kV - Part 2-16: National Normative Aspects (NNA) for NORWAY*, CEN-CENELEC.

[58] E. W. W. D. AS) and C. Aastrop, "Mastedokumentasjon Sentrale områder på Østlandet Sommer og høst 2011" 2012.

[59] NVE, "Hol – Oslo." [Online]. Available: https://www.nve.no/om-nve/nves-utvalgte-kulturminner/kraftledninger/hol-oslo/#begrunnelse

[60] E. Widenoja, "Visuell tilpasning av mastetyper i regionalnettet," 2019, vol. 60-2019.

[61] L. Li, C. Lin, and X. Wu, *Research On Windage Yaw Of V-Type Composite Insulators In Ultra-High Voltage*. 2017.

[62] P. Catchpole, *Structural Engineering of Transmission Lines*. London: London: ICE Publishing, 2014.

[63] Statnett, "Ertsmyra–Tjørhom–Lyse Spenningsoppgradering fra 300 til 420 kV" [Online]. Available: https://www.nve.no/om-nve/nves-utvalgte-kulturminner/kraftledninger/hasle-borgvik/#landskap-og-miljo

[64] Statnett, "Ertsmyra–Tjørhom–Lyse Spenningsoppgradering fra 300 til 420 kV. " 2020. [Online]. Available: https://www.statnett.no/vare-prosjekter/region-sor/vestre-korridor/ertsmyra-tjorhom-lyse/
[65] *NEK 60383-1:1996*, NEK.
[66] F. Kiessling, P. Nefzger, U. Kaintzyk, and J. F. Nolasco, *Overhead Power Lines: Planning, Design, Construction*. Springer Science & Business Media, 2003.
[67] D. Douglass, M. Gaudry, D. Douglass, and S. Hoffmann, "Sag-Tension calculation methods for overhead lines," in "TECHNICAL BROCHURES: ," CIGRE, Task Force B2.12.3, 2016.
[68] K. O. Papailiou, *Overhead Lines* (International Council on Large Electric Systems (CIGRE) Study Committee B2: Overhead Lines). Springer International Publishing Switzerland 2017, 2007.
[69] *NEK IEC TR 61597:2021*, NEK.
[70] A. Association, "Stress-Strain-Creep Curves for Aluminum Overhead Electrical Conductors," 1974.
[71] L. L. Grigsby, *Electric Power Generation, Transmission, and Distribution: The Electric Power Engineering Handbook*, 3 ed. CRC Press, 2012.
[72] Statnett, "Refsdal – Fardal," November 11th, 2015. [Online]. Available: https://www.nve.no/om-nve/nves-utvalgte-kulturminner/kraftledninger/refsdal-fardal/#begrunnelse
[73] Kinectrics, "Conductor Fatigue Test." [Online]. Available: https://www.kinectrics.com/Case-Studies/Pages/Conductor-Fatigue-Testing-.aspx
[74] CIGRE, *Fatigue Endurance Capability of Conductor/Clamp Systems - Update of Present Knowledge* (Technical Brochures). TF B2.11.07, 2007.
[75] S. Goudreau, F. Lévesque, A. Cardou, and L. Cloutier, "Strain Measurements on ACSR Conductors During Fatigue Tests III—Strains Related to Support Geometry," *Power Delivery, IEEE Transactions on,* vol. 25(4), pp. 3007-3016, 11/01 2010, doi: 10.1109/TPWRD.2010.2045399.
[76] S. Lalonde, R. Guilbault, and S. Langlois, "Modeling multilayered wire strands, a strategy based on 3D finite element beam-to-beam contacts - Part II: Application to wind-induced vibration and fatigue analysis of overhead conductors," *International Journal of Mechanical Sciences,* vol. 126, pp. 297-307, 2017/06/01/ 2017, doi: https://doi.org/10.1016/j.ijmecsci.2016.12.015.
[77] Statnett. "Composite and aluminium towers." https://www.statnett.no/en/about-statnett/innovation-and-technology-development/our-prioritised-projects/composite-and-aluminium-towers/ (accessed.
[78] I. B. (STATNETT) and H. J. F. R.-T. AS), "Høyspentmaster for 420 kV i kompositttmaterialer," in *Polymerdagene 2014*, 2014.
[79] T. Jahangiri, Q. Wang, F. F. da Silva, and C. Leth Bak, "Overview of Composite-Based Transmission Pylons," (Lecture Notes in Electrical Engineering. Cham: Cham: Springer International Publishing, 2019, pp. 1-13.
[80] E. A. R. ingeniører, "Research & Development project of new tower type." [Online]. Available: https://www.efla-engineers.com/about-us/news/r-d-project-of-new-tower-type
[81] Hyndla, "132 kV project with Elvia." [Online]. Available: https://www.hyndla.com/tower-projects/132-kv-project-with-elvia
[82] I. W. o. A. I. o. S. (IWAIS). https://iwais2019.is (accessed.
[83] *Forskrift om elektriske forsyningsanlegg*, D. f. s. o. b. (DSB), 20. December 2005.
[84] *NEK 445:2016 Luftledninger over 1kV*, NEK.
[85] *IEC 61774:1997 Overhead lines - Meteorological data for assessing climatic loads*, I. E. Commission.
[86] *NS-EN 1991-1-4:2005/NA:2009*.
[87] *NS-EN 1993-3-1:2006/AC:2009*.
[88] P. L. Systems. https://www.powerlinesystems.com/about (accessed.
[89] B. Chen, W.-h. Guo, P.-y. Li, and W.-p. Xie, "Dynamic Responses and Vibration Control of the Transmission Tower-Line System: A State-of-the-Art Review," *ScientificWorldJournal,* vol. 2014, pp. 538457-20, 2014, doi: 10.1155/2014/538457.
[90] G. I. Ramsli, "Monsterlinja skulle koste 1,4 milliardar, men vert fire gonger så dyr," *Firda Media AS*. [Online]. Available: https://www.firda.no/nyheiter/statnett/orskog/monsterlinja-skulle-koste-1-4-milliardar-men-vert-fire-gonger-sa-dyr/s/5-15-209839

[91] *NS-EN 1993-1-1:2005+A1:2014+NA:2015*.
[92] *NS-EN 10056-1:2017*.
[93] *Torsional Section Properties of Steel Shapes*, C. I. o. S. Construction, 2002.
[94] R. Stephen, D. Douglass, M. Gaudry, R. Kimata, and S. Hoffmann, *Conductors for the Uprating of Overhead Lines*. CIGRE, TF B2.12, 2004.
[95] O. Papailiou and Schmuck, *Silicone Composite Insulators* (Materials, Design, Applications). Springer, 2012.
[96] M. Adolfsen, "Høyspentmast havarerte i vinden," *Europower AS*. [Online]. Available: https://www.europower-energi.no/nett/mastehavari-for-statnett-i-nordland/1-2-294609
[97] Ø. L. Kraft, "Høyspentmast havarerte i vinden," *Teknisk Ukeblad Media AS*. [Online]. Available: https://www.tu.no/artikler/hoyspentmast-havarerte-i-vinden/234127
[98] *DNVGL-CG-0128,* Edition October 2015.
[99] *NS-EN 1993-1-1:2005+A1:2014+NA:2015*.
[100] *NS-EN 1993-1-3:2006+NA:2015*.
[101] *M. Kraus R. Kindmann*, U. o. B. Institute for Steel and Composite Structures, Germany, Proceedings of the Nordic Steel Construction Conference 2009.
[102] L. Hou, L. Wang, and Z.-c. Guan, "Dynamics characteristic of V-string composite insulators for 330kV overhead transmission line," *2006 IEEE Conference on Electrical Insulation and Dielectric Phenomena,* pp. 429-432, 2006.
[103] S. Malwande, T. Ngonda, and M. Kaunda, "Experimental investigation of self-damping characteristics of the ACSR Beresford and TERN transmission line conductors using log-decrement and quality factor methods," *Materials Today: Proceedings,* vol. 56, pp. 1653-1658, 2022/01/01/ 2022, doi: https://doi.org/10.1016/j.matpr.2021.10.181.
[104] J. Li, H.-N. Li, and X. Fu, "Stability and Dynamic Analyses of Transmission Tower-Line Systems Subjected to Conductor Breaking," *International Journal of Structural Stability and Dynamics,* vol. 17, p. 1771013, 03/24 2017, doi: 10.1142/S0219455417710134.
[105] A. B. (COMSOL), "Connecting the Dots Between Theory, Model, and App," in *COMSOL Blog*, ed, June 29, 2016.